Coordination Chemistry Reviews 253 (2009) 343–409

Contents lists available at ScienceDirect

Coordination Chemistry Reviews

journal homepage: www.elsevier.com/locate/ccr

Review

Lanthanides and actinides: Annual survey of their organometallic chemistry covering the year 2006

Frank T. Edelmann*

Chemisches Institut der Otto-von-Guericke-Universität Magdeburg, D-39106 Magdeburg, Germany

Contents

* Fax: +49 391 6712933.
E-mail address: frank.edelmann@ovgu.de.

0010-8545/$ – see front matter
doi:10.1016/j.ccr.2008.03.003

ARTICLE INFO

Article history:
Received 3 March 2008
Accepted 4 March 2008
Available online 14 March 2008

Keywords:
Lanthanides
Actinides
Cyclopentadienyl complexes
Cyclooctatetraenyl complexes
Organometallic chemistry

ABSTRACT

This review summarizes the progress in organo-f-element chemistry during the year 2006. A continuing trend in organolanthanide research is a strong emphasis on applications of organolanthanide complexes in homogeneous catalysis and, to a lesser extent, materials science. Only little more than 10% of all relevant papers published in 2006 were in the area of organoactinide chemistry, although the latter has produced some truly spectacular results.

1. Introduction

This review summarizes the progress in organo-f-element chemistry during the year 2006. A continuing trend in organolanthanide research is a strong emphasis on applications of organolanthanide complexes in homogeneous catalysis and, to a lesser extent, materials science. Only little more than 10% of all relevant papers published in 2006 were in the area of organoactinide chemistry, although the latter has produced some truly spectacular results (*cf.* Section 3.4). In this review only regular scientific papers are covered, while patents, conference abstracts, etc. have been excluded.

2. Lanthanides

2.1. Lanthanide carbonyls

Isolable binary lanthanide carbonyls still remain elusive, but transient species continue to be subjects of experimental and theoretical investigations. Reactions of laser-ablated scandium and yttrium atoms with dilute carbon monoxide molecules in solid argon were investigated using matrix-isolation infrared spectroscopy. An absorption at 1193.4 cm^{-1} was assigned to the C–O stretching vibration of the $Sc_2[\eta^2(\mu_2\text{-C,O})]$ molecule, which has a single bridging CO that is tilted to the side. This CO-activated molecule undergoes UV/vis-photoinduced rearrangement to the CO-dissociated molecule, *c*-$Sc_2(\mu\text{-C})(\mu\text{-O})$. The cyclic *c*-$Sc_2(\mu\text{-C})(\mu\text{-O})$ molecule has a bridging carbon on one side of the Sc_2 unit and a bridging oxygen on the other. The analogous $Y_2[\eta^2(\mu_2\text{-C,O})]$ molecule was not observed, but the CO-dissociated *c*-$Y_2(\mu\text{-C})(\mu\text{-O})$ molecule was detected in the Y + CO experiments. DFT calculations of the geometry structures, vibrational frequencies, and IR intensities strongly supported the assignments [1]. Reactions of laser-ablated La atoms with CO molecules in solid argon were also studied. The neutral lanthanum monocarbonyl LaCO, produced upon sample deposition at 7 K, exhibits a C–O stretching frequency of 1772.7 cm^{-1}. This is apparently the lowest yet observed value for a terminal CO in a neutral metal-carbonyl molecule (MCO, M = metal atom), implying anomalously enhanced metal-to-CO back-bonding. An infrared (IR) absorption band at 1145.9 cm^{-1} was assigned to the C–O stretching mode of the side-on-bonding CO in the $La_2[\eta^2(\mu_2\text{-C,O})]$ molecule. Like its yttrium lighter homologue [1], this CO-activated molecule undergoes an UV/vis-photoinduced rearrangement to the CO-dissociated molecule *c*-$La_2(\mu\text{-C})(\mu\text{-O})$ [2]. In an analogous manner, reactions of cerium atoms and dicerium molecules with CO were investigated using matrix-isolation infrared absorption spectroscopy. The cerium carbonyls CeCO and Ce_2CO were produced spontaneously on annealing, and they were photochemically rearranged to the CCeO and *c*-$Ce_2(\mu\text{-C})(\mu\text{-O})$ isomers, where Ce and Ce_2 are inserted into the CO triple bond. Theoretical calculations indicated that CeCO is an end-on-bonded carbonyl with a quintet ground state, whereas Ce_2CO is a rare dinuclear lanthanide carbonyl complex with CO serving as an asymmetrically bridged side-on ligand. The CCeO molecule was theoretically characterized to have a linear structure with a singlet ground state. In addition, evidence was presented for the $CeCO^-$ anion and other cerium carbonyls with higher coordination numbers [3]. Using the same experimental method, mononuclear $Gd(CO)_x$ ($x = 1, 3$) and dinuclear $Gd_2(CO)_y$ ($y = 1, 2$) gadolinium carbonyls were produced and characterized. The $Gd(CO)_x$ complexes are CO terminal-bonded carbonyls, whereas the Gd_2CO and $Gd_2(CO)_2$ carbonyl complexes were characterized to have asymmetrically bridging and side-on-bonded CO, which are drastically activated with remarkably low C–O stretching frequencies. The cyclic *c*-$Gd_2(\mu\text{-C})(\mu\text{-O})$ and *c*-$Gd_3(\mu\text{-C})(\mu\text{-O})$ molecules in which the C–O triple bond is completely cleaved were also formed on annealing. The $Gd_2(CO)_2$ complex rearranged to the more stable *c*-$Gd_2(\mu\text{-O})(\mu\text{-CCO})$ isomer, which also has a four-membered ring structure with one CO being completely activated [4].

In a related study, laser-ablated scandium, yttrium, and lanthanum atoms were reacted with CS_2 and COS molecules in an argon matrix. Products of the type SLnCX and S–Ln(η^2-CX) (Ln = Sc, Y, La; X = S or O) were formed on sample deposition. Photolysis favored the S–Ln(η^2-CX) complex, while annealing increased the more stable SLnCX isomer [5].

2.2. Lanthanide hydrocarbyls

2.2.1. Neutral homoleptic compounds

A theoretical study of the small ScC_n, ScC_n^+, and ScC_n^- ($n = 1$–10) cyclic clusters was carried out employing the B3LYP density functional method. Predictions for several molecular properties that could help in their possible experimental characterization, such as equilibrium geometries, electronic structures, dipole moments, and vibrational frequencies, were reported. For all neutral, cationic, and anionic clusters it was found that cyclic species are more stable than their open-chain counterparts. Therefore, cyclic structures are the most interesting possible targets for an experimental search of scandium-doped carbon clusters [6].

Following the successful synthesis of solvent-free, amorphous trimethylyttrium, $[YMe_3]_n$, the fundamental reactivity of this simple homoleptic trialkyl was representatively examined. As illustrated in Scheme 1, it reacts toward trimethylgallium as a Lewis acid, toward 9-fluorenone as a carbonyl substrate, and toward tetramethyldisilazane as a Brønsted acid [7].

Agostic Ln···H–C interactions were detected in a series of homoleptic lanthanide arylthiolates containing the bulky "supermesityl" thiolate ligand SMes* (Mes* = $C_6H_2Bu_3^t$-2,4,6). The compounds $Ln(SMes^*)_3$ were prepared in very high yields by protonolysis of $Ln[N(SiMe_3)_2]_3$ with HSMes* in cyclohexane [8].

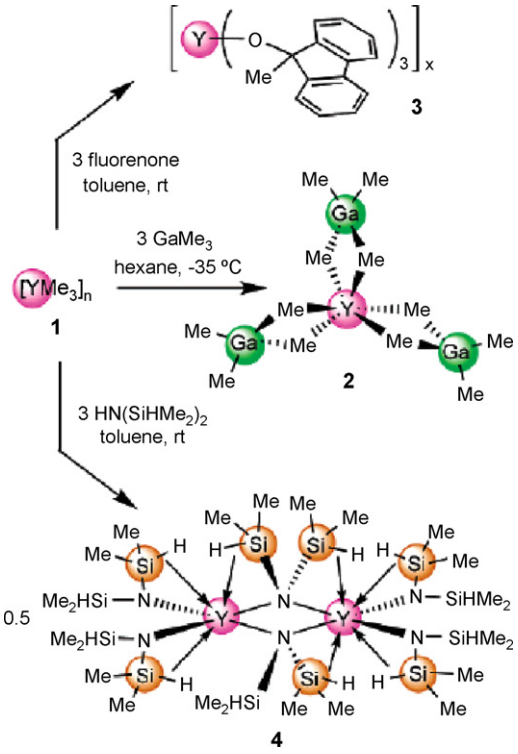

Scheme 1.

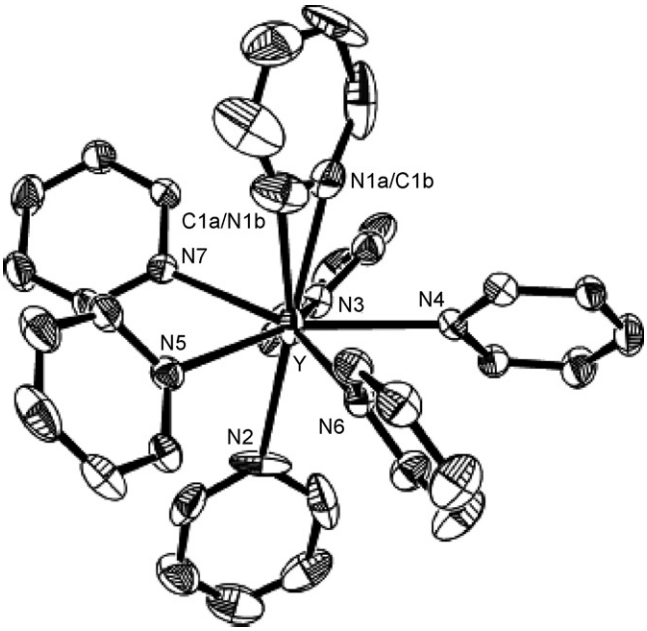

Fig. 1. Molecular structure of the cation in $[Y\{\eta^2\text{-}(C,N)\text{-}C_5H_4N\}(C_5H_5N)_6]^{2+}[BPh_4]_2^-$ [11].

2.2.2. Heteroleptic compounds

Density functional theory (DFT) and Hartree–Fock effective core potential calculations were performed to investigate the reactivity of neutral f-block atoms toward methane C–H bond activation. The first step of the methane dehydrogenation process, which corresponds to an oxidative insertion and formation of $HLnCH_3$, was studied for all lanthanides [9]. In a related paper an *ab initio* dynamic study of the reaction of $RLaCl_2$ (R = H, Me) with H_2 was published [10].

The activation of pyridine by the dicationic yttrium methyl complex $[YMe(THF)_6]^{2+}[BPh_4]_2^-$ to give the structurally characterized cationic rare-earth metal η^2-pyridyl complex $[Y\{\eta^2\text{-}(C,N)\text{-}C_5H_4N\}(C_5H_5N)_6]^{2+}[BPh_4]_2^-$ (Scheme 2) was reported. According to the X-ray structural analysis (Fig. 1), the η^2-pyridyl complex adopts a pentagonal bipyramidal coordination geometry with the η^2-pyridyl ligand in the axial position. Kinetic data demonstrated that this complex forms *via* the substitution product $[YMe(C_5H_5N)_6]^{2+}[BPh_4]_2^-$ [11].

A series of heteroleptic complexes of lanthanum(III) and neodymium(III) with oxygen- or nitrogen-functionalized tris(triorganosilyl)methyl ligands were synthesized through metathetical reactions between either $LaI_3(THF)_3$ or $NdI_3(THF)_{3.5}$

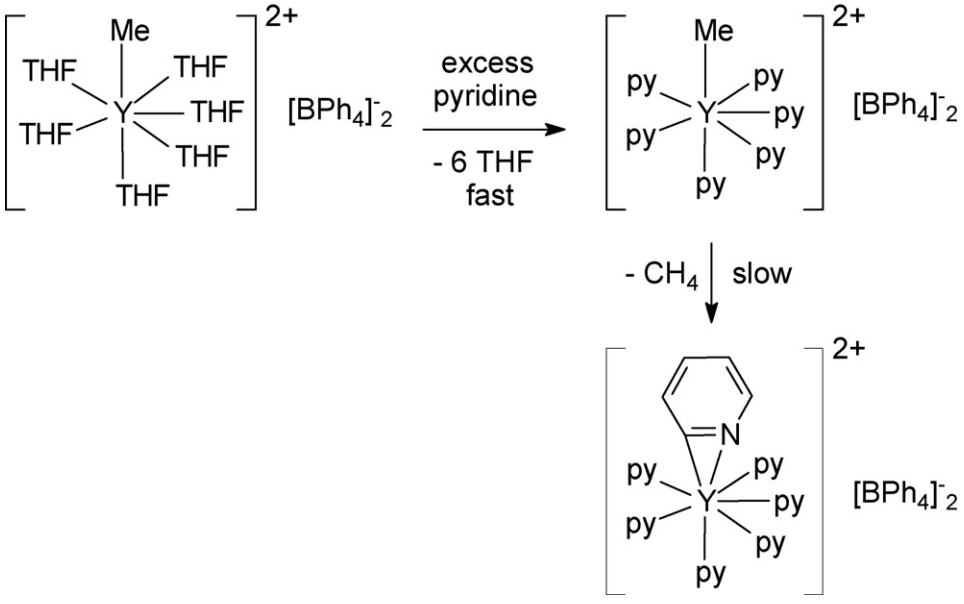

Scheme 2.

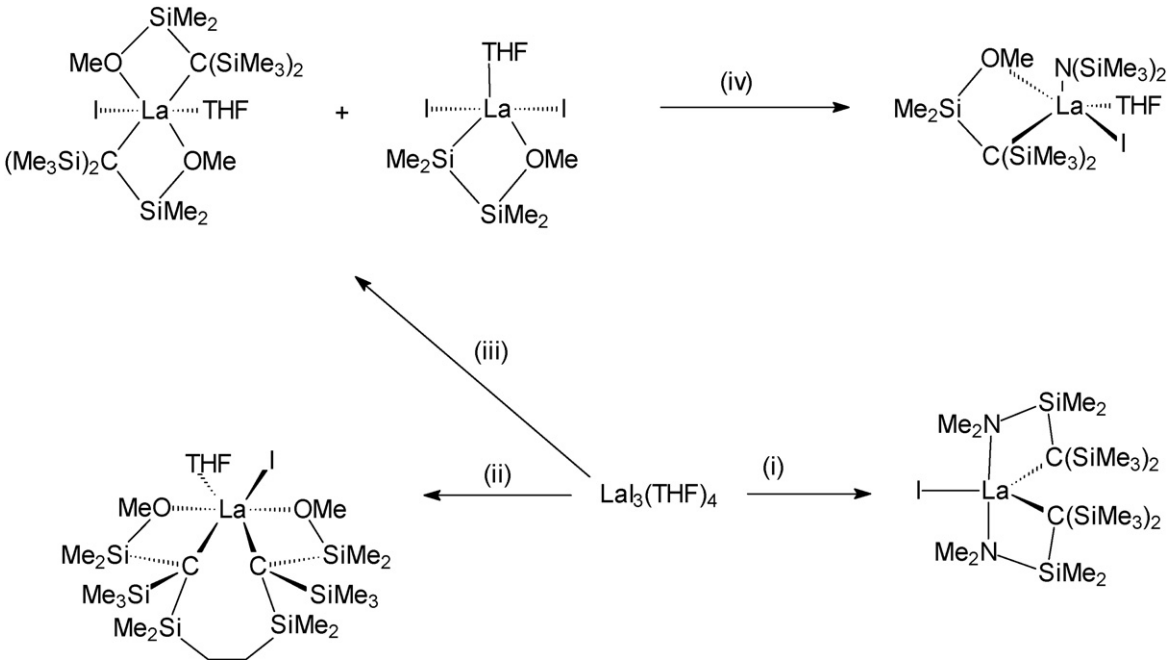

Scheme 3. Reagents: (i) 2K[$(Me_3Si)_2${$Me_2(Me_2N)Si$}C], THF; (ii) $K_2[(Me_3Si)(Me_2MeOSi)C(SiMe_2CH_2)]_2$, THF; (iii) 2K[$(Me_3Si)_2${$Me_2(MeO)Si$}C], THF; (iv) $KN(SiMe_3)_2$, THF.

and the respective functionalized potassium alkyl reagents. The outcome of these preparations was found to be highly dependent upon the nature of the ligands, the metal center, and the precise reaction conditions. Scheme 3 illustrates the different products obtained with lanthanum [12].

Simple tribenzyl complexes of lanthanum, $La(CH_2C_6H_4R\text{-}p)_3(THF)_3$ (R = H, Me), were prepared in a remarkably straightforward fashion from $LaBr_3(THF)_4$ and potassium benzyl reagents according to Scheme 4 [13].

Single crystal X-ray diffraction studies on both La derivatives revealed a *fac*-arrangement of the three THF ligands and η^2-coordination of the benzyl groups. Fig. 2 depicts the structure of the parent tribenzyl derivative [13].

The tribenzyl complexes were shown to be convenient precursors to other organolanthanum complexes. Reaction of $La(CH_2Ph)_3(THF)_3$ with the amidine ArN=CPhNHAr (Ar = $C_6H_3{}^iPr_2$-2,6) afforded the corresponding mono(amidinato) dibenzyl derivative (Scheme 5) in 70% isolated yield. Treatment of the tri-*p*-tolyl derivative with 1 equiv. of *p*-$LiCH_2C_6H_4Me$ generated the ionic compound $[Li(THF)_4][La(CH_2C_6H_4Me\text{-}p)_4]$ which was isolated as red-orange crystals in 52% yield (Scheme 5). Both products were structurally characterized by X-ray diffraction. Fig. 3 depicts the molecular structure of the amidinate derivative. In this complex one of the two remaining benzyl groups is again η^2-coordinated, while the second approaches an η^3-like bonding. In the anion in $[Li(THF)_4][La(CH_2C_6H_4Me\text{-}p)_4]$ all four benzyl groups are η^2-coordinated [13].

Reactions of the two lanthanum tribenzyl complexes with 1 or 2 equiv. of $[HNMe_2Ph][B(C_6H_5)_4]$ as illustrated in Scheme 6 produced the corresponding mono- and dicationic benzyl species, which were structurally characterized [13].

Heteroleptic perfluorophenyl complexes of the type $Ln(OAr^{OMe})_2(C_6F_5)$ were postulated as intermediates in redox transmetallation/ligand exchange reactions of lanthanide metals

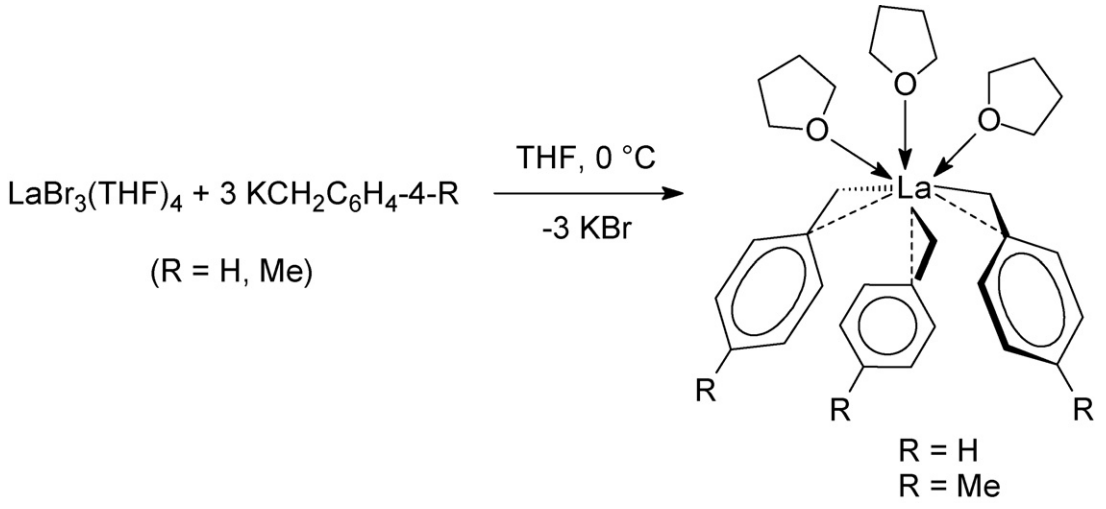

Scheme 4.

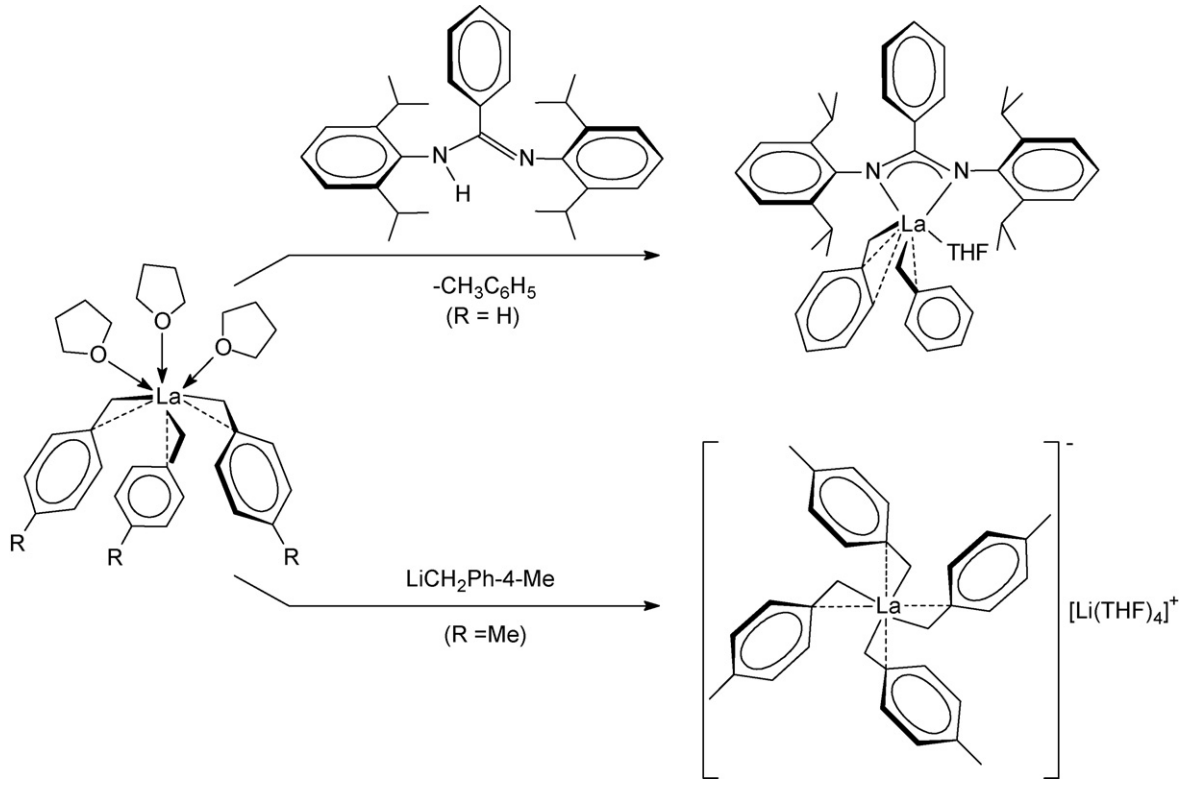

Scheme 5.

(Ln), $Hg(C_6F_5)_2$, and $HOAr^{OMe}$ ($Ar^{OMe} = C_6H_2Bu^t$-2,6-OMe-4) in THF. However, these are unstable and decompose under formation of mixed fluoro aryloxide species as illustrated in Scheme 7 [14].

An interesting series of neutral and cationic heteroleptic rare-earth metal silanolate complexes have been prepared starting with protonolysis of the appropriate tris(alkyl) complexes $Ln(CH_2SiMe_3)_3(THF)_n$ (Ln = Y, Tb, Lu; $n = 2$, 3) with tri(*tert*-butoxy)silanol in pentane. Several cationic monoalkyl species were also prepared by the reactions illustrated in Scheme 8 [15].

The initial products, $[Ln\{\mu,\eta^2\text{-}OSi(O^tBu)_3\}(CH_2SiMe_3)_2]_2$ (Ln = Y, Tb, Lu), are dimers which can be described by the two resonance forms A and B shown in Scheme 9. The molecular structure of the yttrium derivative is shown in Fig. 4 [15].

Somewhat related to these silanolates are novel diamidosilylether complexes, which were reported for yttrium(III). The

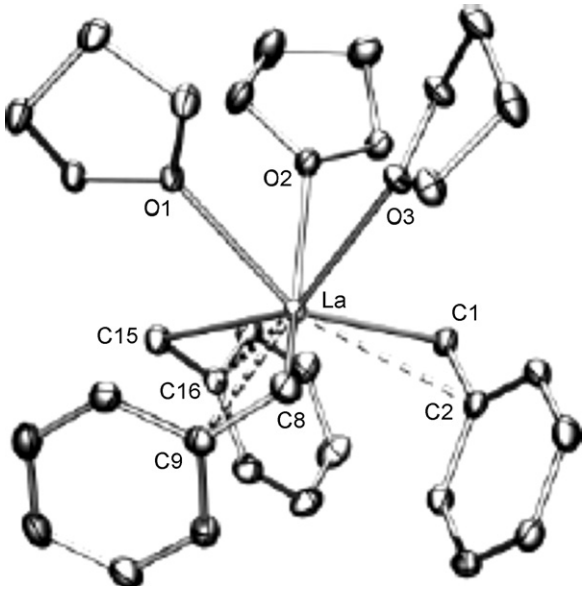

Fig. 2. Molecular structure of $La(CH_2Ph)_3(THF)_3$ [13].

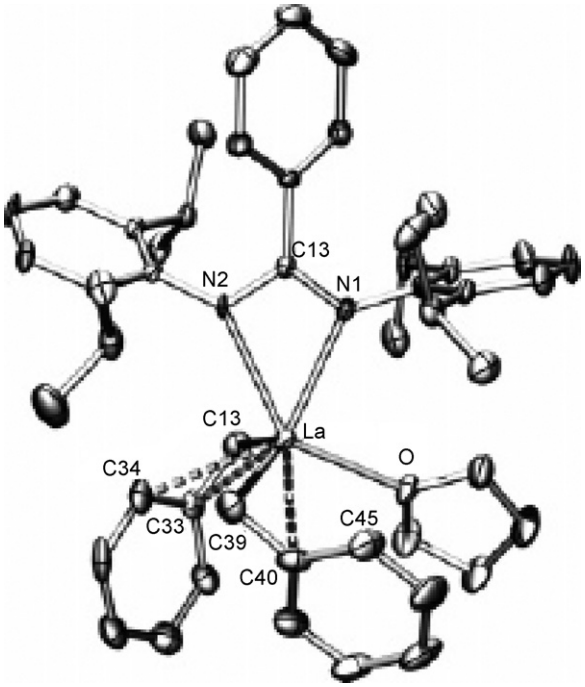

Fig. 3. Molecular structure of $[PhC(NAr)_2]La(CH_2Ph)_2(THF)$ ($Ar = C_6H_3{}^iPr_2$-2,6) [13].

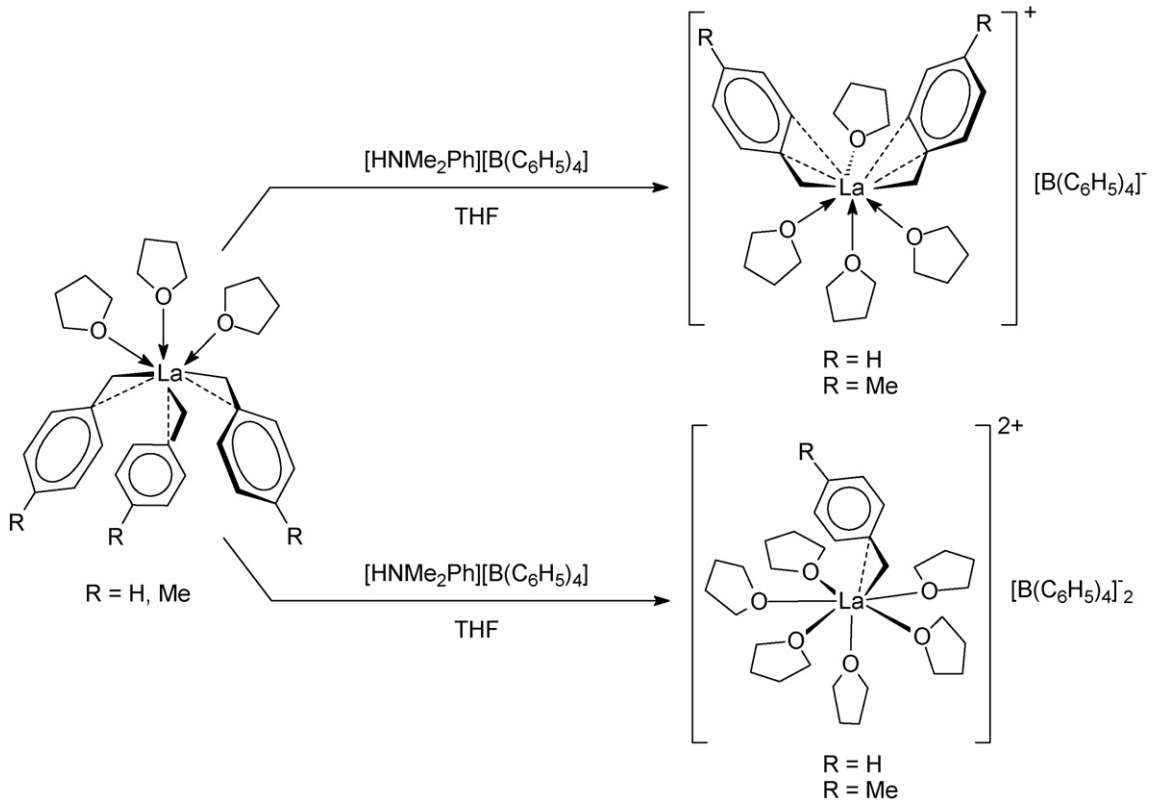

Scheme 6.

synthetic routes leading to these compounds are summarized in Scheme 10. True organometallic species among the series are the bis(trimethylsilyl)methyl and the mono(cyclopentadienyl) derivatives [16].

In a similar synthetic approach a novel N_3 donor heteroscorpionate ligand has been developed and successfully employed in the synthesis of scandium and yttrium alkyl complexes. Scheme 11 illustrates the preparative routes leading to neutral dialkyls as well as a cationic monoalkyl complex. The neutral scandium dialkyl was structurally characterized by X-ray diffraction (Fig. 5). The new N_3 donor heteroscorpionate ligand adopts the expected *fac* coordination mode and the overall geometry at scandium is square-base pyramidal [17].

The readily available neutral 6-amino-6-methyl-1,4-diazepine group has been introduced as an ancillary ligand framework for neutral and cationic scandium and yttrium alkyls. Treatment of the trialkyl complexes $M(CH_2SiMe_3)_3(THF)_3$ (M = Sc, Y) with the free permethylated ligand according to Scheme 12 afforded the complexes (6-amino-6-methyl-1,4-diazepine)$M(CH_2SiMe_3)_3$ in high isolated yields (Sc: 94%; Y: 95%). A single-crystal X-ray analysis of the Sc complex revealed an approximately octahedral coordination geometry around scandium (Fig. 6) [18].

The neutral trialkyl complexes could be converted in THF solution to the dialkyl cations [(6-amino-6-methyl-1,4-diazepine) $M(CH_2SiMe_3)_2]^+$ (M = Sc, Y) by reaction with $[PhMe_2NH][BAr_4]$ (Ar = Ph, C_6F_5) (Scheme 12) [18]. Two new ligands were pre-

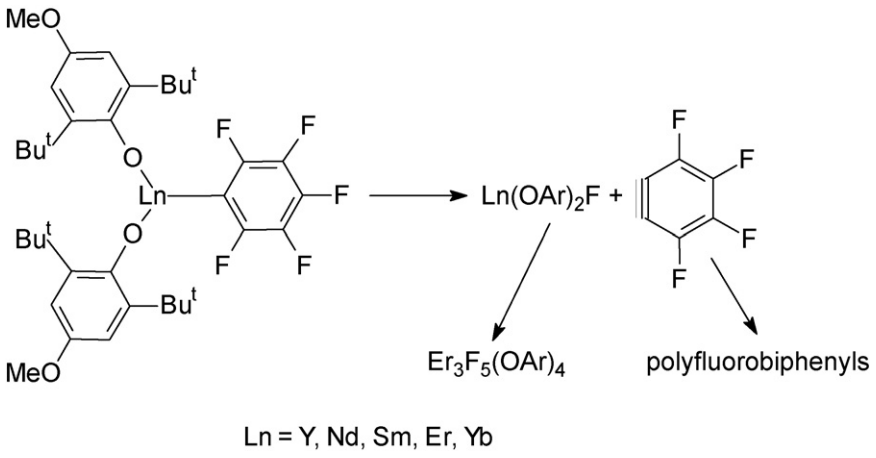

Scheme 7.

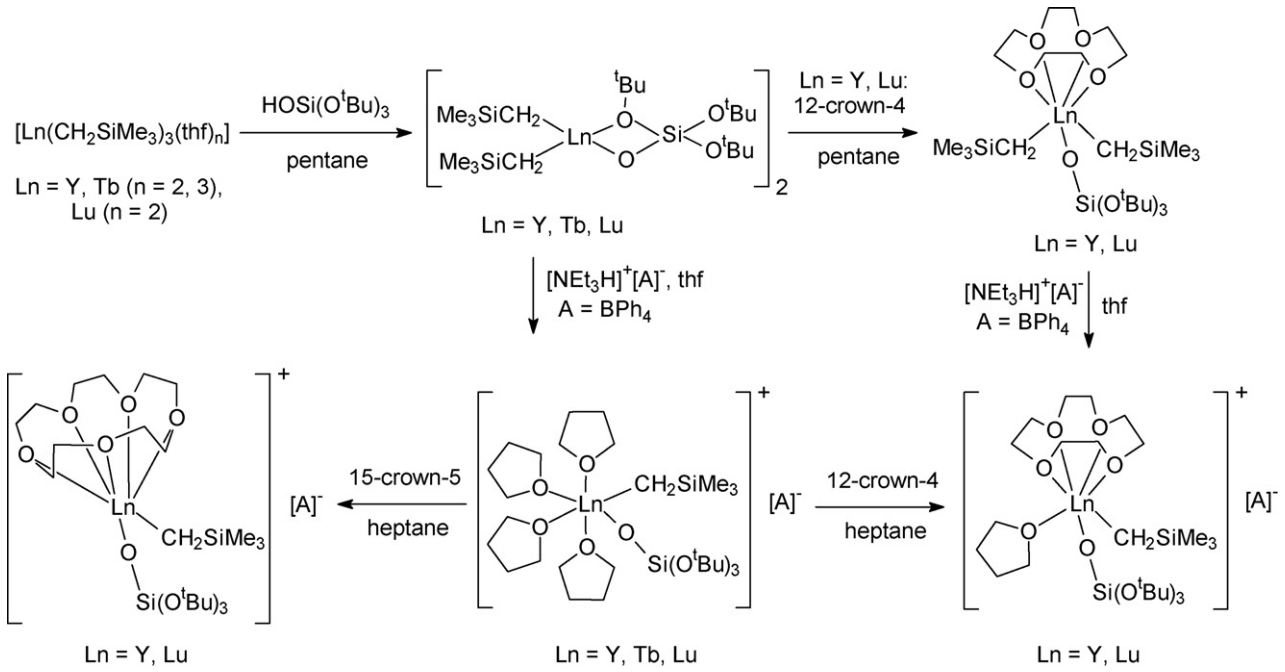

Scheme 8.

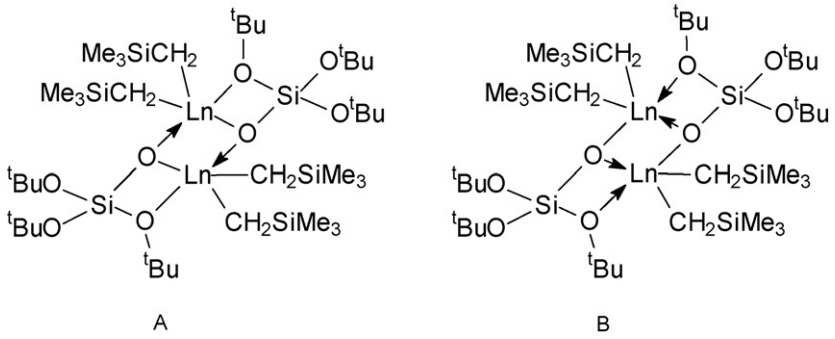

Scheme 9.

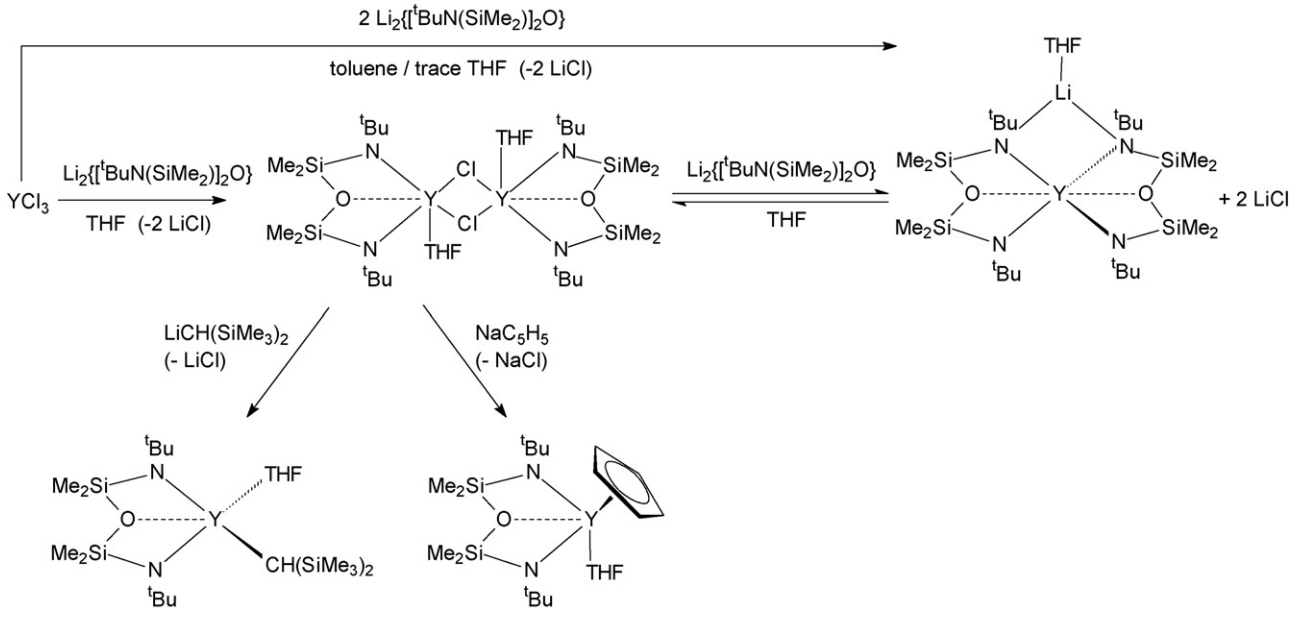

Scheme 10.

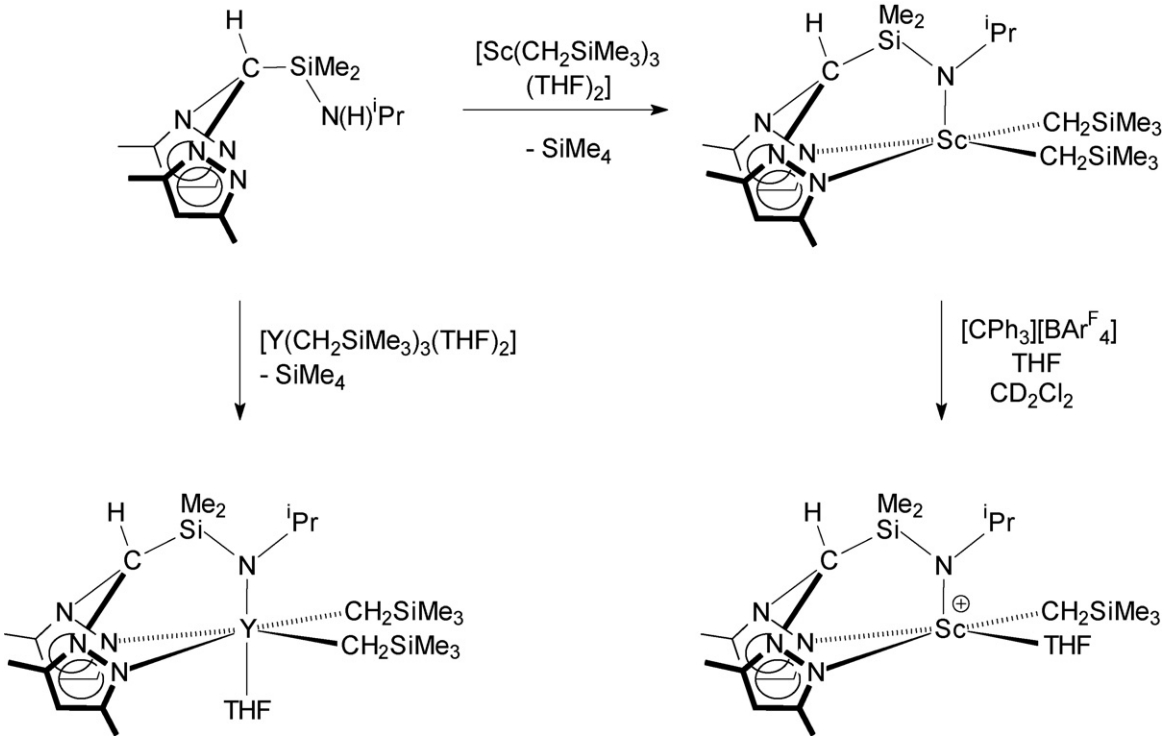

Scheme 11.

pared by the acid-catalyzed condensation of the 1,4-dimethylated 6-amino-6-methyl-1,4-diazepine with benzaldehyde and with *o*-hydroxybenzaldehyde and employed in the subsequent preparation of the corresponding yttrium dialkyl complexes as illustrated in Scheme 13 [18].

In closely related work, yttrium and lanthanum dialkyl complexes with the isopropyl-substituted triazacyclononane-amide monoanionic ligands $[^{i}Pr_2TACN\text{-}(B)\text{-}NBu^{t}]^{-}$ (B = $(CH_2)_2$ (=**L1**), $SiMe_2$ (=**L2**)) were reported. The ligand synthesis as illustrated in Scheme 14 starts from the known 1,4-diisopropyl-1,4,7-triazacyclononane in both cases [19].

For yttrium, the dialkyl complexes were obtained by reaction of $Y(CH_2SiMe_3)_2(THF)_2$ with H**L**, whereas for La *in situ* peralkylation of $LaBr_3(THF)_4$ preceded reaction with H**L** (Scheme 15). Cationic monoalkyl complexes were subsequently generated upon treatment of the dialkyls with $[PhNMe_2H][BAr_4]$ (Ar = Ph, C_6F_5) [19].

Bis(guanidinato)lanthanide alkyls containing the $-CH_2SiMe_3$ ligand were prepared according to Scheme 16 using either the dimeric chloro species (Ln = Nd, Sm) or the closely related "ate" complexes (Ln = Y, Gd, Yb) as starting materials [20].

In some cases closely related bis(guanidinato)lanthanide alkyl derivatives were also obtained in an unexpected manner from

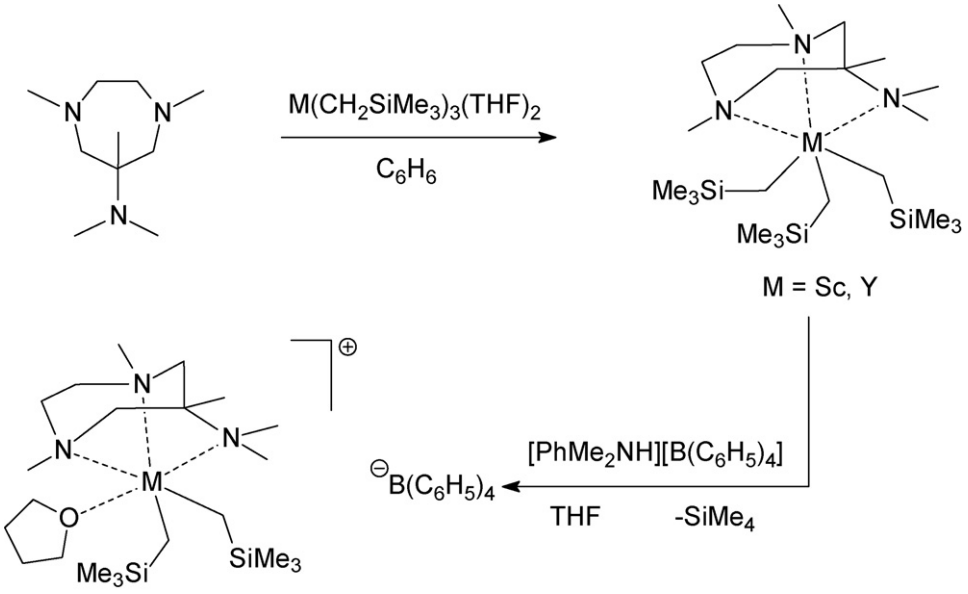

Scheme 12.

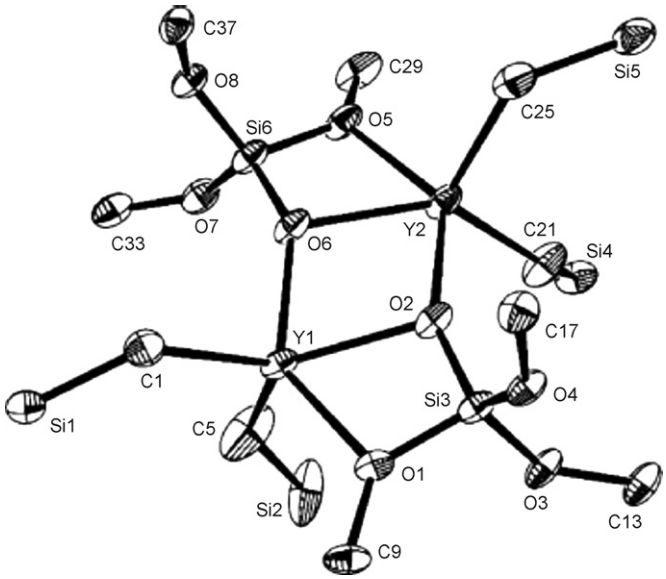

Fig. 4. Molecular structure of $[Y\{\mu,\eta^2\text{-}OSi(O^tBu)_3\}(CH_2SiMe_3)_2]_2$ (hydrogen atoms and methyl groups omitted for clarity) [15].

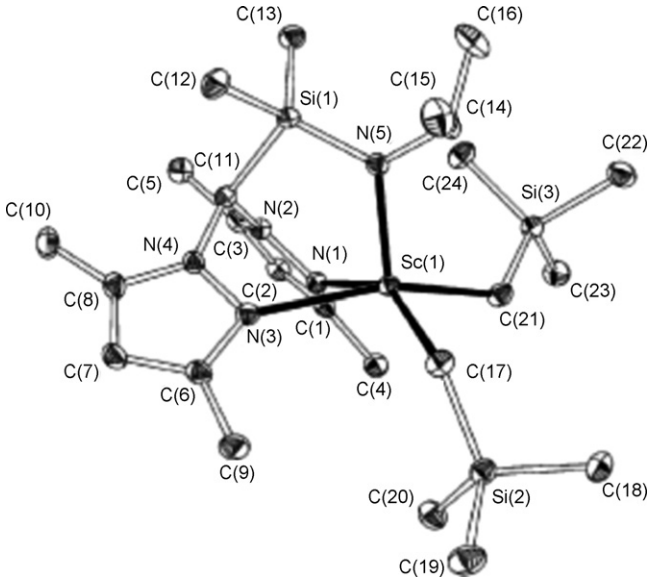

Fig. 5. Molecular structure of $[(Me_2pz)_2CHSiMe_2N^iPr]Sc(CH_2SiMe_3)_2$ [17].

mono(guanidinato) precursors [21]. As shown in Scheme 17, reaction of a dimeric chloro complex with 4 equiv. of ^{t}BuLi unexpectedly afforded the corresponding bis(guanidinato) monoalkyl complex in 42% yield. Apparently in the reaction with ^{t}BuLi redistribution of the guanidinate ligands occurs, and all attempts to isolate other organoyttrium complexes from the reaction mixture failed [21].

The guanidinate ligand redistribution was also observed in the reaction of a mono(guanidinato) dichloro yttrium precursor with two molar equivalents of $LiCH_2SiMe_3$ in hexane at 0 °C (Scheme 18). This reaction afforded the *ate*-complex $[(Me_3Si)_2NC(NCy)_2]_2Y(\mu\text{-}CH_2SiMe_3)_2Li$ in 34% yield. Fig. 7 displays the molecular structure of this compound as determined by X-ray diffraction. The most interesting feature of this compound is the extremely low coordination number of the lithium ion, which is coordinated only by two methylene carbon atoms (Fig. 7) [21].

Alkylation of the dimeric chloro precursor with 4 equiv. of $LiCH_2SiMe_3$ (Scheme 19) was performed in hexane at 0 °C and afforded the mono(guanidinate) dialkyl derivative $[(Me_3Si)_2NC(NCy)_2]Y(CH_2SiMe_3)_2(THF)_2$ as a colorless crystalline solid in 96% yield [21].

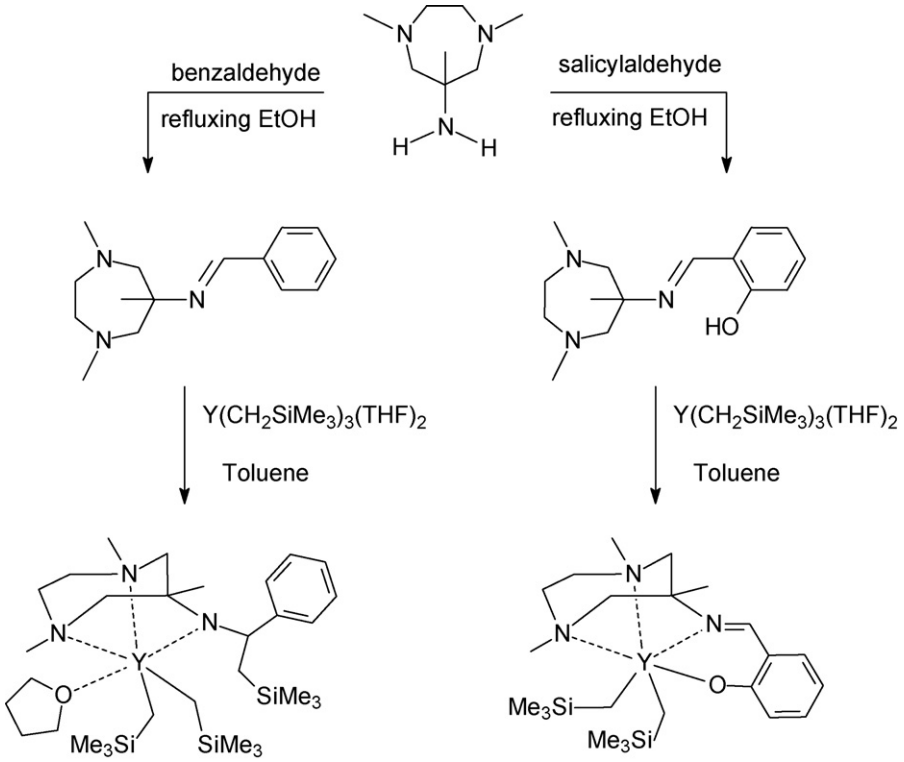

Scheme 13.

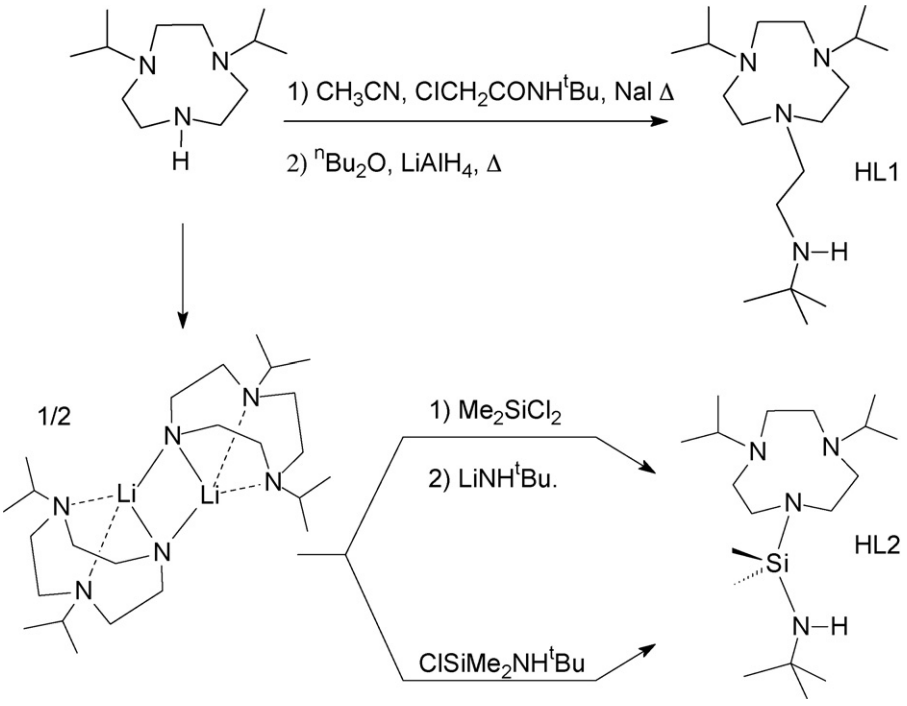

Scheme 14.

The colorless, air- and moisture-sensitive methyl-bridged "ate" complex $[(Me_3Si)_2NC(NCy)_2]Y[(\mu\text{-}Me)_2Li(TMEDA)]_2$ was prepared in a similar manner by reaction of the dimeric chloro complex with eight molar equivalents of MeLi in the presence of TMEDA at 20 °C (Scheme 20) [21].

The bis(guanidinato) alkyl complexes in turn served as starting materials for a new family of base-free hydrido complexes of rare-earth metals supported by guanidinate ligands (Scheme 21). Single-crystal X-ray and solution NMR studies revealed that these complexes are dimeric both in the solid state and in $[D_6]$benzene. The dimeric hydrido complexes can adopt eclipsed (Nd, Sm, Gd) or staggered (Y, Yb, Lu) conformations depending on the ionic radius of the metal [20].

Closely related chloro, alkyl, and aryl complexes supported by the bulky tetrasubstituted guanidinate ligand $[(Me_3Si)_2NC(NCy)_2]^-$ were also reported. The synthesis of the chloro precursors is summarized in Scheme 22. It was found that the nature of the products depended on the use of either the lithium or the sodium salt of the guanidinate anion. In the case of the Li salt, "ate" complexes were obtained, while in the case of the Na salt the products were simple THF adducts without incorporated alkali metal chloride [56].

Subsequent treatment of the yttrium precursor with RLi (R = Me, Bu^t, Ph) afforded the hydrocarbyl complexes $[(Me_3Si)_2NC(NCy)_2]_2Y(\mu\text{-}Me)_2Li(TMEDA)$, $[(Me_3Si)_2NC(NCy)_2]_2YBu^t$, and $[(Me_3Si)_2NC(NCy)_2]_2YPh(THF)$, respectively. Agostic interactions between the yttrium atom and the *tert*-butyl group in $[(Me_3Si)_2NC(NCy)_2]_2YBu^t$ in the solid state as well as in solution were substantiated by ^{13}C NMR spectroscopy and X-ray analysis (Fig. 8) [22].

Selected homoleptic metal β-diketiminates, including several ytterbium species, were studied by cyclic voltammetry (CV) as well as DFT calculations [23]. Attempts were made to synthesize β-diketiminato scandium complexes containing terminal imido ligands by deprotonation of the corresponding cationic amido precursors. Treatment of the β-diketiminato-supported scandium amido methyl derivatives $[ArNC(^tBu)CHC(^tBu)NAr]Sc(Me)(NHR)$ ($Ar = C_6H_3{}^iPr_2$-2,6; $R = {}^tBu$, $C_6H_3{}^iPr_2$-2,6) with 1 equiv. of $B(C_6F_5)_3$

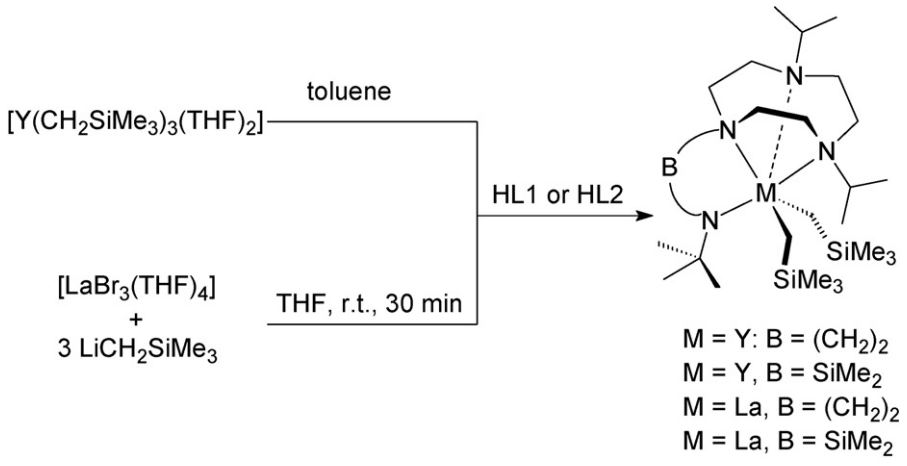

Scheme 15.

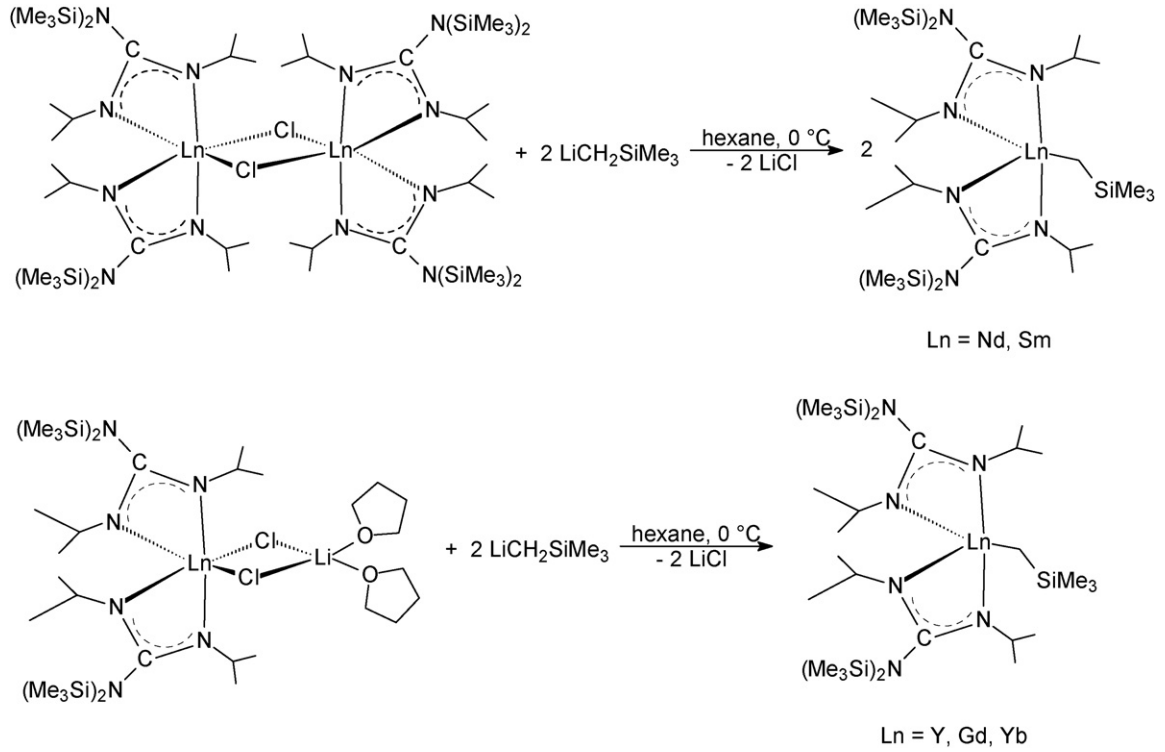

Scheme 16.

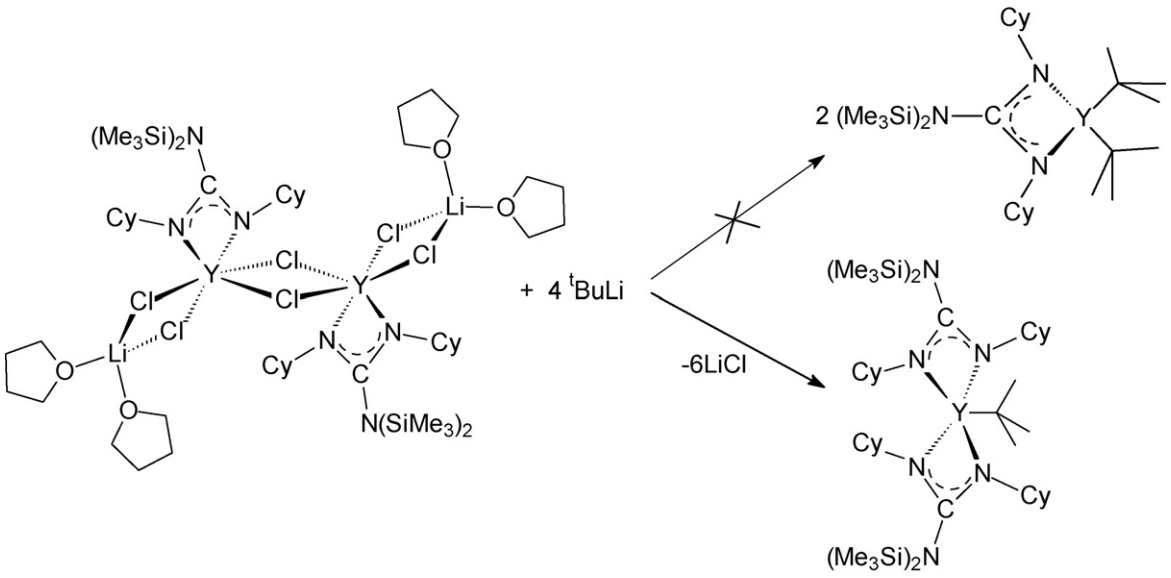

Scheme 17.

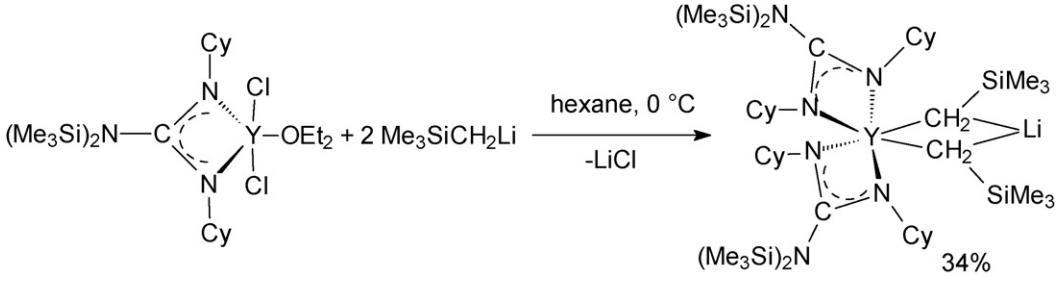

Scheme 18.

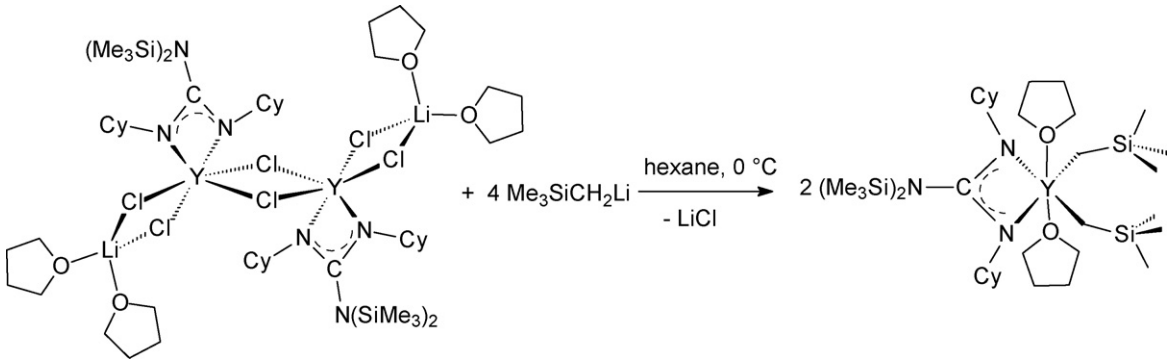

Scheme 19.

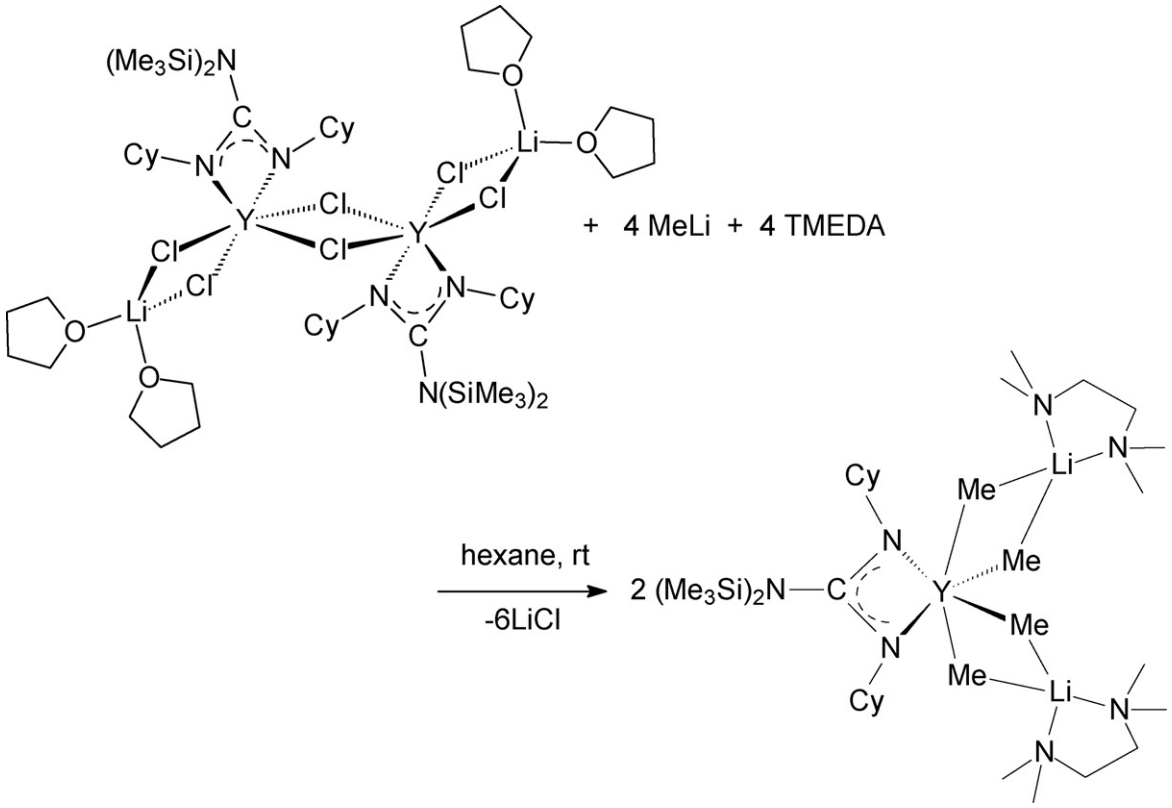

Scheme 20.

resulted in the formation of the scandium amido ion pairs depicted in Scheme 23 in good yields. A single-crystal X-ray analysis of the compound with R = ^{t}Bu was carried out, and two crystallographically independent molecules were observed in which one contains an N–H···F–C hydrogen bond while the other does not [24].

Several attempts to deprotonate the amido ligand to yield a neutral scandium imido species containing an Sc=NR moiety resulted

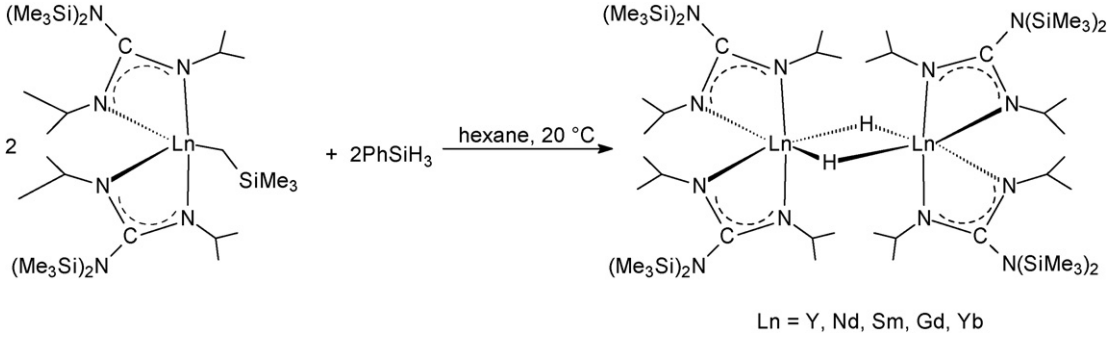

Scheme 21.

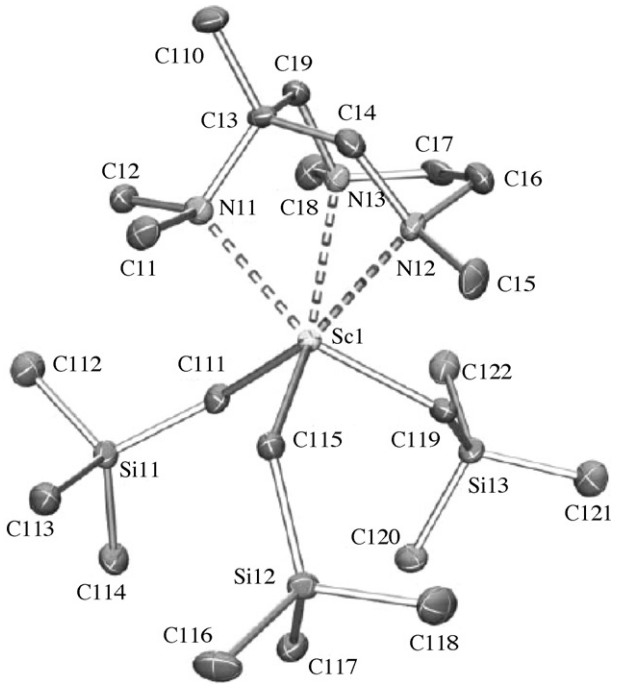

Fig. 6. Molecular structure of (6-amino-6-methyl-1,4-diazepine)Sc(CH_2SiMe_3)$_3$ [18].

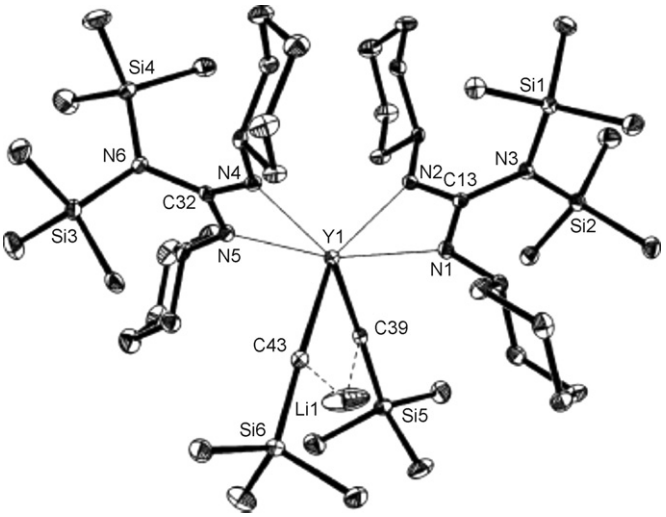

Fig. 7. Molecular structure of [$(Me_3Si)_2NC(NCy)_2$]$_2$Y(μ-CH_2SiMe_3)$_2$Li [21].

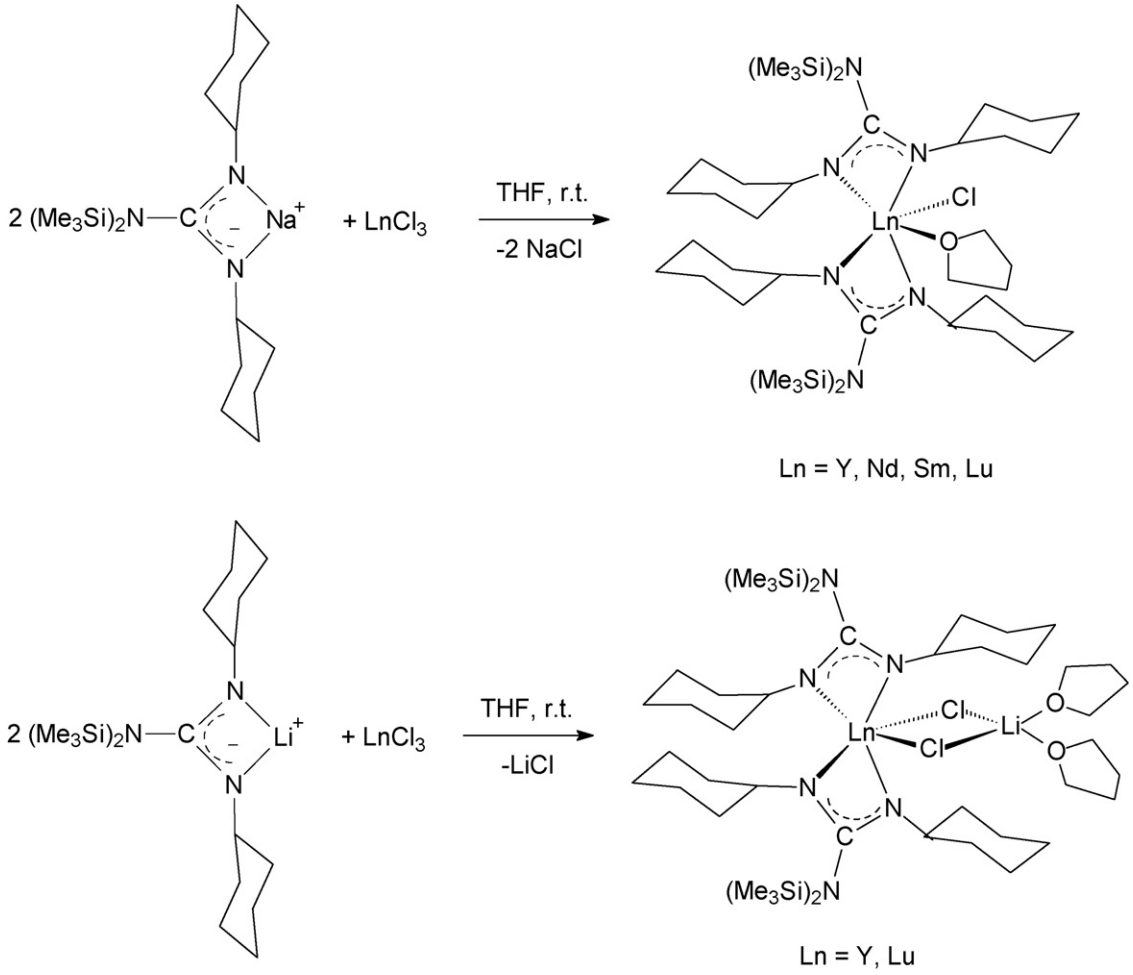

Scheme 22.

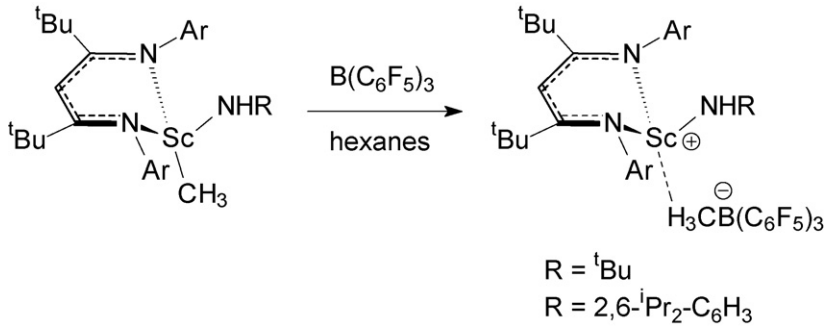

Scheme 23.

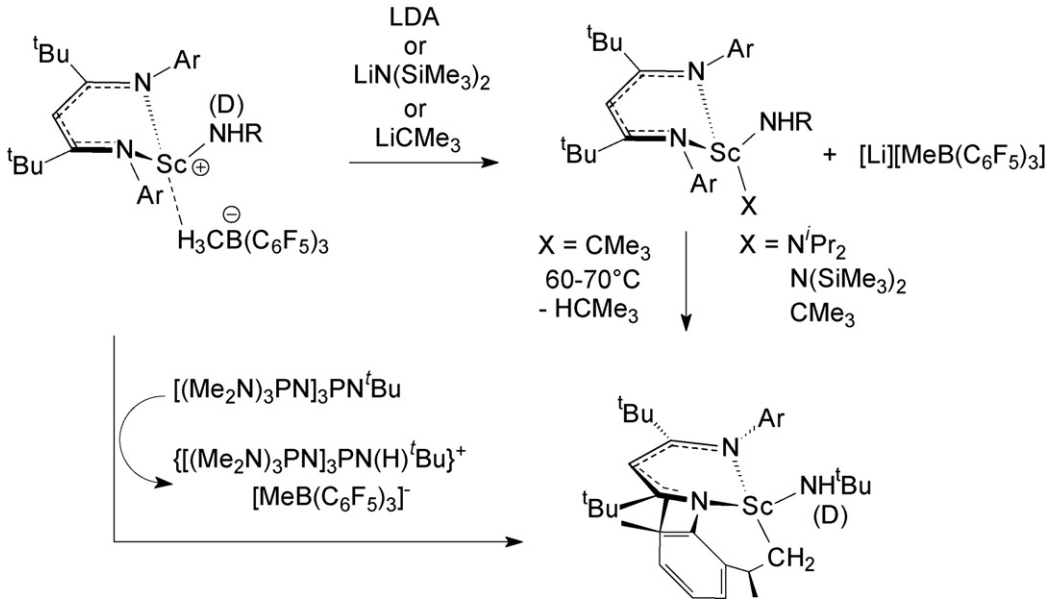

Scheme 24.

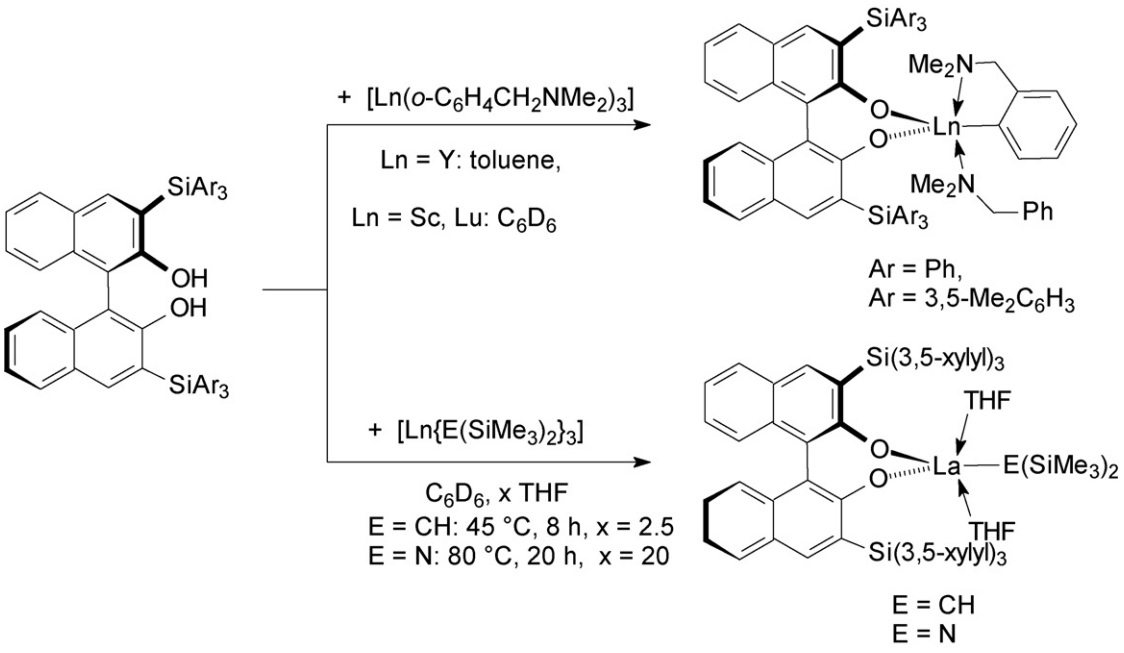

Scheme 25.

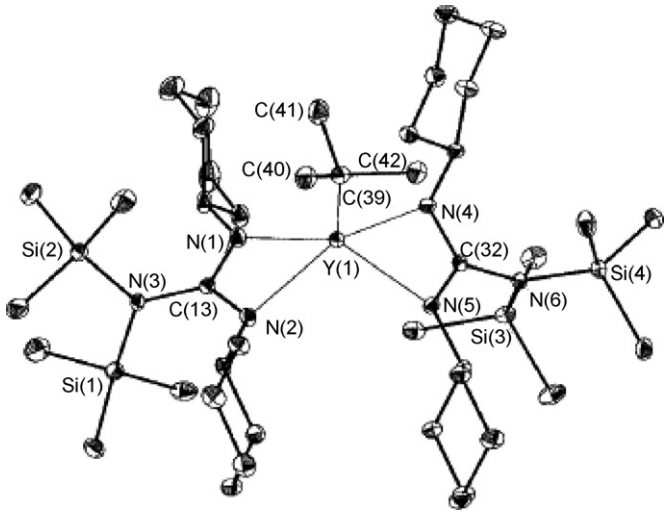

Fig. 8. Molecular structure of $[(Me_3Si)_2NC(NCy)_2]_2YBu^t$ [22].

in either attack of the base at the metal center or deprotonation of the β-diketiminato ligand (Scheme 24). For example, treatment of [ArNC(^{t}Bu)CHC(^{t}Bu)NAr]Sc(NH^{t}Bu)(μ-Me)B(C_6F_5)$_3$ with *tert*-butyllithium gave [ArNC(^{t}Bu)CHC(^{t}Bu)NAr]Sc(^{t}Bu)(NH^{t}Bu), while treatment with the phosphazene base $[(Me_2N)_3P{=}N]_3P{=}N^tBu$ gave a previously reported metalated complex (Scheme 24). Deuterium labelling experiments indicated that the metalated product is produced *via* direct deprotonation of the aryl isopropyl group and not *via* a transient scandium imido derivative [13].

Several chiral 3,3′-bis(triarylsilyl)-substituted binaphtholate rare-earth metal complexes were prepared according to Scheme 25 by facile protonation reaction of the free binaphtholes with suitable aryl, alkyl, or amido lanthanide precursors [25].

The small class of well characterized lanthanide silyl complexes has been expanded in 2006 by a number of interesting members by exploring the use of "hypersilyl" potassium, $KSi(SiMe_3)_3$, as a silylation or deprotonation agent for some lanthanide bis(trimethylsilyl)amides. Thus, a reaction with $Yb[N(SiMe_3)_2]_2$ afforded the addition product $K[Yb\{Si(SiMe_3)_3\}\{N(SiMe_3)_2\}]$ in high yield which contains a three-coordinate ytterbium atom (Scheme 26) [26].

The deprotonation of *N*-heterocyclic carbenes (=NHC) to afford heterobimetallic organolanthanide complexes was investigated. As shown in Scheme 27, treatment of an amido-tethered *N*-heterocyclic carbene complex of yttrium with potassium naphthalenide resulted in regiospecific deprotonation at the NHC backbone to generate an Y(III)–K heterobimetallic complex. This compound reacts quantitatively with Me_3SiCl to eliminate KCl to give the corresponding silylated yttrium carbene complex (Scheme 27) [27].

Treatment of the corresponding samarium NHC complex with potassium naphthalenide resulted in formation of an analogous heterobimetallic product (Scheme 28), which was isolated in the form of yellow crystals. Similar reaction with KC_8 did not afford a samarium(II) complex but instead a bis(methoxide)-bridged species, presumably a product of metal-mediated radical C–O activation and cleavage of the DME solvent [27].

The synthesis and molecular structures of mono- and trisphenoxo-tethered *N*-heterocyclic carbene (=NHC) yttrium complexes was also reported. Reaction of $LiY(N^iPr_2)_4$ with H_2LCl (L = *O*-4,6-di-^{t}BuC_6H_2-2-CH_2[C{N(CHCH)N^{i}Pr}]) and ^{n}BuLi in the molar ratio of 1:3:2 at −78 °C afforded an yttrium complex supported by three anionic NHC ligands, L_3Y (Scheme 29). The reaction temperature was found to have a great effect on the reaction outcome. The same reaction at room temperature yielded a monoanionic NHC yttrium complex co-supported by a bridged bis(phenoxo) group, LY[(*O*-4,6-di-

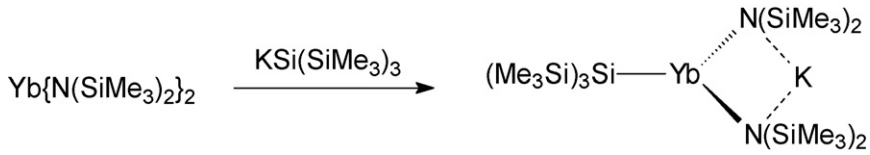

Scheme 26.

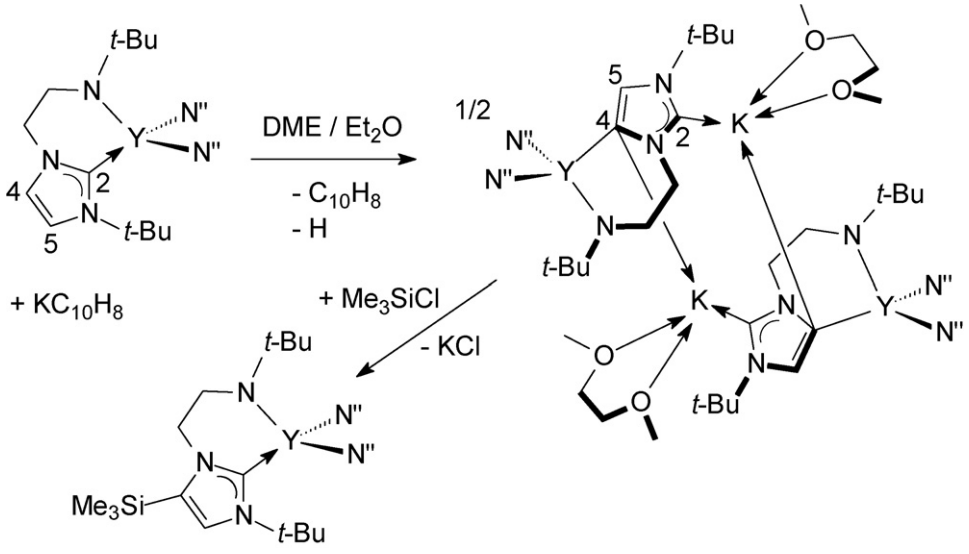

Scheme 27.

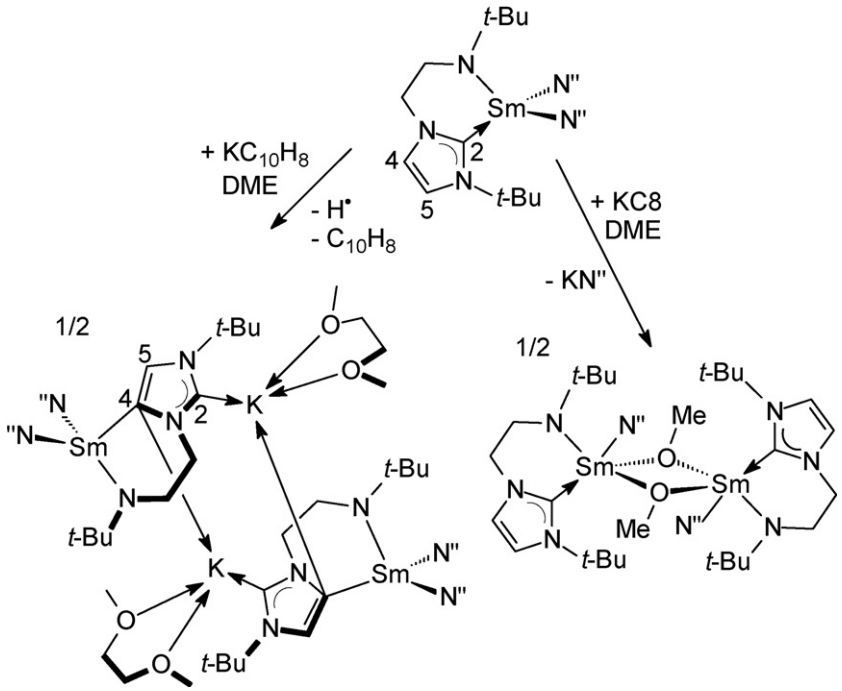

Scheme 28.

$^{t}BuC_6H_2)_2(CH_2)][^{i}PrIm]_2$ ($^{i}PrIm$ = *N*-isopropylimidazole) formed from the cleavage of NHC [28].

Analogous ytterbium(III) complexes containing the aryloxo-functionalized *N*-heterocyclic carbene ligands were obtained according to Scheme 30 by the same transamination route using the anionic homoleptic amido ytterbium complex $LiYb(N^{i}Pr)_4$ as starting material. The products were structurally characterized by X-ray diffraction methods. Fig. 9 displays the molecular structure of the complex with R = Me [29].

The first thulium alkylidene complexes were synthesized using a stable dianionic precursor as illustrated in Scheme 31. The resulting iodide-bridged dimer is analogous to the previously reported Sm congener [30].

When 1/2 equiv. of the thulium alkylidene complex was treated with 1 equiv. of benzophenone (Scheme 32), immediate and complete transformation into the expected alkene was observed. This product could not be obtained by the reaction of the dianion of the ligand itself with benzophenone. This result clearly established the carbenic nature of the Ln=C bond and its nucleophilic character, where Ln is a late-lanthanide element such as Tm [30].

Addition of 2 equiv. of the dianionic precursor to $TmI_3(THF)_{3.5}$ led to the formation of the first homoleptic thulium bis(alkylidene) complex (Scheme 33), which is again an analogue of the previously reported samarium complex. Single crystals of the product exhibited a phase transition near 177 K, which allowed the determination of two significantly different structures at 150 and 230 K. In the low-

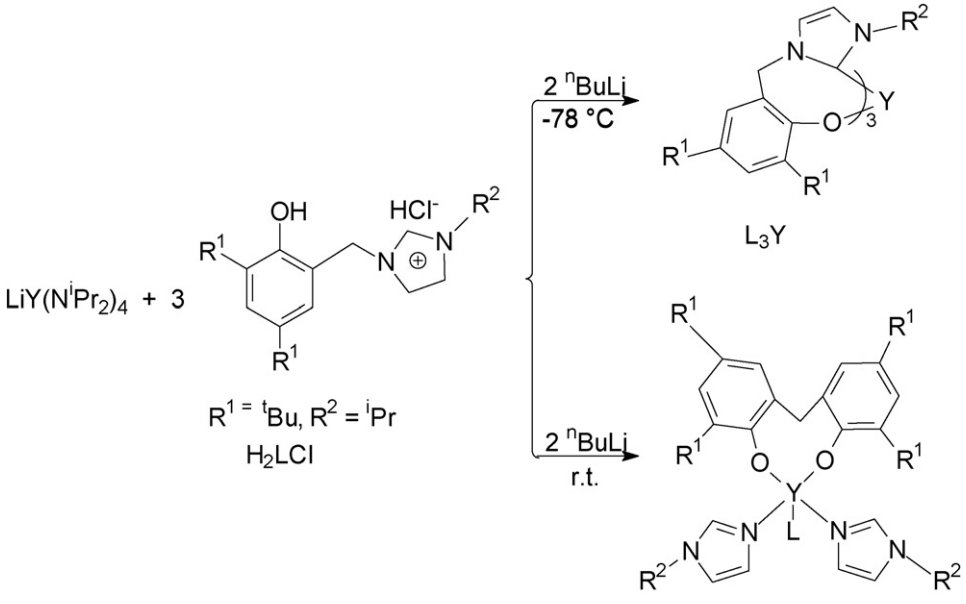

Scheme 29.

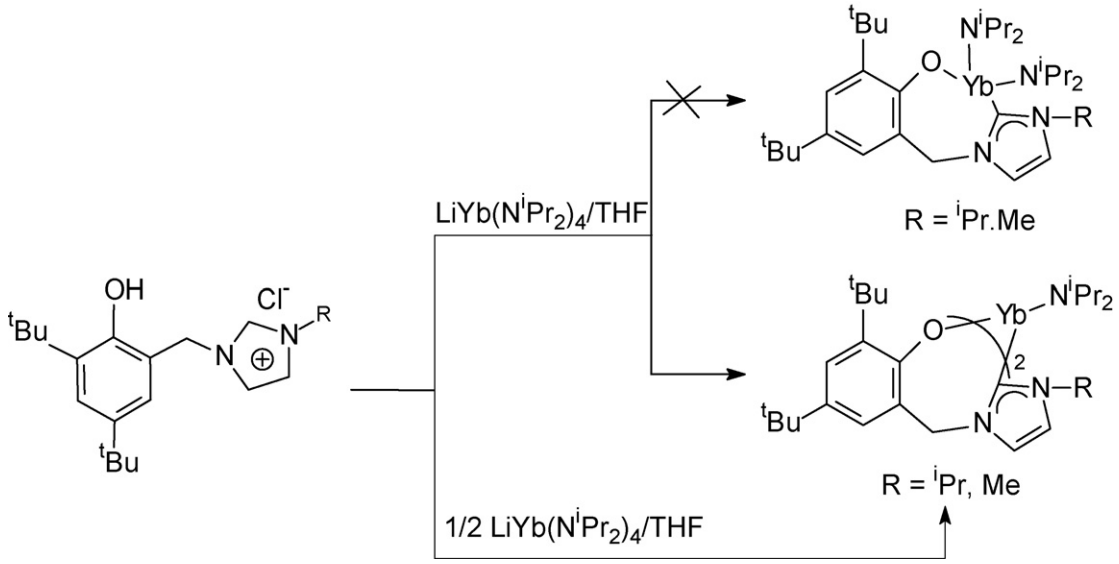

Scheme 30.

temperature structure the two carbenic moieties are geometrically different, whereas they are identical in the structure measured at 230 K [30].

The synthesis and molecular structures of the first phosphoranylidene complexes of rare-earth metals were reported. Metalation of the donor-functionalized ylide ligand $Ph_3P{=}CH(C_6H_4OMe\text{-}o)$ with homoleptic alkyl and aryl complexes of yttrium and lutetium afforded unprecedented phosphoranylidene complexes featuring a central μ-M_2C_2 core (Scheme 34) [31].

Deprotonation on the periphery occurred during the reaction of $KSi(SiMe_3)_3$ with the tris(amides) $Ln[N(SiMe_3)_2]_3$ (Ln = Y, Yb), and compounds of the type $K[CH_2Si(Me)_2N(SiMe_3)Ln\{N(SiMe_3)_2\}]$ were isolated (Scheme 35). Crystallization of the yttrium derivative from a mixture of benzene and heptane afforded the bis(benzene) solvate $[(C_6H_6)_2K][CH_2Si(Me)_2N(SiMe_3)Y\{N(SiMe_3)_2\}]$ (Fig. 10) [26].

The reaction between the strong bases ^{n}BuLi/tetramethylethylenediamine (=TMEDA) or ^{t}BuLi with $Y[N(SiMe_3)_2]_3$ or $Yb[N(SiMe_3)_2]_3$ yielded the deprotonation product $[(TMEDA)Li][CH_2Si(Me)_2N(SiMe_3)Y\{N(SiMe_3)_2\}]$ and the reduction product $Li[Yb\{N(SiMe_3)_2\}_3]$, respectively (Scheme 36). The trigonal-planar coordination geometry around ytterbium in the latter is augmented by two additional intramolecular Yb···C contacts of 2.801(5) and 2.847(5) Å to two trimethylsilyl carbon atoms (Fig. 11) [26].

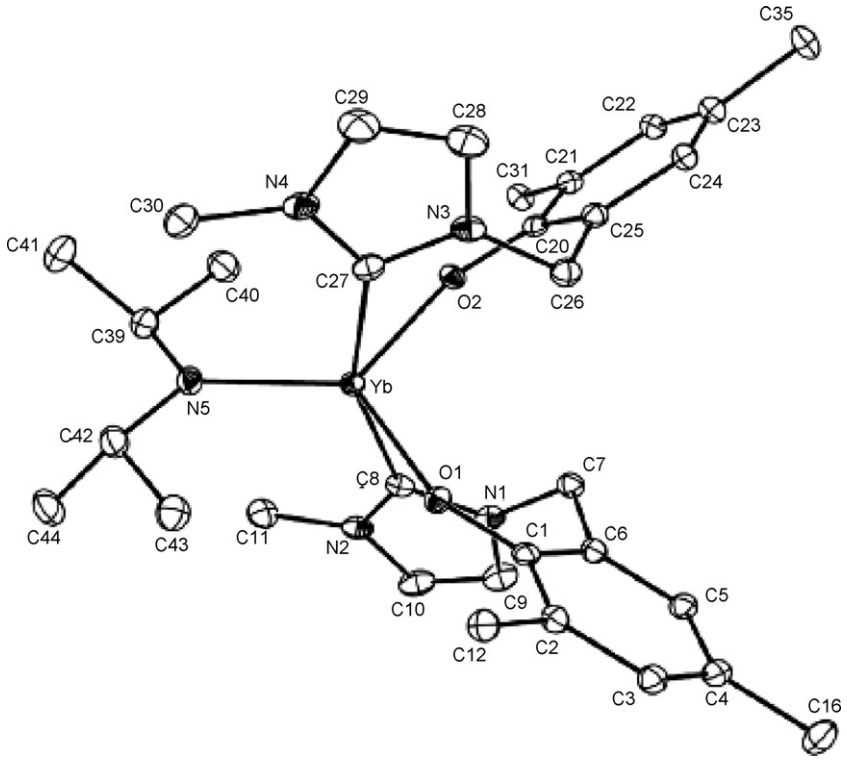

Fig. 9. Molecular structure of $^{i}Pr_2NYb[(O\text{-}4,6\text{-}di\text{-}^{t}BuC_6H_2)_2(CH_2)][^{i}PrIm]_2$ (^{i}PrIm = *N*-isopropylimidazole) [29].

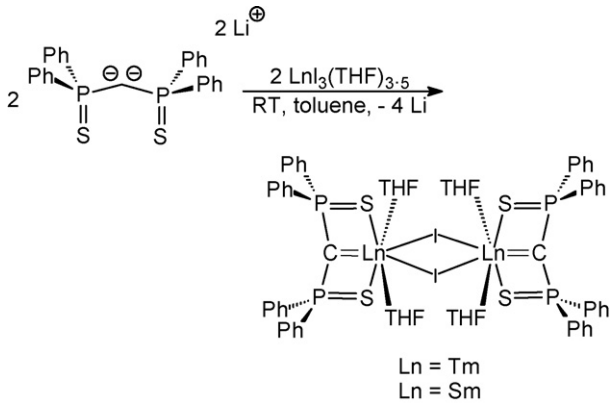

Scheme 31.

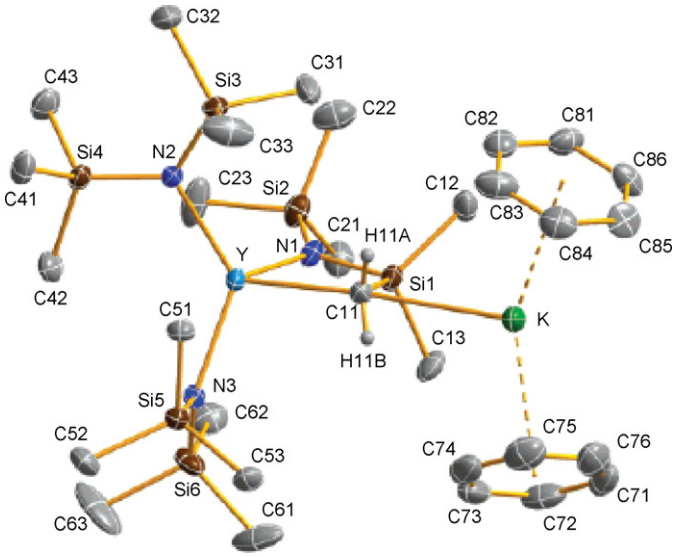

Fig. 10. Molecular structure of $[(C_6H_6)_2K][CH_2Si(Me)_2N(SiMe_3)Y\{N(SiMe_3)_2\}]$ [26].

Instead of the expected bimetallic product, the neutral complex $[Y\{H_2Si(Me)_2N(SiMe_3)\}\{N(SiMe_3)_2\}(THF)]_2$ was isolated in good yield from the reaction between ytterbium(II) diiodide and 2 equiv. of $K[CH_2Si(Me)_2N(SiMe_3)Y\{N(SiMe_3)_2\}]$ (Scheme 37). The most prominent feature of this complex is a ladder-like structure shown in Fig. 12 [26].

2.3. Lanthanide alkenyl and alkynyl compounds

The reaction of scandium monoxide molecules (ScO) with acetylene has been studied in solid argon with infrared absorption spectroscopy. The ScO molecules were prepared by laser-evaporation of a bulk oxide target. The ground-state scandium monoxide molecules reacted with acetylene to form the species

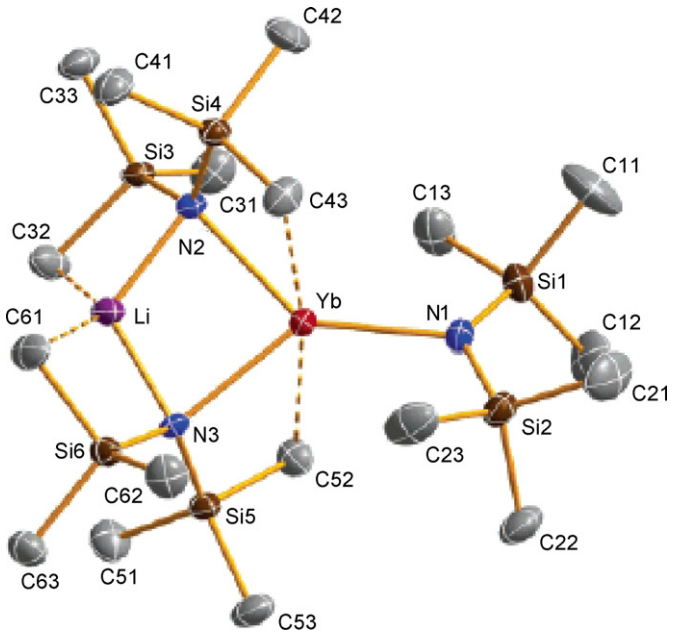

Fig. 11. Molecular structure of $Li[Yb\{N(SiMe_3)_2\}_3]$ [26].

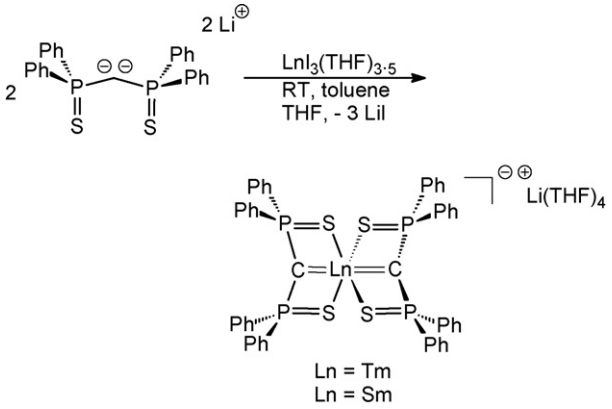

Scheme 33.

$OSc(\eta\text{-}C_2H_2)$ spontaneously on annealing, which was identified on the basis of isotopic IR studies with $^{13}C_2H_2$ and C_2D_2, as well as density functional calculations. The results implied that the $OSc(\eta\text{-}C_2H_2)$ adduct is a typical π-complex [32]. Heteroleptic aryloxide/alkynyl complexes of the type $Ln(OAr^{OMe})_2(C{\equiv}CPh)(THF)_2$ ($Ar^{OMe} = C_6H_2Bu^t$-2,6-OMe-4) were obtained from redox transmetalation/ligand exchange reactions of lanthanide metals (Ln), $Hg(C{\equiv}CPh)_2$ and $HOAr^{OMe}$ (Ln = Y, Er, Lu). Oxidation of the divalent ytterbium aryloxide $Yb(OAr^{OMe})_2(THF)_3$ by $Hg(C{\equiv}CPh)_2$ in THF afforded the analogous ytterbium(III) species $Yb(OAr^{OMe})_2(C{\equiv}CPh)(THF)_2$. The structurally characterized

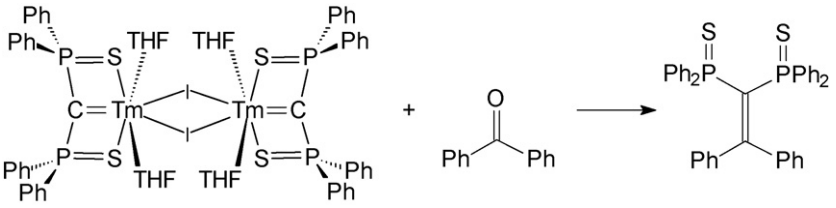

Scheme 32.

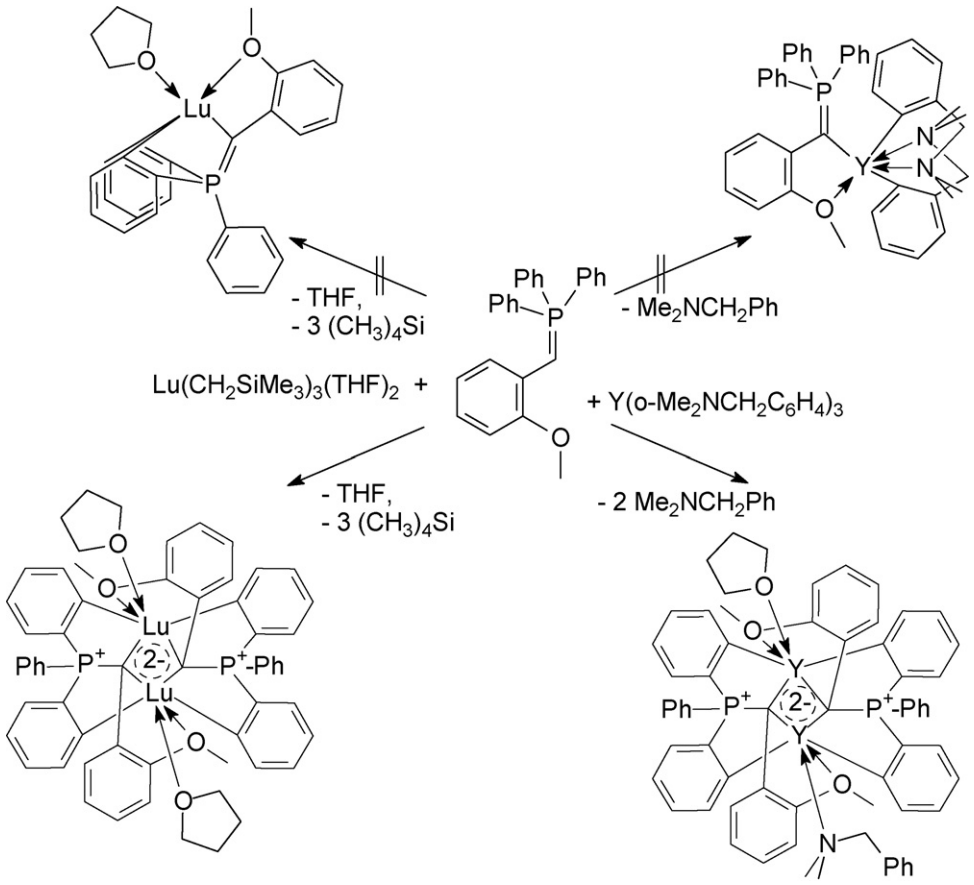

Scheme 34.

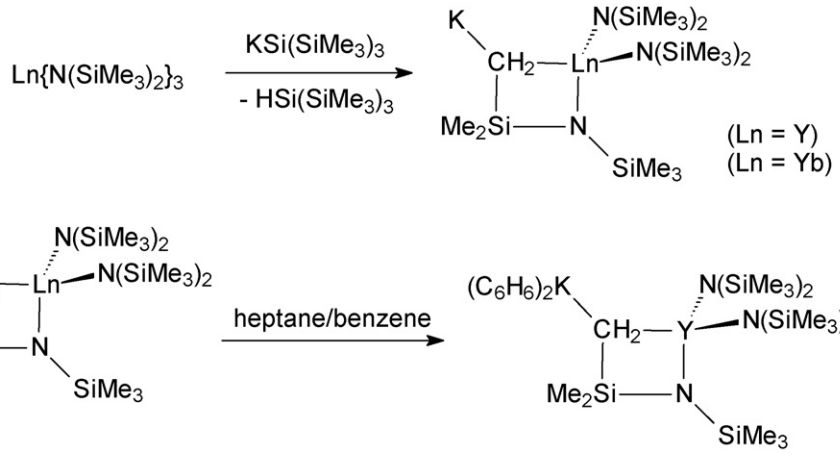

Scheme 35.

erbium alkynide $Er(OAr^{OMe})_2(C{\equiv}CPh)(THF)_2{\cdot}0.25C_6H_{14}$ has distorted square-pyramidal stereochemistry with transoid OAr^{OMe} and THF ligands in the basal plane and a rare (for Ln) terminal alkynide ligand in the apical position (Fig. 13) [14].

Several unusual dinuclear alkynyllanthanide(II) dicationic complexes with pentaphenylcyclopentadienyl or di-*tert*-butyldiphosphacyclopentadienyl counter ions were reported, including their structural characterization by X-ray diffraction. The synthetic routes are outlined in Scheme 38. The starting material, $[(C_5Ph_5)Yb(C{\equiv}CPh)(THF)]_2$, was prepared either from $Yb(C{\equiv}CPh)_2$ and HC_5Ph_5 or from Yb metal, PhHg(C≡CPh) and

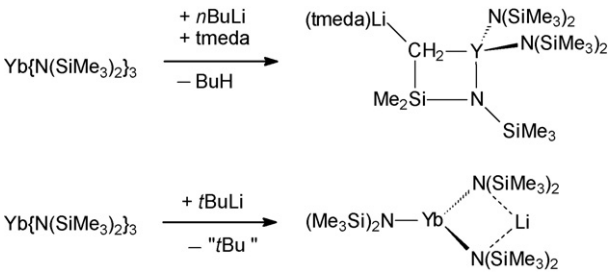

Scheme 36.

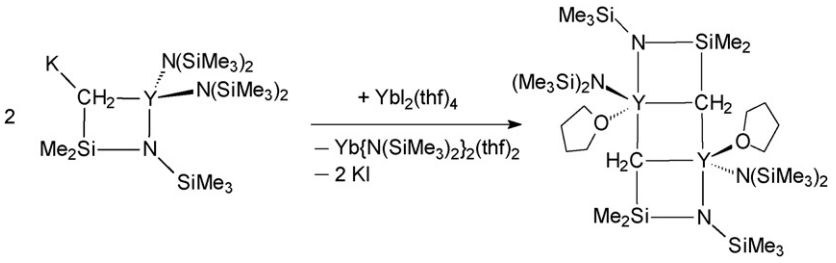

Scheme 37.

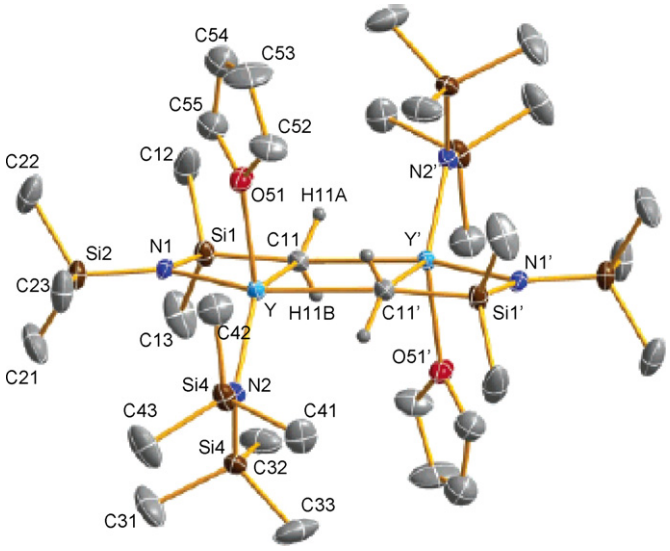

Fig. 12. Molecular structure of L[Y{$H_2Si(Me)_2N(SiMe_3)$}{$N(SiMe_3)_2$}(THF)]$_2$ [26].

HC_5Ph_5. Reactions of this intermediate with a controlled amount of diglyme produced the cationic species with uncoordinated $C_5Ph_5^-$ anions in the crystal lattice. A related europium derivative with tri-*tert*-butylphosphacyclopentadienyl counter ions, $[Eu(C{\equiv}CPh)(diglyme)_2]_2[P_2C_3{}^tBu_3]_2$, was obtained as a few single crystals by the addition of diglyme to the product mixture from the reaction of the phosphaalkyne $^tBuC{\equiv}P$ with a THF solution of $Eu(C{\equiv}CPh)_2$ [33].

2.4. Lanthanide allyls

Reactions of different magnesium/lanthanide allyl complexes with the diketimine 2-(2,6-diisopropylphenyl)amino-4-(2,6-diisopropylphenyl)imino-2-pentene (=BDI–H) have been investigated. As shown in Scheme 39, no lanthanide-containing product could be isolated. Instead, magnesium β-diketiminato complexes were formed as a result of ligand transfer reactions [34].

The unexpected generation of dimethylsilylene and allylidene holmium complexes from trimethylsilylated allyl ligands has been reported. It was found that treatment of rigorously anhydrous holmium triflate with 3 equiv. of the potassium salt of the 1,3-

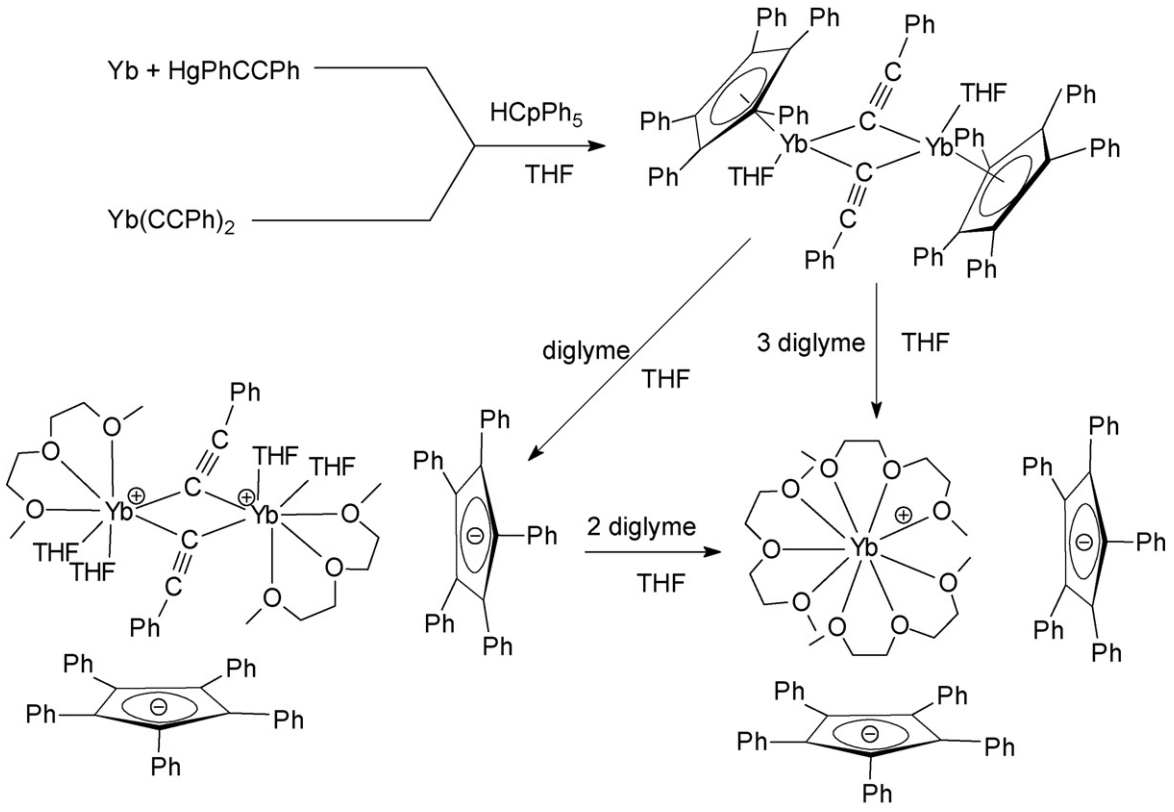

Scheme 38.

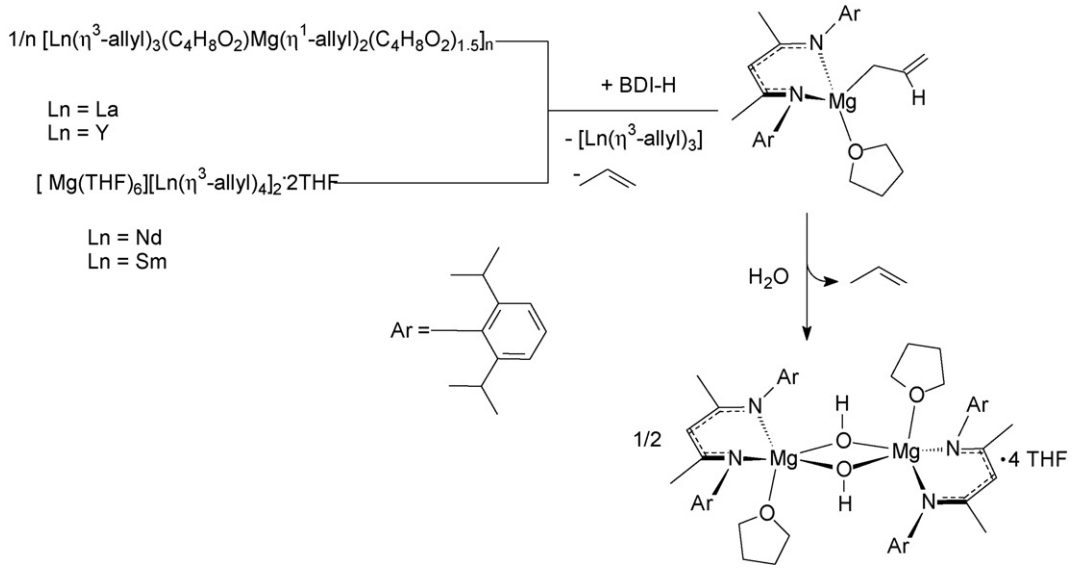

Scheme 39.

bis(trimethylsilyl)allyl anion produces a homoleptic allyl complex, shown as the starting material in Scheme 40. However, it was found that even vacuum-dried $Ho(OTf)_3$ retains traces of coordinated water, and it can alter the outcome of reactions. Thus the same reaction carried out with holmium triflate containing *ca.* 3% of water produced an orange solution, from which a different hydrocarbon-soluble yellow-orange complex could be isolated in 74% yield. An X-ray diffraction study revealed the presence of a dimer in which one η^3-coordinated allyl ligand is bound to each metal, but hydrogen abstraction from a trimethylsilyl group had occurred on a second allyl ligand associated with each metal center, forming dimethylsilylene units that bridge the holmium atoms (Scheme 40). When the reaction that produced the dimeric dimethylsilylene complex was allowed to continue for more than 20 h before work-up, a second yellow-orange dinuclear product could be isolated. The X-ray structure analysis of crystals grown from hexane revealed that, in addition to two dimethylsilylene bridges, the metal centers are joined with a μ-η^1,η^3-allylidene ligand (Scheme 40, Fig. 14). A THF ligand completes the coordination sphere of each metal. This study clearly showed that trimethylsilyl groups on allyl ligands cannot always be assumed to be completely unreactive in f-element complexes [35].

A series of new bulky terpyridyl-ytterbium complexes were synthesized according to Scheme 41 to determine the effect of allyl ligands on the internal charge-transfer process that exists in these materials. Compared to the pentamethylcyclopentadienyl-ytterbocene compound $Cp^*_2Yb(tpyCN)$ (tpyCN = 4′-cyano-2,2′:6′2″-terpyridine) with $\nu_{C\equiv N} = 2172\,cm^{-1}$, the symmetrically substituted allyl complex $[1,3\text{-}(Me_3Si)_2C_3H_3]_2Yb(tpyCN)$ (Scheme 41) possesses a markedly lowered C≡N frequency of $2130\,cm^{-1}$. The differences in these frequencies can be attributed to differences in the ligands' steric and electronic character. Single-crystal X-ray characterization of $[1,3\text{-}(Me_3Si)_2C_3H_3]_2Yb(tpy)$ (Fig. 15) revealed that the allyl moiety possesses shorter Yb–C and Yb–N bond lengths than the Cp* analogue. The magnetic susceptibility data for $[1,3\text{-}(Me_3Si)_2C_3H_3]_2Yb(tpy)$ departs dramatically from the Curie law, with a room-temperature magnetic moment of $2.95\mu_B$ [36].

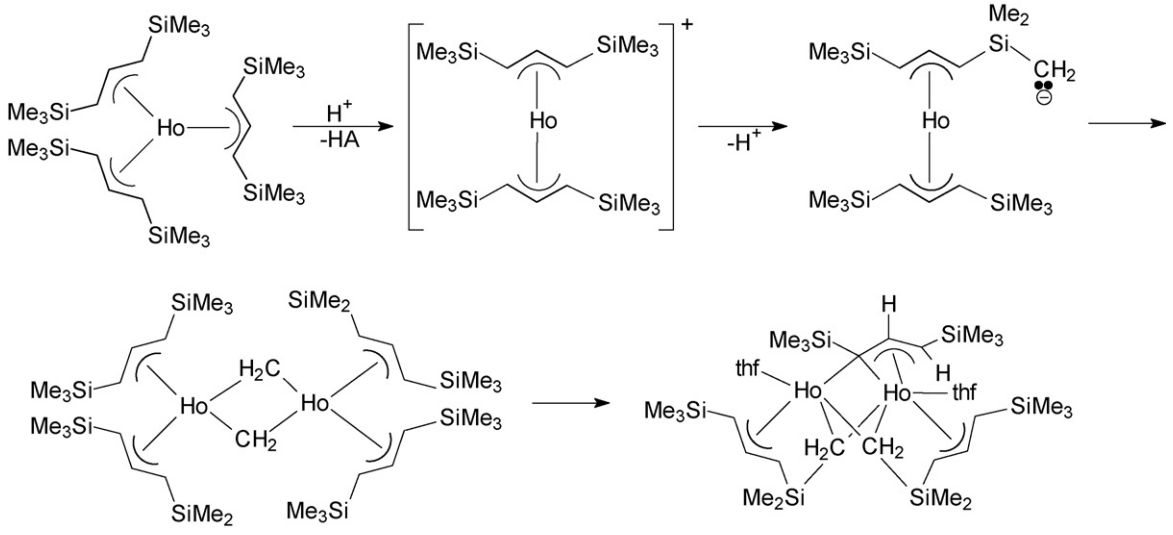

Scheme 40.

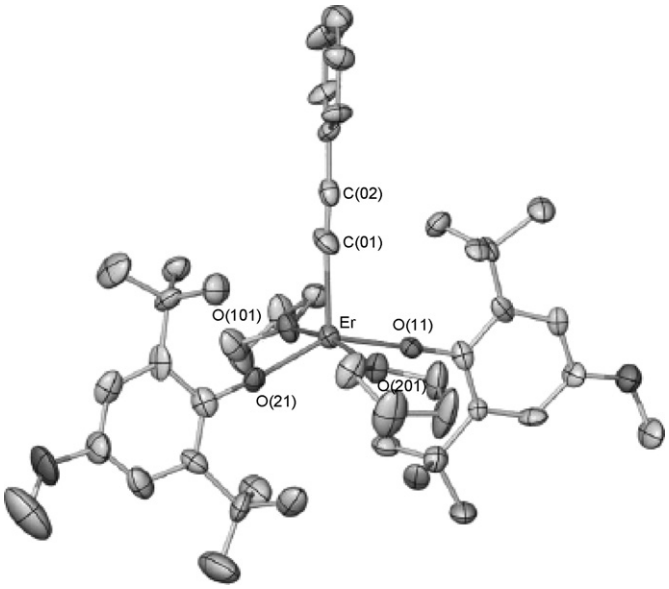

Fig. 13. Molecular structure of $Er(OAr^{OMe})_2(C{\equiv}CPh)(THF)_2{\cdot}0.25C_6H_{14}$ [14].

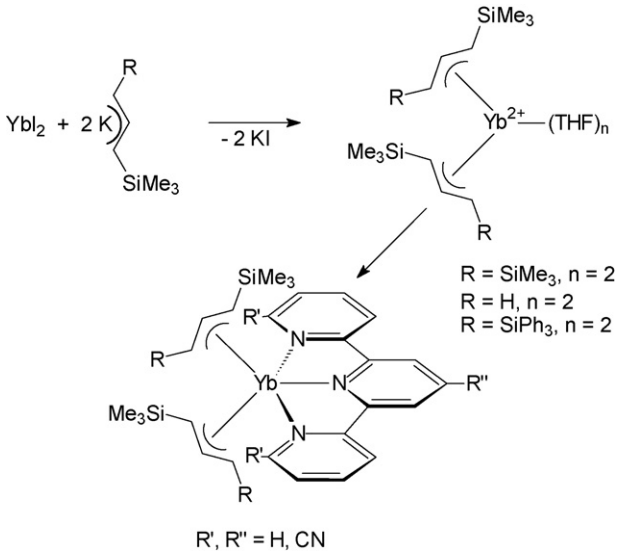

Scheme 41.

2.5. Lanthanide cyclopentadienyl complexes

2.5.1. Cp_2Ln compounds

The synthesis of a new stable, neutral organothulium(II) complex by reduction of a thulium(III) precursor was reported. Dark purple $(Cp^{ttt})_2Tm$ [Cp^{ttt} = 1,2,4-tris(*tert*-butyl)cyclopentadienyl] was obtained either by direct reaction of $NaCp^{ttt}$ with TmI_2 or by reduction of $(Cp^{ttt})_2TmI$ by KC_8 in non-polar solvents. Especially the latter route was found to be very useful for the isolation of neutral "non-classical" low-valent organolanthanide species. After treatment of $(Cp^{ttt})_2Tm$ with THF and pentane, extremely air-sensitive crystals with the composition $(Cp^{ttt})_2Tm(THF)$ were obtained, which were structurally characterized by X-ray crystallography (Fig. 16) [37].

2.5.2. $CpLnX_2$ compounds

Density functional theory calculations were used to study a given complex for the whole series of lanthanide cations: $CpLn(C_3H_5)(OMe)$ (Scheme 42, Ln = La–Lu) except for the radioactive promethium. Contrary to the common assumptions, the calculations suggested a significant, albeit indirect, contribution of f-electrons to the bonding. Relativistic effects were considered in the calculations of the bonding energies, as well as in geometry optimizations in both spin-restricted and unrestricted formalisms. The unrestricted orbitals were finally used for the analysis of the charges and the composition of the frontier orbitals. It was con-

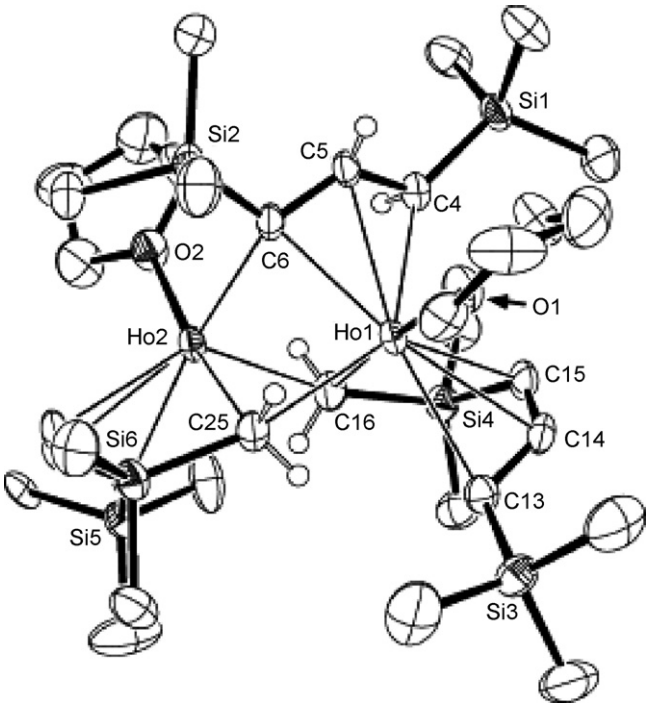

Fig. 14. Molecular structure of the dimeric holmium μ-η^1,η^3-allylidene complex [35].

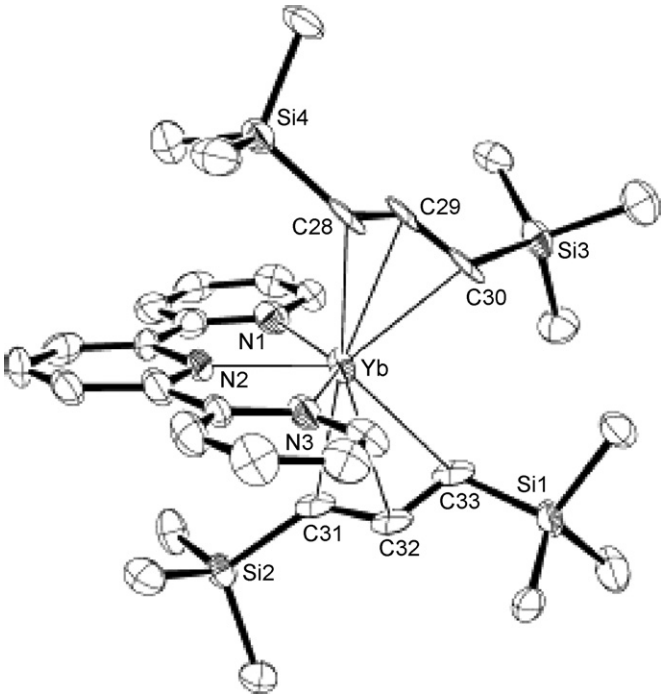

Fig. 15. Molecular structure of $[1,3\text{-}(Me_3Si)_2C_3H_3]_2Yb(tpy)$ [36].

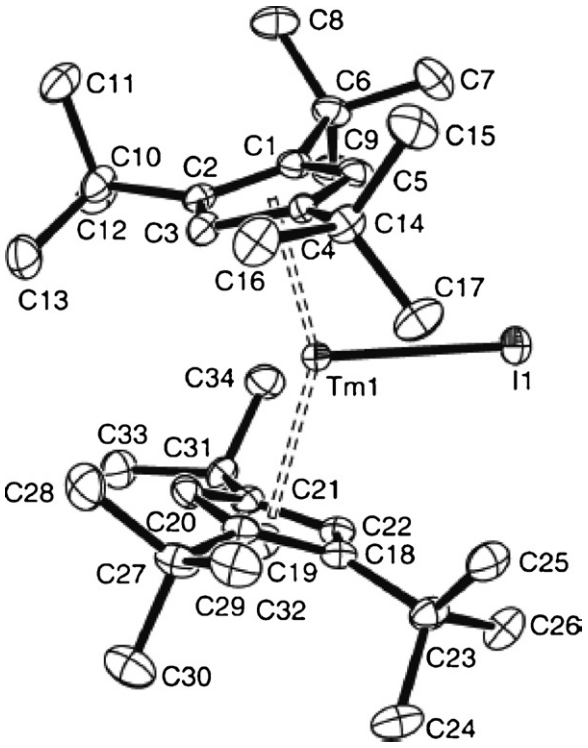

Fig. 16. Molecular structure of $(Cp^{ttt})_2Tm(THF)$ [37].

firmed that the ionic character was more pronounced for complexes of the late lanthanides [38].

The mono(cyclopentadienyl)lanthanide(III) diiodides $CpLnI_2(THF)_3$ (Ln = Nd, Dy) were isolated after recrystallization from THF from the reaction of NdI_2 or DyI_2, respectively, with vanadocene in benzene at 85 °C. The vanadium-containing reaction product was bis(benzene)vanadium [39].

The mixed-ligand cyclopentadienyl/alkoxide complexes $[CpGd(OCMe_2{}^iPr)_2]_2$, $[CpSm(OCMe_2{}^iPr)_2]_2$, and $Cp_3Sm_2(OCMe_2{}^iPr)_3$ were synthesized by allowing the respective Cp_3Ln precursors to react with $HOCMe_2{}^iPr$ in hexanes. X-ray crystallographic studies revealed that the three complexes each have two bridging alkoxide ligands linking two lanthanide atoms. The coordination geometries at the metals are distorted *pseudo*-tetrahedral [40]. A new chelating β-diketonate/phenoxide ligand has been developed and found to react with Cp_3Sc after prolonged heating to 70 °C under formation of a mono(cyclopentadienyl) complex in which the ligand is coordinated to scandium *via* both the β-diketonate and the phenoxide functionalities (Scheme 43). Protonolysis of the second cyclopentadienyl ring of Cp_3Sc appears to take place by an indirect, Cp_3Sc-catalyzed pathway [41].

A series of "constrained geometry" yttrium and lutetium alkyl complexes $(C_5Me_4ZNR)Ln(CH_2SiMe_3)(THF)_n$ (Ln = Y, Lu; Scheme 44) were prepared by treatment of the tris(trimethylsilylmethyl) precursors $Ln(CH_2SiMe_3)_3(THF)_2$ with different linked

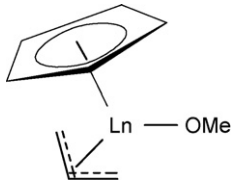

Scheme 42.

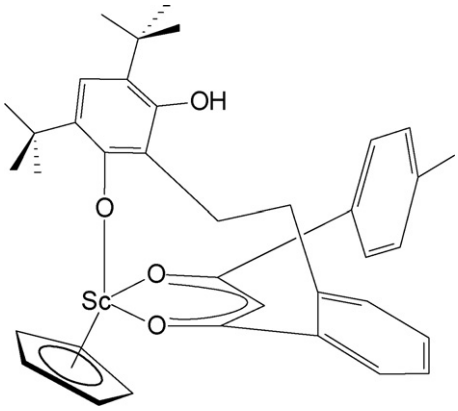

Scheme 43.

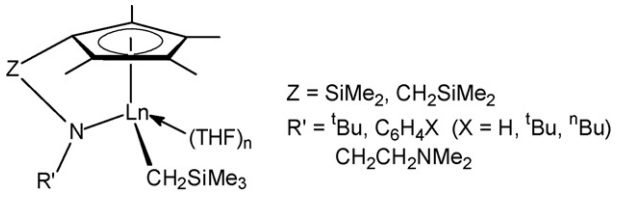

Scheme 44.

aminocyclopentadienes of the type $(C_5Me_4H)ZNHR$ (Z = $SiMe_2$, CH_2SiMe_2; R = ^{t}Bu, Ph, $C_6H_4{}^tBu$-*p*, $C_6H_4{}^nBu$-*p*) [42].

A half-sandwich samarium(III) diketiminate bromide was synthesized by the reaction sequence illustrated in Scheme 45. The compound was shown to be active in methyl methacrylate (MMA) polymerization (*cf.* Section 2.11.2) [43].

An unusual "ate" complex of samarium containing two different kinds of reduced azobenzene species was prepared and structurally characterized. The compound was made by reaction of metallic samarium first with 2 equiv. of azobenzene in THF with the aid of a catalytic amount of iodine and subsequently with 1 equiv. of NaCp as illustrated in Scheme 46. It was found that two-electron

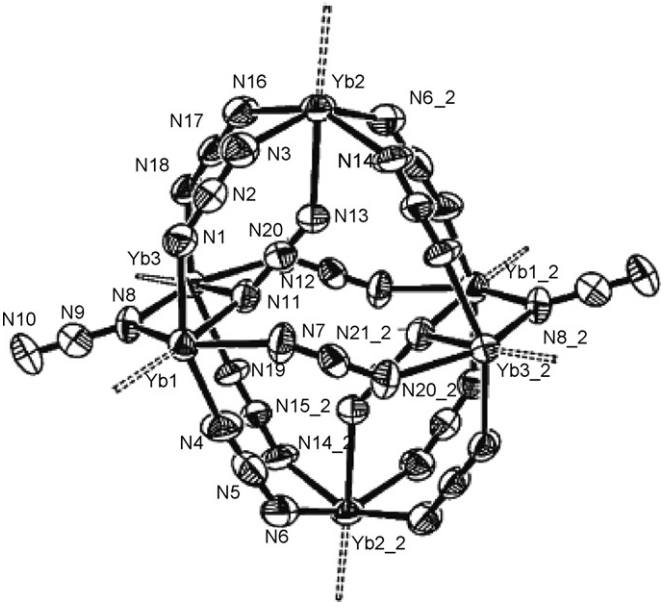

Fig. 17. Structure of the anion in $[Na(DME)_3][Cp^{iPr_4}Yb_6(N_3)_{14}]$ (Cp^{iPr_4} rings omitted for clarity) [45].

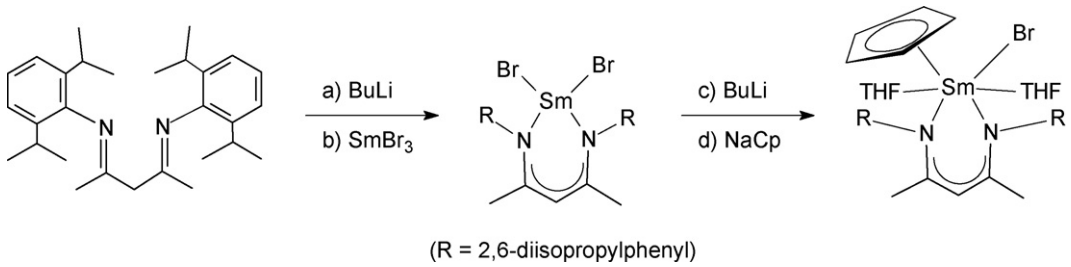

Scheme 45.

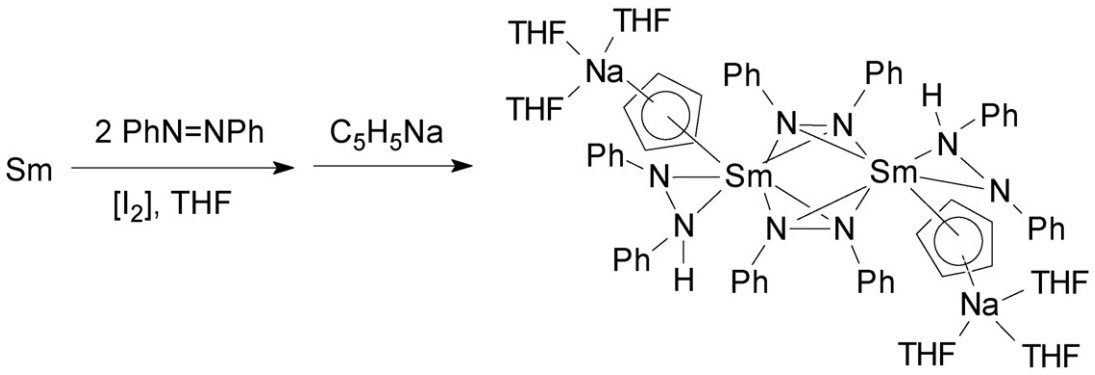

Scheme 46.

reduction and hydride-addition of azobenzene cooperated in this reaction. The hydride-addition reaction happened in the absence of any hydride-reagents. Notably, the product is the first "ate" samarium-azobenzene complex and also the first samarium complex containing two different kinds of reduced azobenzene species [44].

The first mono(cyclopentadienyl)ytterbium azide complex was formed in a slow reaction of the half-sandwich precursor $Cp^{iPr_4}YbCl_2(DME)$ ($Cp^{iPr_4} = C_5H^iPr_4$) with sodium azide in DME at room temperature as shown in Scheme 47 [45].

The product was isolated as red-purple crystals in 58% yield. A single-crystal X-ray diffraction study revealed the presence of a hexanuclear azide-bridged anionic aggregate as shown in Fig. 17 [45].

2.5.3. Cp_2LnX compounds

Cp_2DyI was formed in the reaction of chromocene, Cp_2Cr, with DyI_2 in benzene at ambient temperature. The chromium-containing reaction product was $[CpCr(\mu\text{-}I)]_2$ [39]. The binding of *N*-heterocyclic carbenes (=NHC) to Cp_2MI compounds [M = Ce(III), U(III)] was characterized by quantum chemical methods. Density functional methods were found to be in qualitative agreement with experiment that binding to U(III) is more favorable than to Ce(III) [46].

The reactivity of the lanthanocene hydroxides $[Cp_2Ln(\mu\text{-}OH)(THF)]_2$ (Ln = Y, Er, Yb) toward PhEtC=C=O, PhN=C=O, Cp_3Ln, $[Cp_2Ln(\mu\text{-}Me)]_2$, and the LiCl adduct of $Cp_2Ln^nBu(THF)_x$ was examined. In all cases, OH-centered reactivity was observed. All three complexes reacted with PhEtC=C=O to form the O–H addition products $[Cp_2Ln(\mu\text{-}\eta^1\text{:}\eta^2\text{-}O_2CCHEtPh)]_2$ (Ln = Y, Er, Yb) (Scheme 48) [47].

Similar treatment of $[Cp_2Y(\mu\text{-}OH)(THF)]_2$ with PhN=C=O afforded the addition/CpH-elimination/rearrangement product $(\mu\text{-}\eta^2\text{:}\eta^2\text{-}O_2CNPh)[Cp_2Y(THF)]_2$, which contains an unusual $PhNCO_2^{2-}$ dianionic ligand. The same product as well as the analogous derivatives $(\mu\text{-}\eta^2\text{:}\eta^2\text{-}O_2CNPh)[Cp_2Ln(THF)]_2$ with Ln = Er and Yb could be obtained in a higher yield by treatment of $[Cp_2Y(\mu\text{-}OH)(THF)]_2$ with PhN=C=O followed by reaction with the corresponding Cp_3Ln (Scheme 49) [47].

In the course of this investigation it was also found that reactions of $[Cp_2Yb(\mu\text{-}OH)(THF)]_2$ with either $[Cp_2Yb(\mu\text{-}Me)]_2$ or $Cp_3Yb(THF)$ lead to formation of the same oxo-bridged compound, $(\mu\text{-}O)[Cp_2Yb(THF)]_2$ (yellow-green crystals), in both cases (Scheme 50) [47].

An unusual regioselective substitution reaction liberating 3,5-dimethylpyrazole was observed when the bis(cyclopentadienyl)lanthanide precursors shown in Scheme 51 were treated with *p*-aminothiophenol. The products with Ln = Y, Dy,

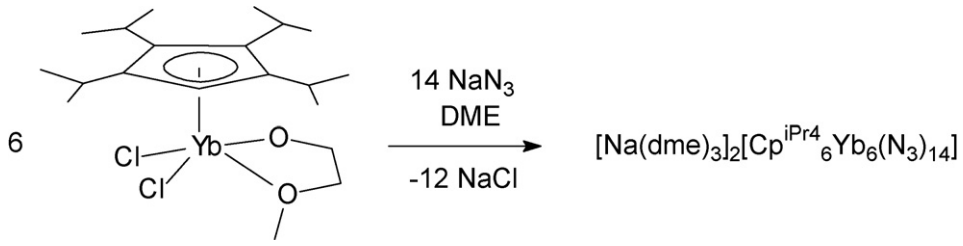

Scheme 47.

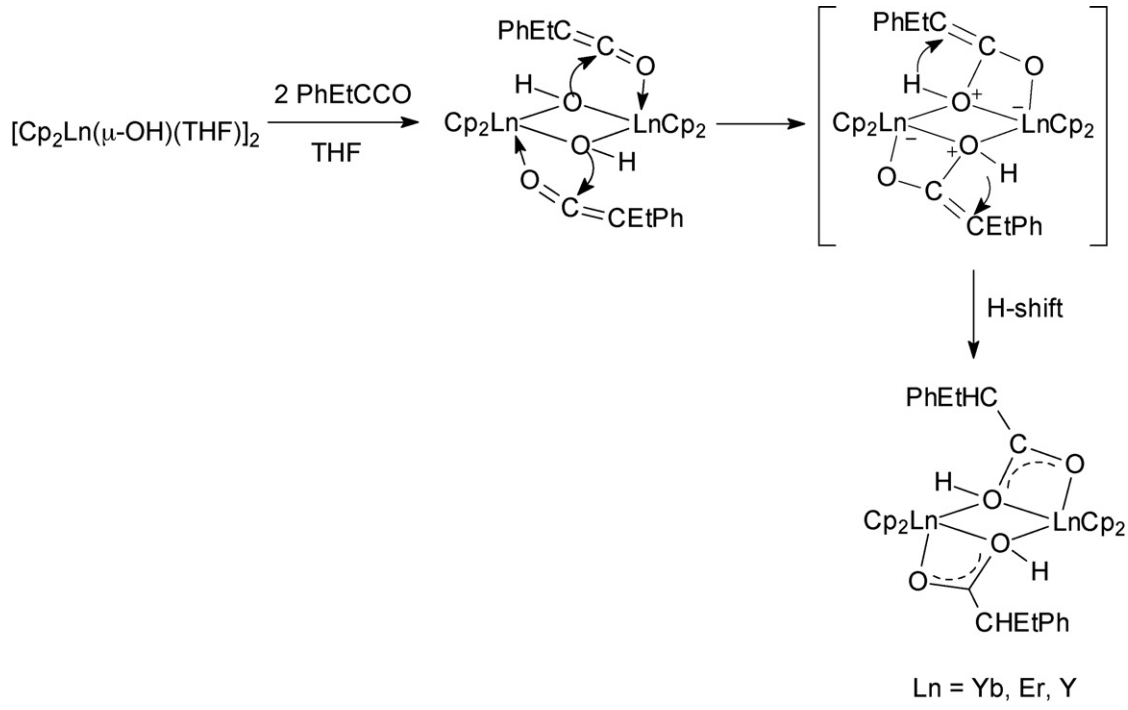

Scheme 48.

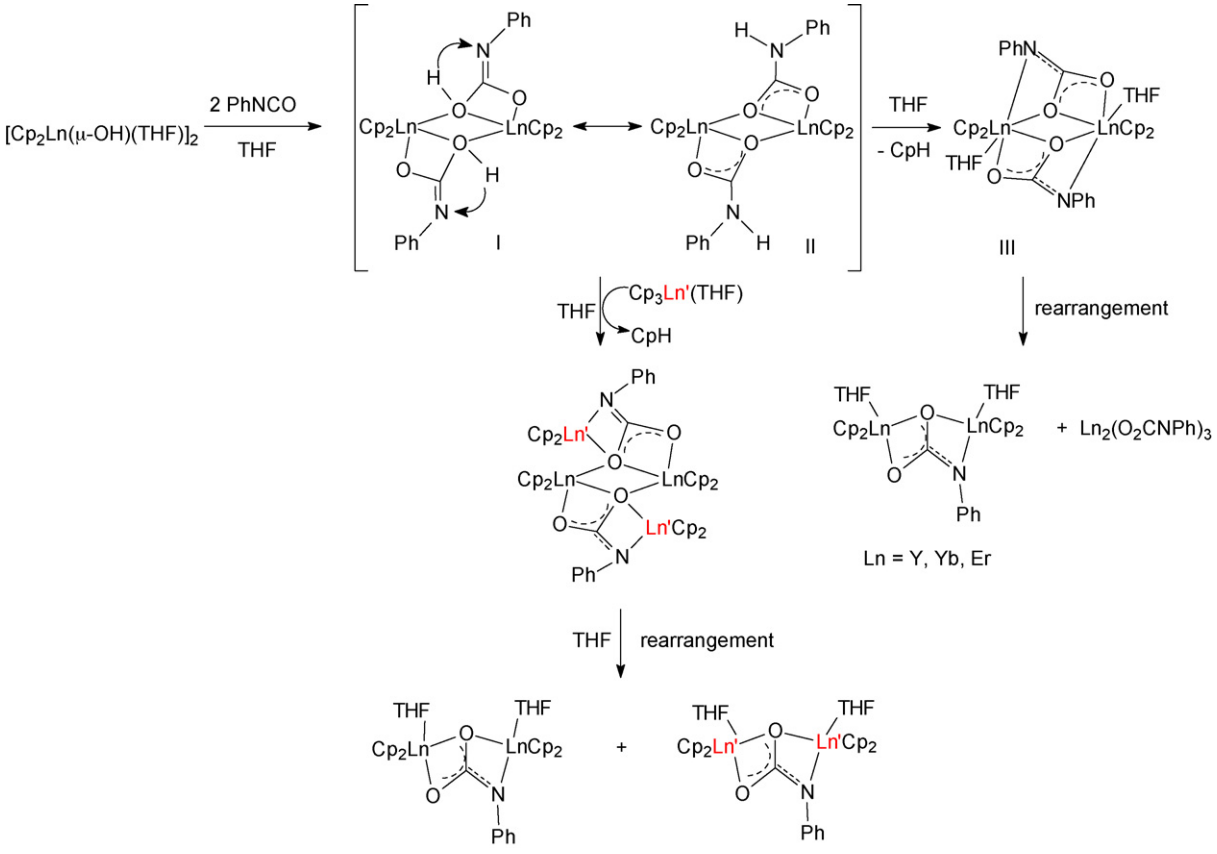

Scheme 49.

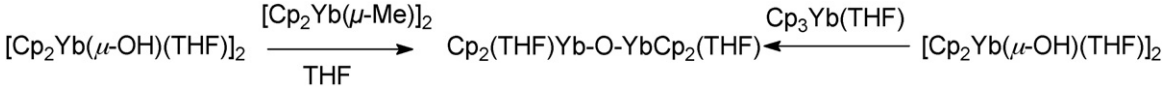

Scheme 50.

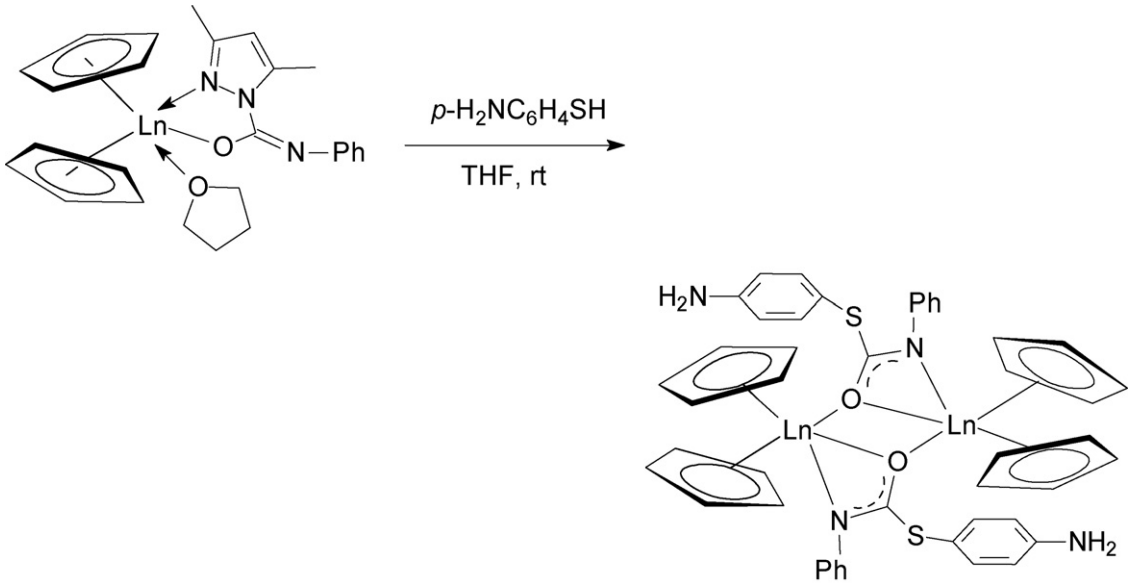

Scheme 51.

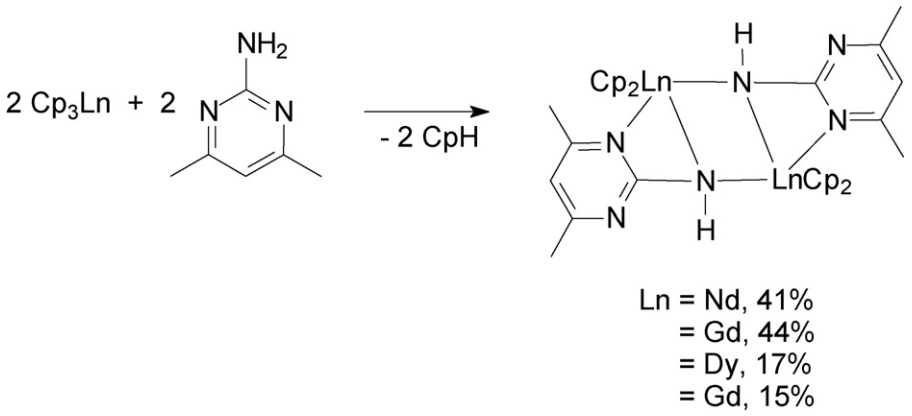

Scheme 52.

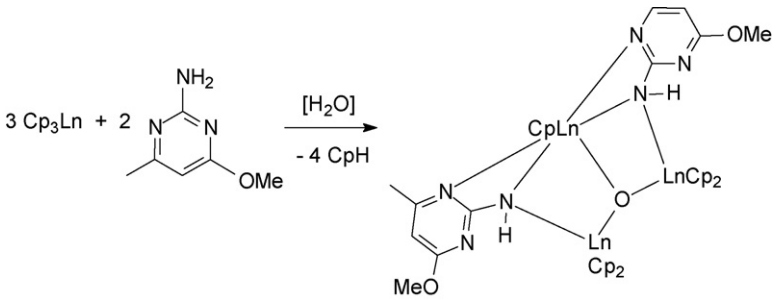

Scheme 53.

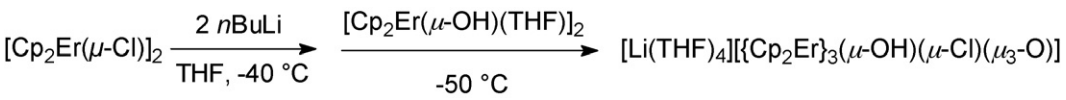

Scheme 54.

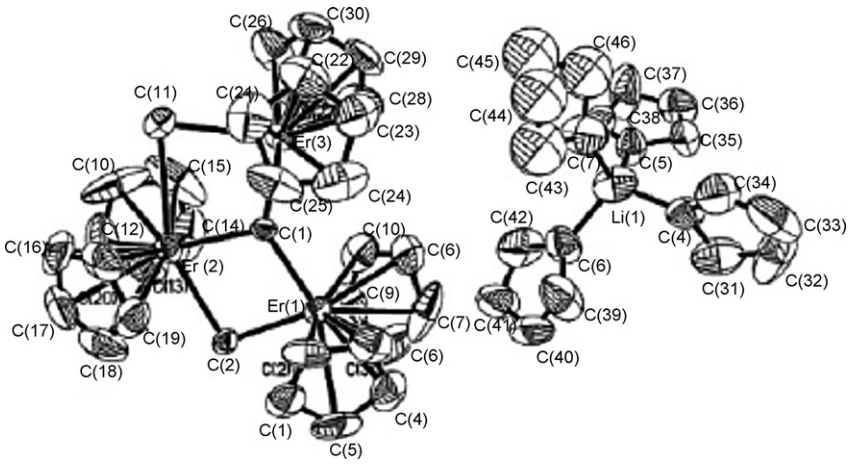

Fig. 18. Molecular structure of $[Li(THF)_4][\{Cp_2Er\}_3(\mu\text{-}OH)(\mu\text{-}Cl)(\mu_3\text{-}O)]$ [47].

Er, and Yb were formed in moderate yields, and the dysprosium derivative was structurally characterized by X-ray diffraction [48].

Synthesis, structures and magnetic properties of the series of dimeric organolanthanide(III) amides $[Cp_2Ln\{2\text{-}NH\text{-}4,6\text{-}Me_2pm\}]_2$ (Ln = Nd, Gd, Dy, Yb; pm = pyrimidine) were reported. These complexes are formed according to Scheme 52 through deprotonation of 2-amino-4,6-dimethylpyrimidine by the corresponding lanthanide tris(cyclopentadienide) [49].

As shown in Scheme 53, the unexpected product $(\mu_3\text{-}O)(YbCp[Cp_2Yb(2\text{-}NH\text{-}4\text{-}MeO\text{-}6\text{-}MeOpm)]_2)$ was formed in a similar deprotonation reaction but in the presence of adventitious water. All compounds shown in Schemes 52 and 53 were structurally characterized by single-crystal X-ray diffraction [49].

Treatment of $[Cp_2Er(\mu\text{-}Cl)]_2$ with ^{n}BuLi in THF followed by reaction with $[Cp_2Er(\mu\text{-}OH)(THF)]_2$ as shown in Scheme 54 resulted in formation of an unexpected μ-oxo lanthanocene cluster, $[Li(THF)_4][\{Cp_2Er\}_3(\mu\text{-}OH)(\mu\text{-}Cl)(\mu_3\text{-}O)]$, in the form of pink crystals. X-ray crystallography revealed that this compound exists as discrete cation and anion pairs (Fig. 18). The anion is comprised of three Cp_2Er units in a triangular array. Two sides of the triangle are bridged by one hydroxide ligand and one chloride ion, respectively, and an additional μ_3-oxo ligand resides in the center of the triangle [47].

In a closely related study the reactivity of lanthanocene amide complexes toward ketenes has been studied. Unprecedented organolanthanide-induced conjugate electrophilic addition reactions of ketenes to arenes were discovered in the course of this study. For example, the reaction of $[Cp_2Ln(\mu\text{-}N^iPr_2)]_2$ with 4 equiv. of $Ph_2C{=}C{=}O$ in toluene afforded the unexpected enolization-dearomatization products $Cp_2Ln[OC\{2,5\text{-}C_6H_5(=CPhCON^iPr_2\text{-}4\}{=}CPh_2]$ (Ln = Er, Yb) in good yields, representing an unprecedented conjugate electrophilic addition to a non-coordinated benzenoid nucleus (Scheme 55). Fig. 19 illustrates the molecular structure of the erbium derivative [50].

Similar treatment of $[Cp_2Ln(\mu\text{-}N^iPr_2)]_2$ with 4 equiv. of $PhEtC{=}C{=}O$ under the same conditions gave the unexpected enolization-

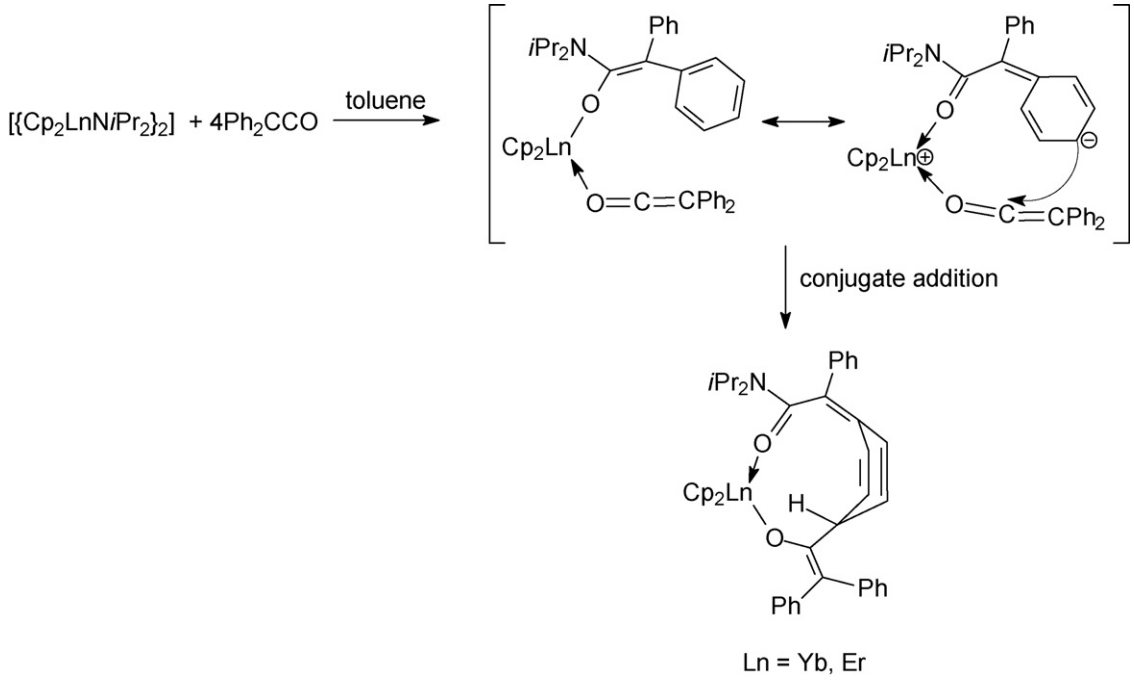

Scheme 55.

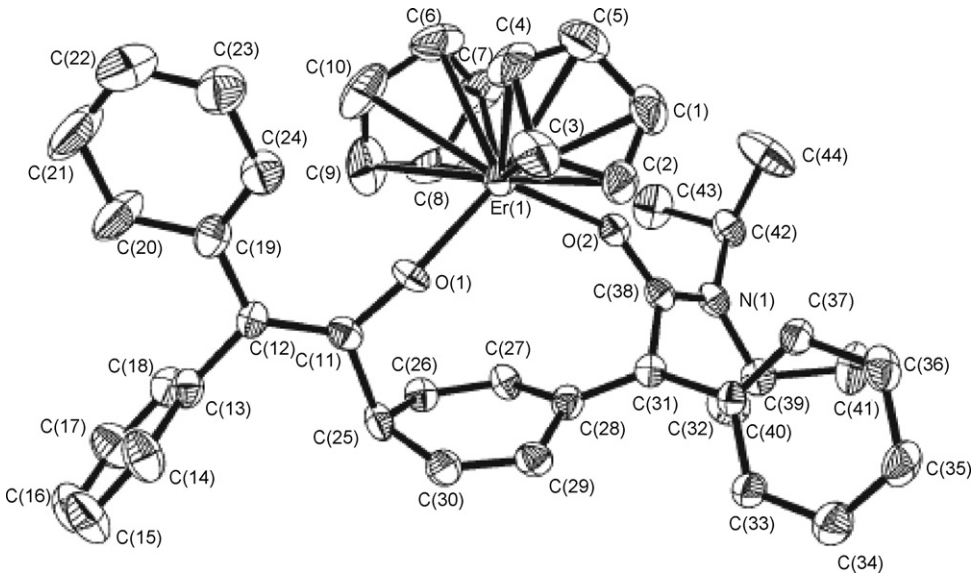

Fig. 19. Molecular structure of $Cp_2Ln[OC\{2,5\text{-}C_6H_5(=CPhCON^iPr_2\text{-}4\}=CPh_2])$ [50].

dearomatization/rearomatization products $[Cp_2Ln(OC\{C_6H_4(p\text{-}CHEtCON^iPr_2)\}=CEtPh)]_2$ (Ln = Dy, Er, Yb) as shown in Scheme 56. Hydrolysis of $[Cp_2Ln(OC\{C_6H_4(p\text{-}CHEtCON^iPr_2)\}=CEtPh)]_2$ afforded the aryl ketone $PhEtCHCOC_6H_4(p\text{-}CHEtCON^iPr_2)$. It is noteworthy that the formation of the dinuclear products is also competing with the insertion of PhEtC=C=O into the Ln–N bonds of $[Cp_2Ln(\mu\text{-}N^iPr_2)]_2$ in toluene. When the reaction with Ln = Yb was carried out in THF, the mononuclear insertion product $Cp_2Yb[OC(N^iPr_2=CEtPh)](THF)$ was isolated as the main product in good yield. Thus the overall formation of aryl ketones provides an alternative route to the acylation of aromatic compounds [50a].

Similar reactions of $[Cp_2Ln(\mu\text{-}NHPh)]_2$ with an excess of PhEtC=C=O afforded only the products resulting from

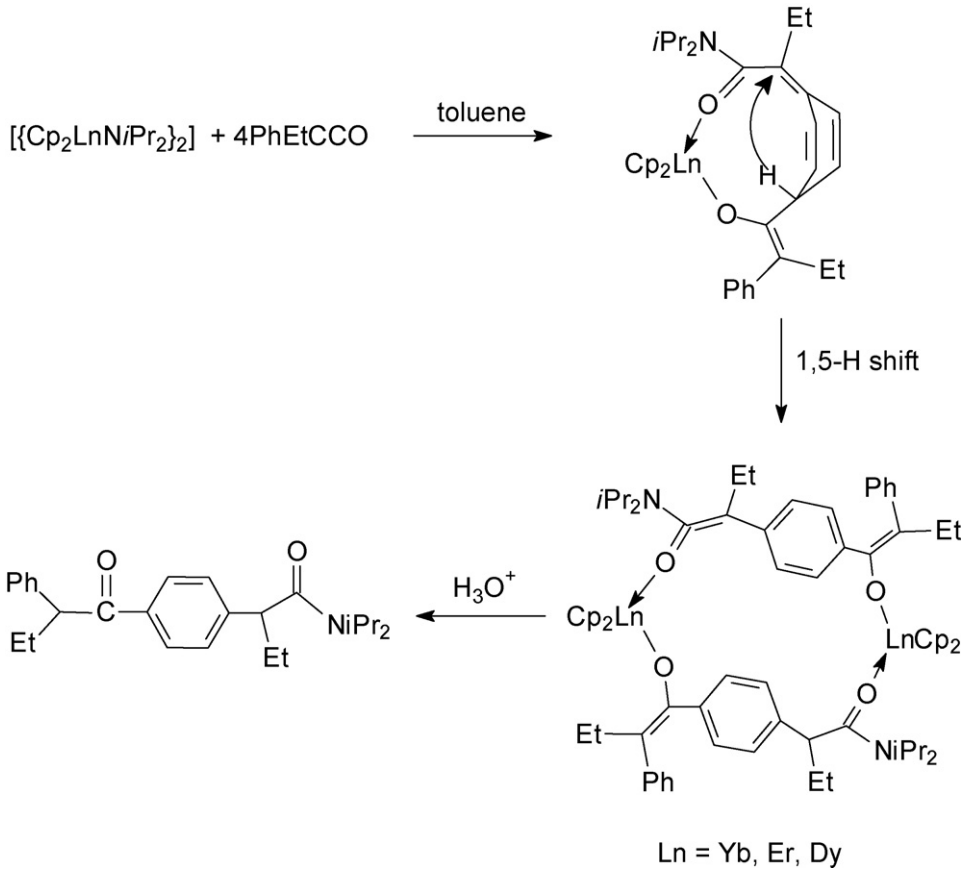

Scheme 56.

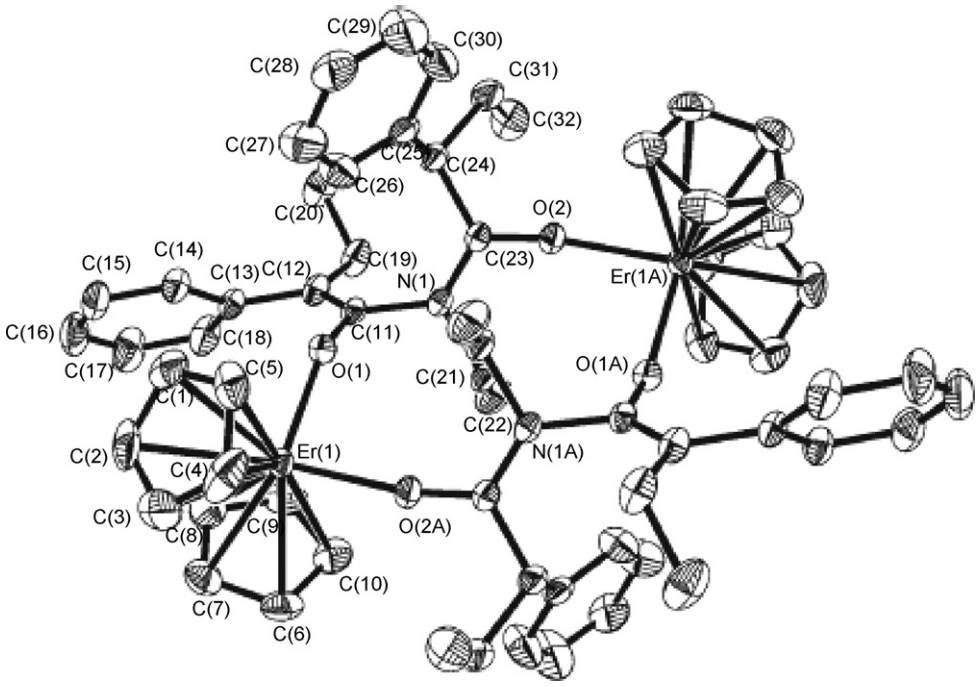

Fig. 20. Molecular structure of $[Cp_2Er\{OC(CHPh_2)NPh\}]_2$ [50a].

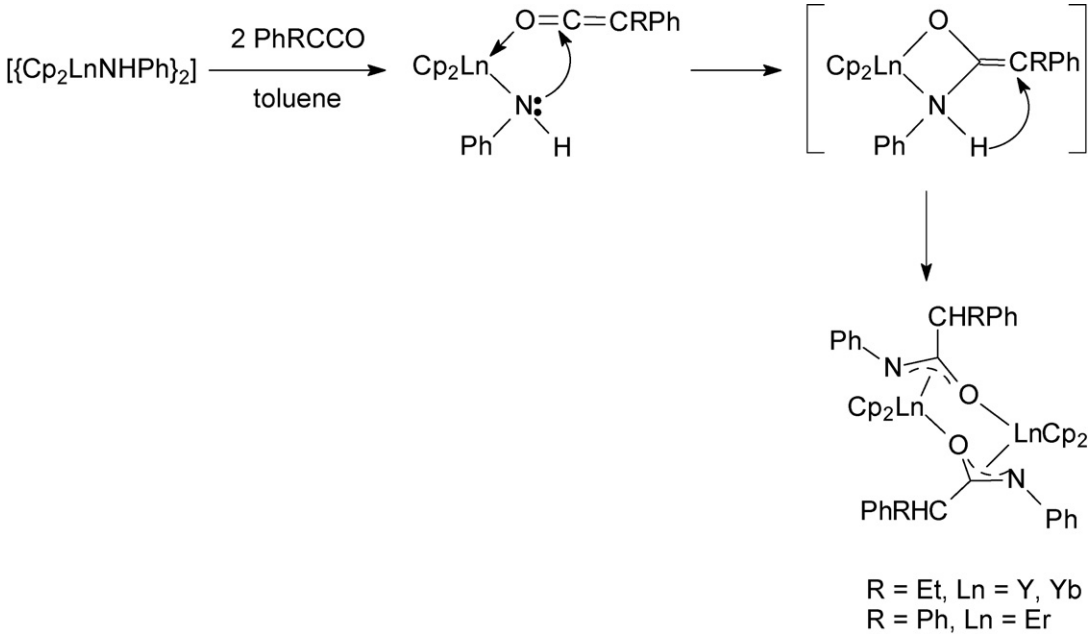

Scheme 57.

formal insertion of the C=C bond of the ketene into the N–H bond, $[Cp_2Ln\{OC(CHEtPh)NPh\}]_2$ (Ln = Y, Yb) or $[Cp_2Er\{OC(CHPh_2)NPh\}]_2$ (Fig. 20), respectively (Scheme 57) [50a].

Analogous insertion reactions of organolanthanide thiolates with ketenes were found to be independent of the nature of the thiolate ligands and the ketene as well as the reaction condition. Treatment of $[Cp_2Ln(\mu\text{-}SR)]_2$ (R = Ph, Ln = Yb; R = CH_2Ph, Ln = Y, Er, Yb) according to Scheme 58 yielded dimers of the ketene monoinsertion products. These reactions provide an efficient method for the synthesis of organolanthanide complexes containing α-thiolate-substituted enolate ligands [50b].

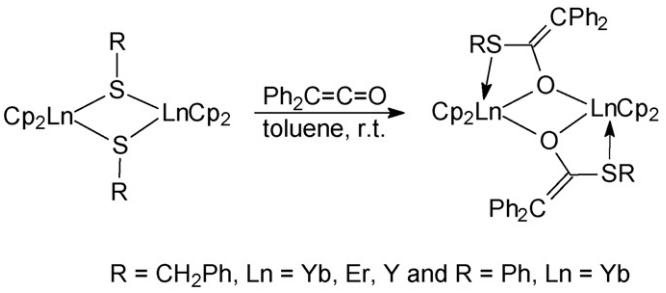

Scheme 58.

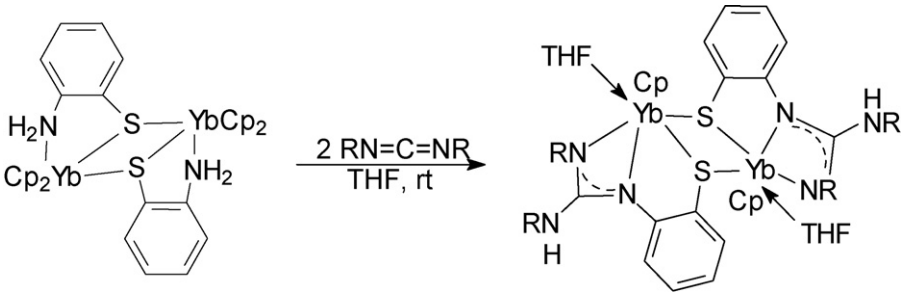

Scheme 59.

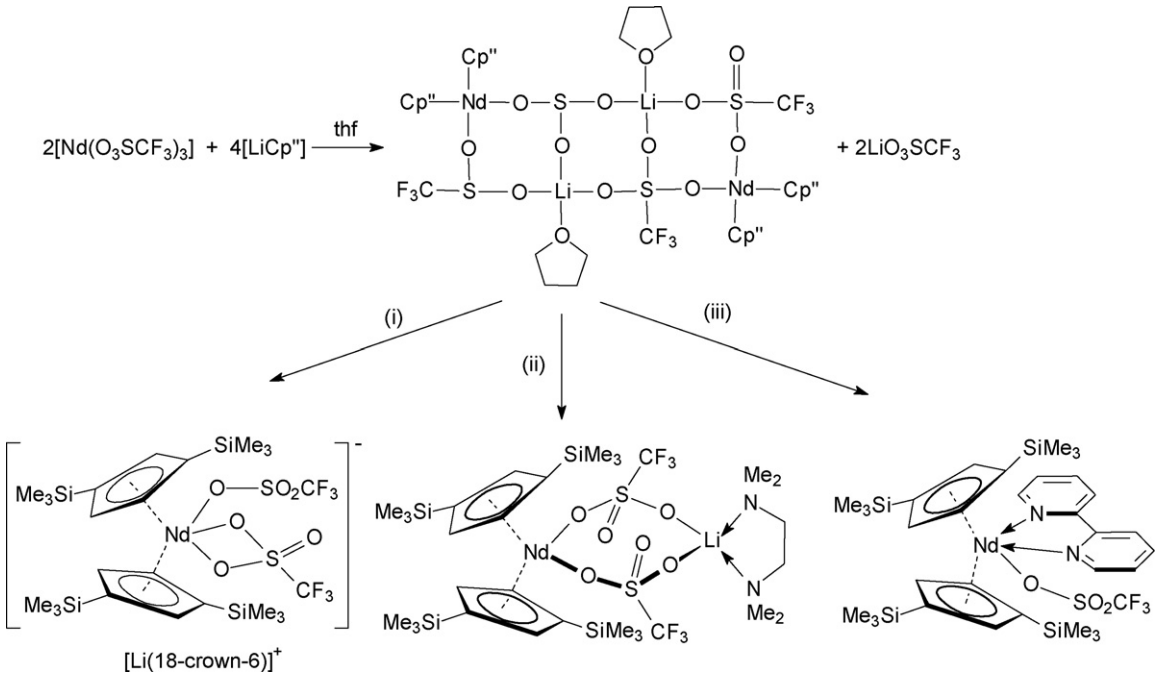

Scheme 60. Reagents and conditions: (i) 18-crown-6, Et_2O, 20 °C; (ii) excess TMEDA, Et_2O, 20 °C, 16 h; (iii) 6 equiv. bipy, Et_2O, 20 °C.

A series of lanthanocene derivatives containing the *o*-aminothiophenolate ligand have been synthesized and their reactivities toward carbodiimides have been investigated. Scheme 59 illustrates a typical reaction sequence. The dimeric starting materials were all prepared by protonolysis of Cp_3Ln (Ln = Dy, Er, Yb) with *o*-aminothiophenol. Subsequent treatment with *N*,*N*′-diisopropylcarbodiimide led to the formation of various insertion products. As illustrated in Scheme 59, these reactions are often accompanied by elimination of a cyclopentadienyl ligand [50c].

The compounds $Cp_2Ce[\eta^3\text{-}N(EPPh_2)_2]$ (E = S, Se) and $Cp_2Ce[\eta^3\text{-}N(SP^iPr_2)(SePPh_2)]$ were synthesized from the protonolysis reactions between Cp_3Ce and $HN(EPPh_2)_2$ or $HN(SP^iPr_2)(SePPh_2)$ in THF. The structures of these compounds were determined by X-ray crystallographic methods. All three compounds have similar structures in which the ligands are coordinated to the Cp_2Ce moiety in an η^3-fashion through the two chalcogen atoms and an N atom. Whereas the ^{77}Se NMR resonances were normal, the ^{31}P NMR resonances were found to be shifted to much lower frequencies than in similar rare-earth complexes [51]. Treatment of the β-diketiminate-supported ytterbium dichloride complex $LYbCl_2(THF)_2$ (L = *N*,*N*′-bis(2,6-dimethylphenyl)-2,4-pentanediiminate) with 2 equiv. of NaCp afforded the complex Cp_2YbL as red microcrystals in 45% yield. The compound was structurally characterized by X-ray methods, showing the expected distorted *pseudo*-tetrahedral coordination geometry [52].

Different triflate coordination modes were found in neodymocene complexes containing bulky 1,3-bis(trimethylsilyl)cyclopentadienyl (=Cp″) ligands. The reaction of $Nd(OTf)_3$ (OTf = O_3SCF_3)

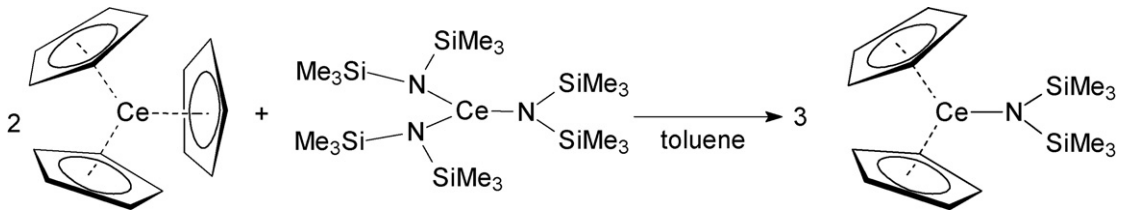

Scheme 61.

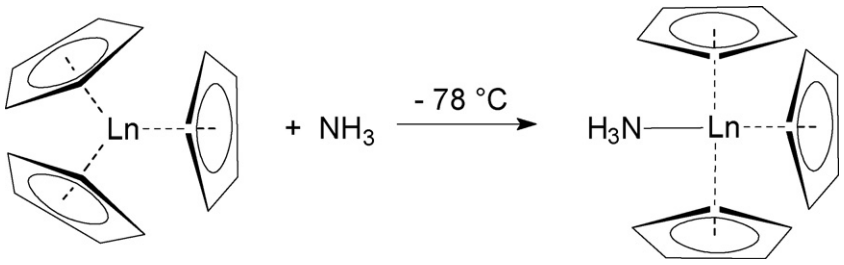

Scheme 62.

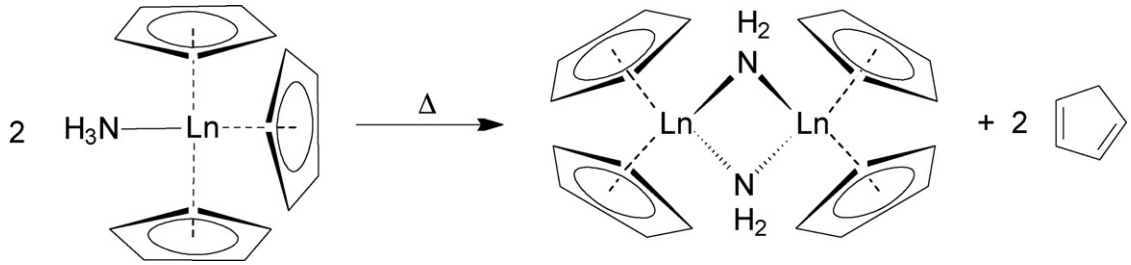

Scheme 63.

with two molar equivalents of LiCp″ according to Scheme 60 generated a blue tetrametallic dimer which was shown by X-ray crystallography to contain a tricyclic, ladder-like scaffold with Nd and Li cations and OTf anions at its core. This compound was found to be relatively labile, being readily cleaved by a variety of donor molecules (Scheme 60). 18-Crown-6 encapsulated the lithium cation to yield a salt-like product. Addition of *N*,*N*,*N*′,*N*′-tetramethylethylenediamine (=TMEDA) afforded a monomeric "ate" complex with bridging triflate ligands, while the more rigid donor 2,2′-bipyridine (=bipy) produced the neutral, Li-free complex $Cp''_2Nd(OTf)(bipy)$ [53].

Lanthanum-containing metallocenes were investigated for the first time by solid-state ^{139}La and ^{15}N NMR spectroscopy. Among the compounds studied in this context was the ^{15}N-enriched dinitrogen complex $(\mu\text{-}^{15}N_2)[(C_5Me_4H)_2La(THF)]_2$ [54].

2.5.4. Cp_3Ln and Cp_3LnL compounds

An experimental and theoretical study of ^{45}Sc NMR interactions in solids has been published. Solid-state ^{45}Sc NMR spectroscopy, *ab initio* calculations, and X-ray crystallography were applied to examine the relationships between ^{45}Sc NMR interactions and molecular structure and symmetry. Besides a number of inorganic and coordination compounds, Cp_3Sc was one of the compounds investigated in this study [55]. The first solid-state ^{139}La NMR spectra of lanthanum-containing metallocenes, including Cp_3La and $(C_5Me_4H)_3La$, were also reported [54]. The crystal structures of three unsolvated tris(cyclopentadienyl)lanthanide complexes were determined using different X-ray diffraction methods. Cp_3Ce and Cp_3Ho crystal data needed special solution and refinement methods, due to the occurrence of intrinsic twinning in these species. The previously published cell constants of Cp_3Ho were redetermined. The space group and unit cell parameters of Cp_3Dy were derived from powder diffraction experiments. High-resolution ^{13}C solid-state NMR data of Cp_3La were also presented, giving evidence of the dynamics and bonding situation of the Cp ligands. Cp_3Ce was found to be a reactive reagent for the synthesis of $Cp_2CeN(SiMe_3)_2$. This compound was obtained as an orange-yellow, extremely air-sensitive solid from the ligand redistribution reaction shown in Scheme 61 [56].

A series of ammine-tris(cyclopentadienyl)lanthanide(III) complexes (Ln = Sm, Gd, Dy, Ho, Er, Yb) were synthesized by the reaction of unsolvated Cp_3Ln complexes with liquid ammonia at −78 °C as shown in Scheme 62 and structurally characterized by X-ray diffraction methods, mass spectrometry and vibrational (IR, Raman) spectroscopy [57].

Heating of the ammine adducts $Cp_3Ln(NH_3)$ in an inert gas atmosphere at temperatures between 240 and 290 °C afforded the corresponding dimeric amido-bridged species $[Cp_2Ln(\mu\text{-}NH_2)]_2$ as illustrated in Scheme 63 [57].

The use of 1,2-phenylenedioxoborylcyclopentadienyl in transition metal and lanthanide chemistry has been explored. In the case of lanthanide elements, three new tris(cyclopentadienyl) derivatives were isolated in the form of their THF adducts as depicted in Scheme 64 [58].

2.5.5. Pentamethylcyclopentadienyl compounds

2.5.5.1. Cp^*_2M compounds. Various 1:1 coordination complexes of Cp^*_2Yb with 4,4′-disubstituted bipyridines, bipy-X, where X is Me, ^tBu, OMe, Ph, CO_2Me, and CO_2Et, were prepared. All of the complexes are paramagnetic, and the values of the paramagnetic susceptibility as a function of temperature showed that these values are less than expected for the cations, $[Cp^*_2Yb(III)(bipy\text{-}X)]^+$, which were isolated as the cation–anion pairs $[Cp^*_2Yb(III)(bipy\text{-}X)]^+[Cp^*_2YbI_2]^-$ [59]. A series of ytterbocene charge-transfer

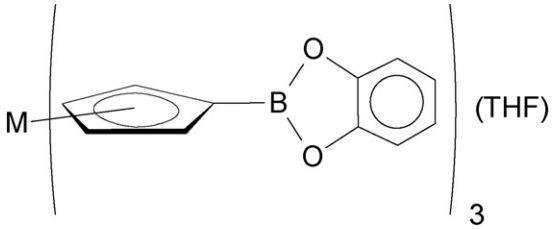

M = La
M = Ce
M = Yb

Scheme 64.

molecular wire complexes shown in Scheme 65 were systematically studied with the aim of determining the effects of increased Yb–Yb separation on the magnetic and electronic properties of these materials. The darkly colored compounds were all prepared by adding a toluene solution of $Cp^*_2Yb(OEt_2)$ to the respective nitrogen bases [60].

The Eu diazadiene complexes $Cp^*_2Eu(^tBuDAD)$ (purple crystals, $^tBuDAD = {}^tBuN{=}CH{-}CH{=}N^tBu$) and $Cp^*_2Eu(C_6F_5DAD)$ (green crystals, $C_6F_5DAD = C_6F_5N{=}C(Me){-}C(Me){=}NC_6F_5$) were prepared by treatment of $Cp^*_2Eu(OEt_2)$ with equimolar quantities of the diazadiene ligands in toluene solution (Scheme 66), and on the basis of characterization by X-ray crystallography, magnetic susceptibility, and ^1H NMR and IR spectroscopy, it was concluded that the Eu oxidation states in these complexes are +2 and +3, respectively. It was found that in the case of $Cp^*_2Eu(C_6F_5DAD)$ the internal redox process is solvent sensitive [61].

2.5.5.2. Mono(pentamethylcyclopentadienyl)lanthanide(III) compounds. An extensive investigation on the chemistry of mono(pentamethylcyclopentadienyl) lanthanide complexes was published in 2006. This study showed that a wide range of mono(pentamethylcyclopentadienyl) lanthanide complexes can be isolated and crystallographically characterized. Several unusual cluster molecules demonstrate the versatility of bridging chlorides and iodides in generating a variety of structures for mono(pentamethylcyclopentadienyl) lanthanide halides. For example, the dysprosium complex $[Cp^*Dy(\mu\text{-}I)_2]_3$ is a trimeric cyclopentadienyl lanthanide halide unusual in that it has six bridging halides that roughly define a trigonal prism. Complete displacement of iodide counterions was found in the acetonitrile complex $[Cp^*Tm(MeCN)_6]I_2$ [62].

2.5.5.3. Bis(pentamethylcyclopentadienyl)lanthanide(III) compounds. Dinitrogen complexes of the type $(\mu\text{-}\eta^2{:}\eta^2\text{-}N_2)[Cp^*_2Ln(THF)]_2$, generated by reduction of dinitrogen with trivalent lanthanide salts and alkali metals, were shown to be strong reductants which provide a useful option in reductive lanthanide chemistry. Hence, lanthanide-based reduction chemistry can be effected in a diamagnetic trivalent system using *e.g.* the dinitrogen reduction product $(\mu\text{-}\eta^2{:}\eta^2\text{-}N_2)[Cp^*_2La(THF)]_2$,

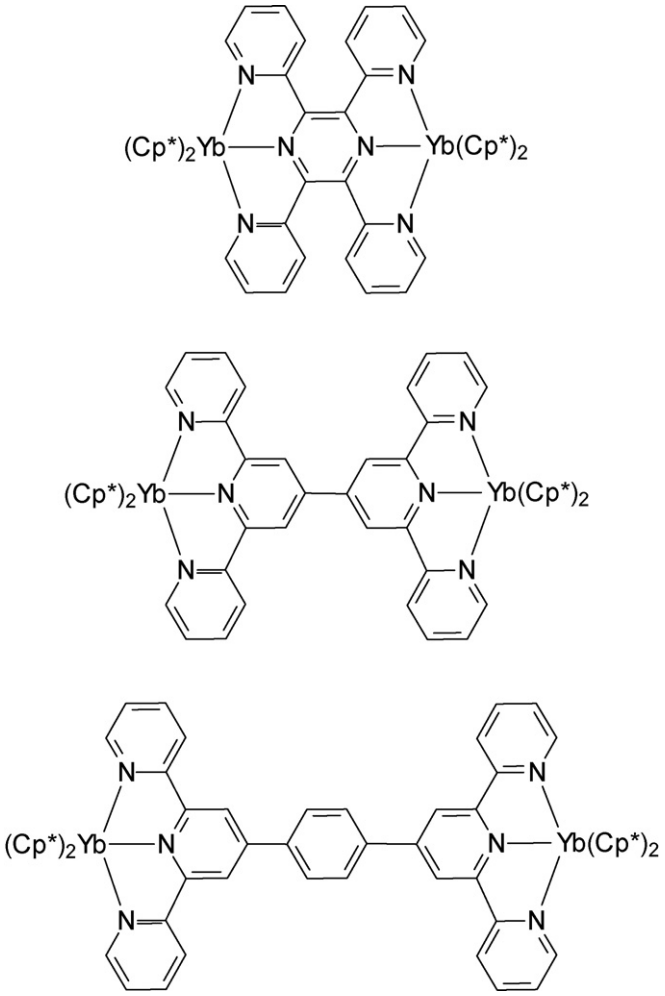

Scheme 65.

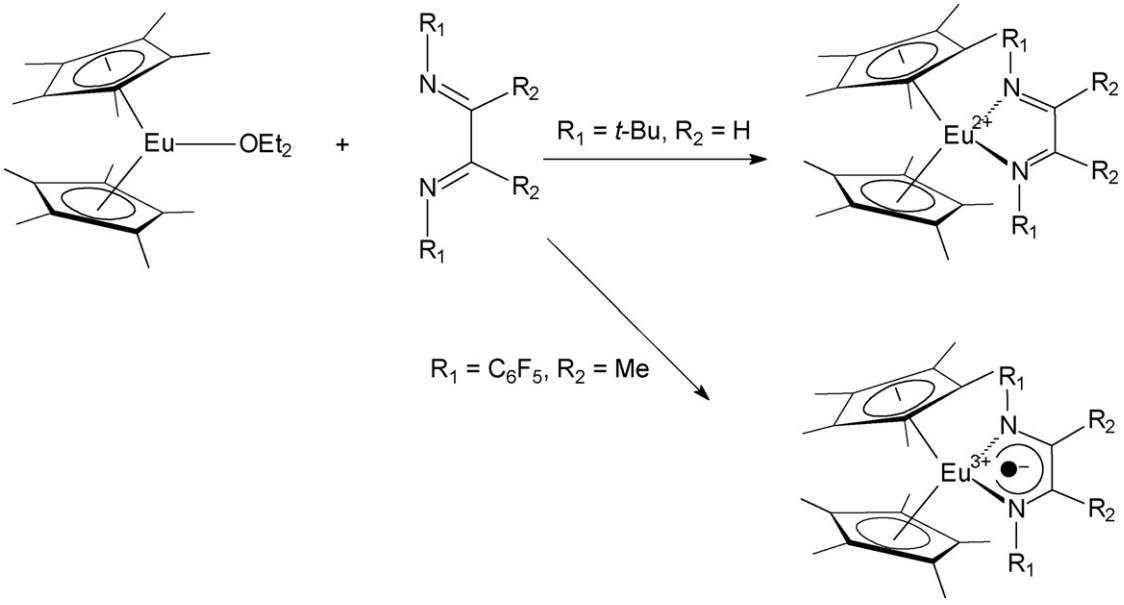

Scheme 66.

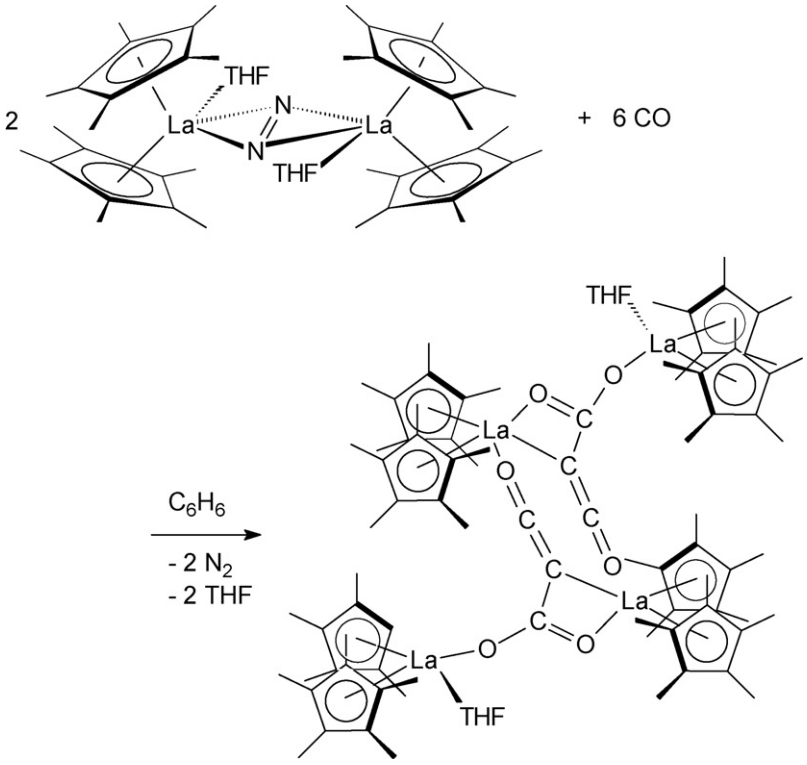

Scheme 67.

readily obtained from $[Cp^*_2La][BPh_4]$, KC_8, and N_2. $(\mu\text{-}\eta^2\text{:}\eta^2\text{-}N_2)[Cp^*_2La(THF)]_2$ reduces phenazine, cyclooctatetraene, anthracene, and azobenzene. Neither stilbene nor naphthalene are reduced by $(\mu\text{-}\eta^2\text{:}\eta^2\text{-}N_2)[Cp^*_2La(THF)]_2$, but the compound reduces CO to make the ketene carboxylate complex $[(\mu\text{-}\eta^4\text{-}O_2C\text{–}C{=}C{=}O)\{Cp^*_2La\}_2(THF)]_2$ (orange crystals) as illustrated in Scheme 67. The ketene carboxylate ligand contains CO-derived carbon atoms completely free of oxygen. Fig. 21 shows the molecular structure of $[(\mu\text{-}\eta^4\text{-}O_2C\text{–}C{=}C{=}O)\{Cp^*_2La\}_2(THF)]_2$ [63].

CO_2 inserts into the Sm–S and Sm–Se bonds of $[Cp^*_2Sm(\mu\text{-}EPh)]_2$ (E = S, Se) according to Scheme 68 to form the first crystallographically characterized $(O_2CEPh)^-$ complexes, $[Cp^*_2Sm(\mu\text{-}O_2CEPh)]_2$. Theses complexes are structurally analogous to $[Cp^*_2Sm(\mu\text{-}O_2CR)]_2$ complexes, but they are less soluble. Fig. 22 shows the molecular structure of $[Cp^*_2Sm(\mu\text{-}O_2CSPh)]_2$. $[Cp^*_2Sm(\mu\text{-}$

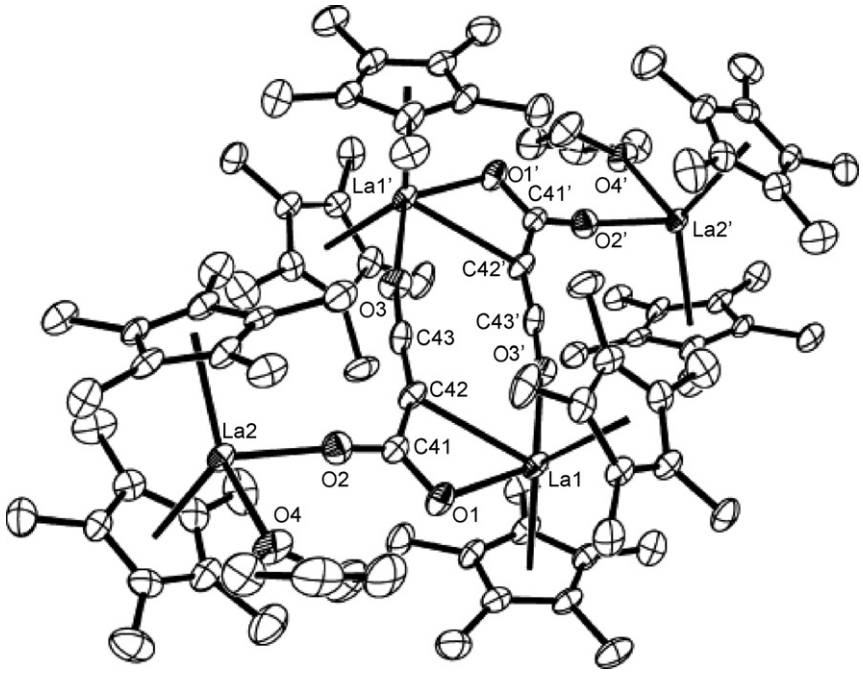

Fig. 21. Molecular structure of $[(\mu\text{-}\eta^4\text{-}O_2C\text{–}C{=}C{=}O)\{Cp^*_2La\}_2(THF)]_2$ [63].

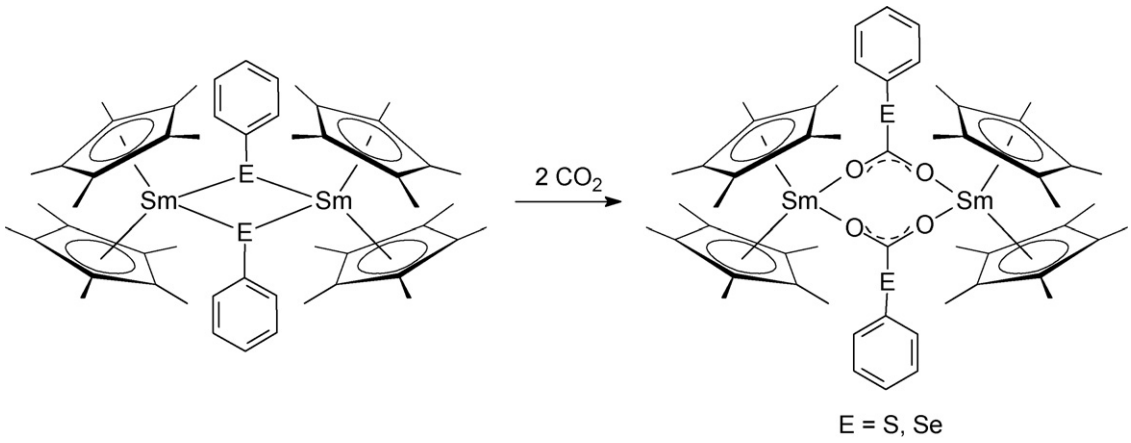

Scheme 68.

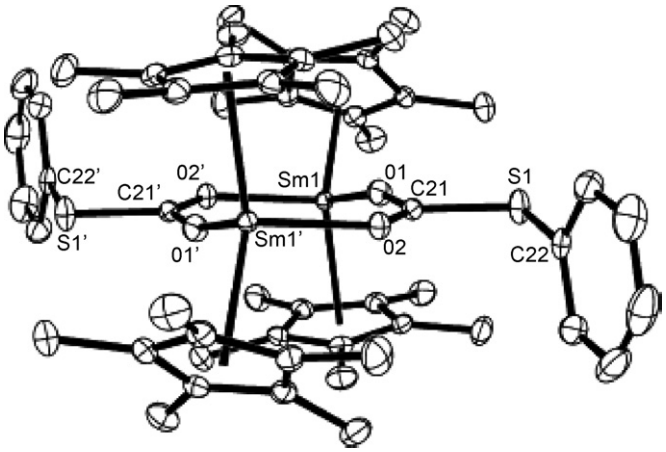

Fig. 22. Molecular structure of $[Cp^*_2Sm(\mu\text{-}O_2CSPh)]_2$ [64].

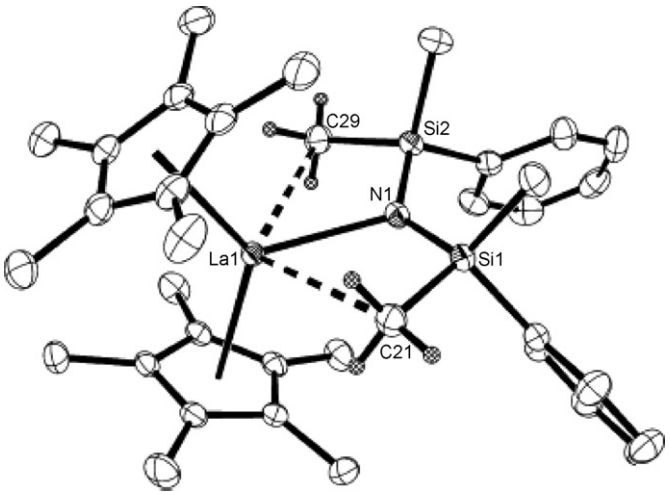

Fig. 23. Molecular structure of $Cp^*_2La[N(SiMe_2Ph)_2]$ [65].

$O_2CSePh)]_2$ decarboxylates in THF to form $Cp^*_2Sm(SePh)(THF)$. The loss of CO_2 rather than COSe with formation of $Cp^*_2Sm(OPh)(THF)$ was established by $^{13}CO_2$ studies and independent synthesis of $Cp^*_2Sm(OPh)(THF)$ from $Cp^*_2Sm[N(SiMe_3)_2]$ and PhOH [64].

The first solid-state ^{139}La NMR spectra of lanthanum-containing metallocenes, including $[Cp^*_2La][BPh_4]$, were reported in 2006 [54]. A lanthanide metallocene derivative of the bis(dimethylsilylphenyl)amide ligand, $[N(SiMe_2Ph)_2]^-$, was obtained by reaction of $K[N(SiMe_2Ph)_2]$ with $[Cp^*_2La][BPh_4]$ according to Scheme 69. Crystals of the product, $Cp^*_2La[N(SiMe_2Ph)_2]$, show agostic interactions between lanthanum and methyl groups of each silyl substituent (Fig. 23) [65].

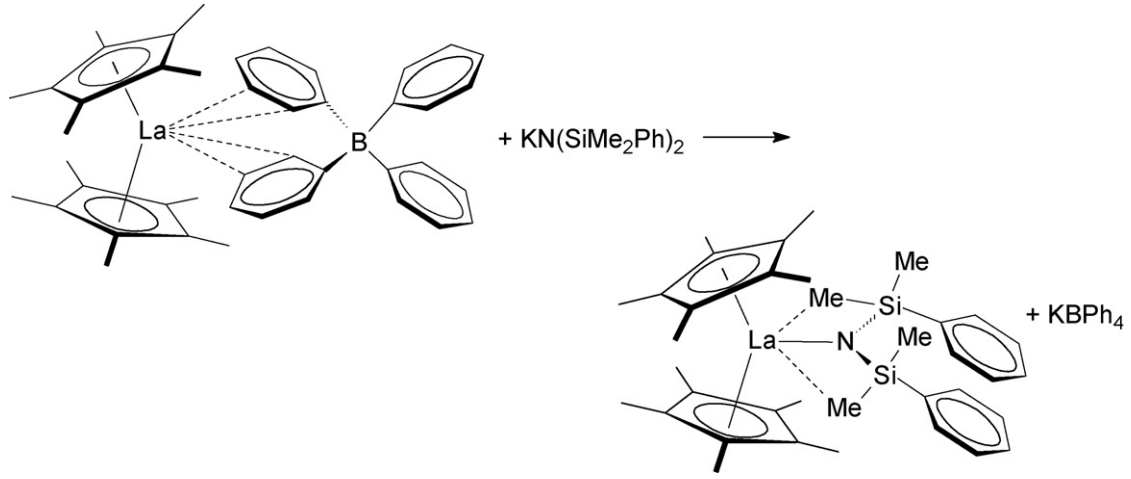

Scheme 69.

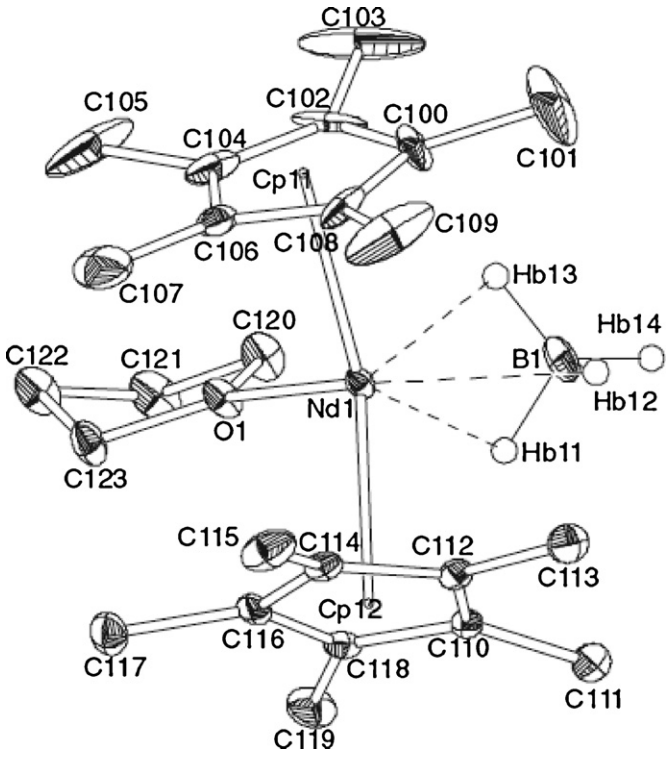

Fig. 24. Molecular structure of $Cp^*_2Nd(BH_4)(THF)$ [66].

$Cp^*_2Nd(BH_4)(THF)$ has been readily obtained in one step from $Nd(BH_4)_3(THF)_3$ and fully characterized. A single-crystal X-ray diffraction analysis revealed a *pseudo*-tetrahedral monomeric structure with a tridentate borohydride ligand as illustrated in Fig. 24. Associated to ^{n}BuEtMg, $Cp^*_2Nd(BH_4)(THF)$ affords a highly active catalyst for ethylene polymerization (*cf.* Section 2.11.2) [66].

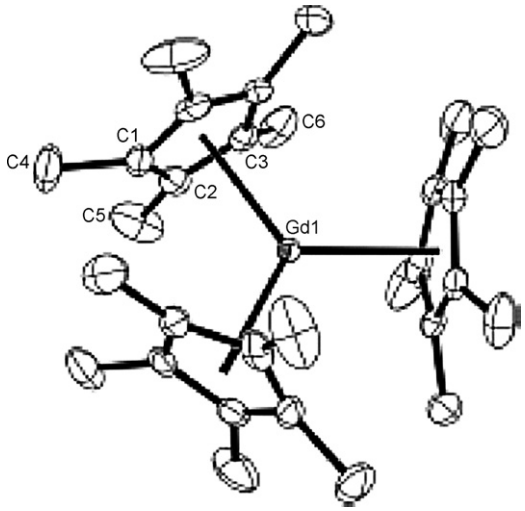

Fig. 25. Molecular structure of Cp^*_3Gd [67].

2.5.5.4. Tris(pentamethylcyclopentadienyl)lanthanide(III) compounds. The successful synthesis of the sterically crowded tris(pentamethylcyclopentadienyl) lanthanide complexes Cp^*_3Ln has demonstrated that organometallic complexes with unconventionally long metal ligand bond lengths can be isolated that provide options to develop new types of ligand reactivity based on steric crowding. Previously, the Cp^*_3Ln complexes were known only with the larger lanthanides La–Sm. The synthesis of even more crowded complexes of the smaller metals Gd and Y was

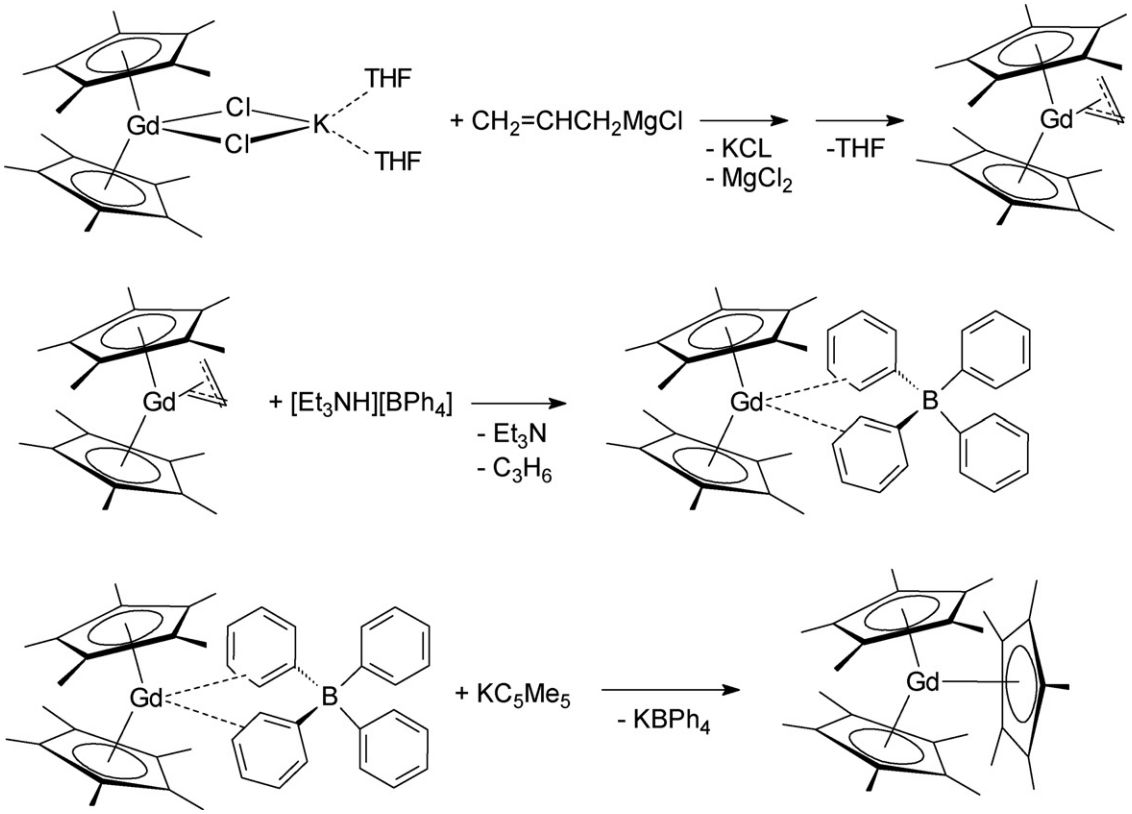

Scheme 70.

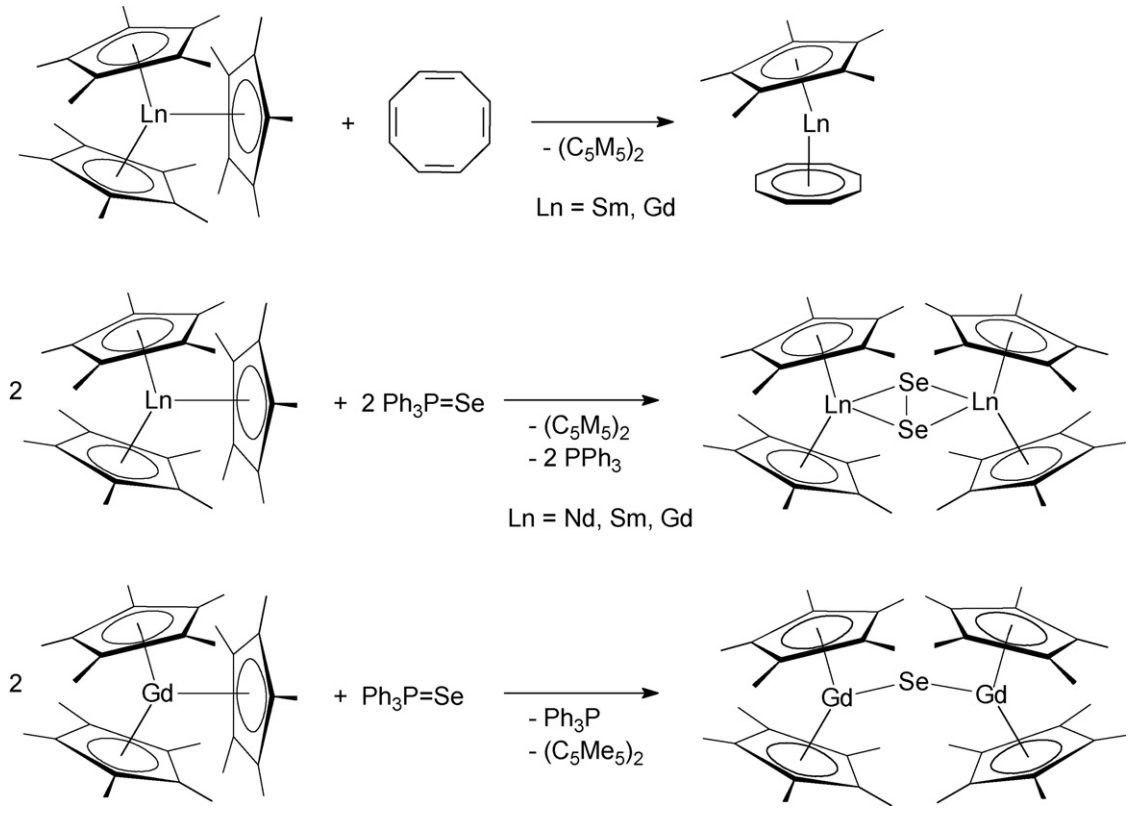

Scheme 71.

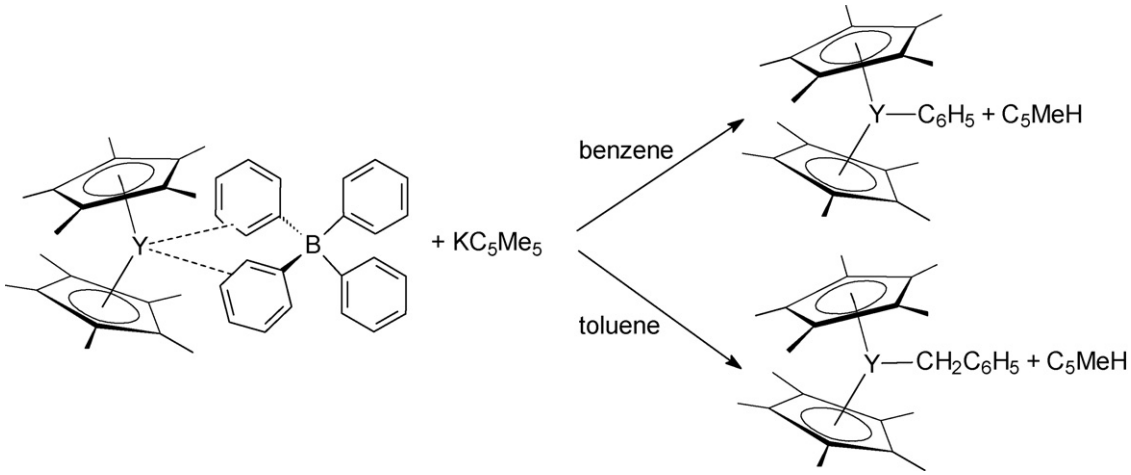

Scheme 72.

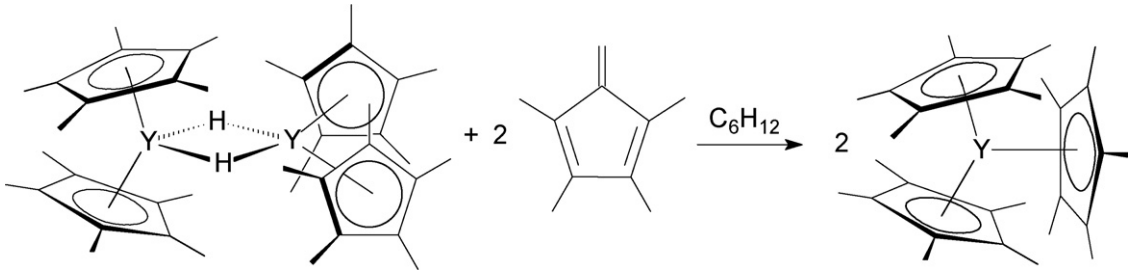

Scheme 73.

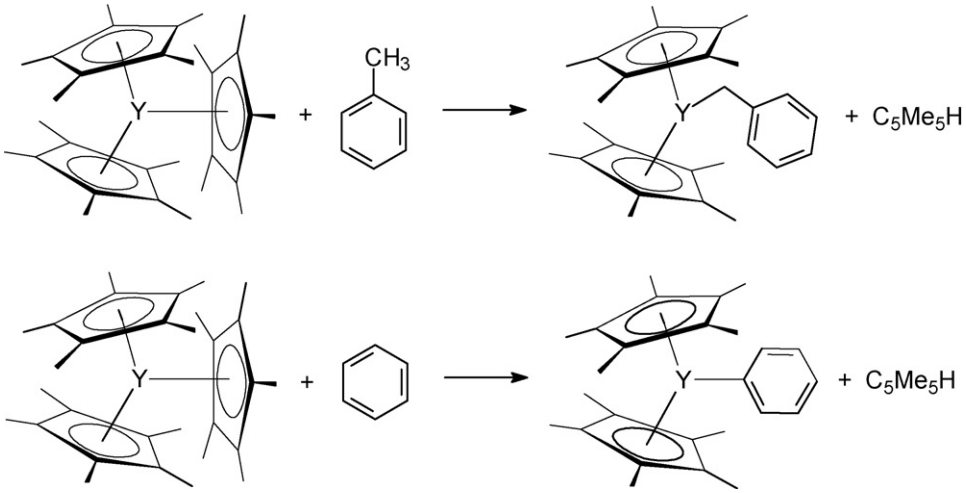

Scheme 74.

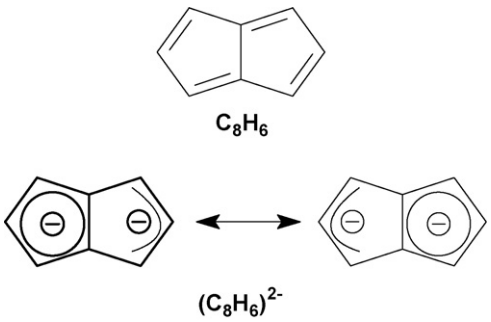

Scheme 75.

reported in 2006. These compounds allowed an evaluation of the size/reactivity correlations previously limited to the larger metals and demonstrated a previously undescribed type of Cp*-based reaction, namely C–H bond activation. Cp^*_3Gd was prepared from $GdCl_3$ through $Cp^*_2Gd(\mu\text{-}Cl)_2K(THF)_2$, $Cp^*_2Gd(C_3H_5)$, and $[Cp^*_2Gd][BPh_4]$ as shown in the reaction sequences shown in Scheme 70. The identity of Cp^*_3Gd was established by X-ray crystallography (Fig. 25) [67].

Although Gd^{3+} is redox-inactive, Cp^*_3Gd functions as a reducing agent in reactions with cyclooctatetraene (=COT) and triphenylphosphine selenide to make Cp*Gd(COT), $(\mu\text{-}Se_2)[Cp^*_2Gd]_2$, and $(\mu\text{-}Se)[Cp^*_2Gd]_2$ depending on the stoichiometry used (Scheme 71) [67].

When the analogous synthetic method as shown in Scheme 71 was attempted with yttrium in arene solvents (benzene, toluene), the previously characterized Cp^*_2YR complexes (R = Ph, CH_2Ph) were isolated instead, *i.e.* C–H bond activation of solvent occurred (Scheme 72) [67].

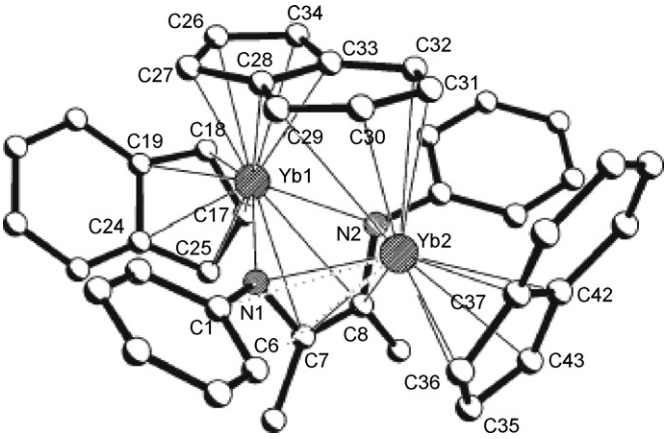

Fig. 26. Molecular structure of $Yb_2(\mu\text{-}\eta^5\text{:}\eta^4\text{-}C_9H_7)(\eta^5\text{-}C_9H_7)_2[\mu\text{-}\eta^4\text{:}\eta^4\text{-}PhNC(Me)\text{=}C(Me)NPh]$ [69].

To avoid this problem, Cp^*_3Y was synthesized according to Scheme 73 form $[Cp^*_2Y(\mu\text{-}H)]_2$ and tetramethylfulvene in aliphatic solvents. This method afforded pure Cp^*_3Y as an orange powder in 81% yield [67].

Once isolated, Cp^*_3Y was found to metalate benzene and toluene with concomitant formation of Cp*H (Scheme 74), a reaction contrary to the normal pK_a values of these hydrocarbons. In this case, the normally inert Cp^{*-} ligand engages in C–H bond activation due to the extreme steric crowding [67].

2.5.6. Pentalenyl, indenyl and fluorenyl compounds

DFT calculations with full geometry optimization were carried out on a series of real and hypothetical compounds containing

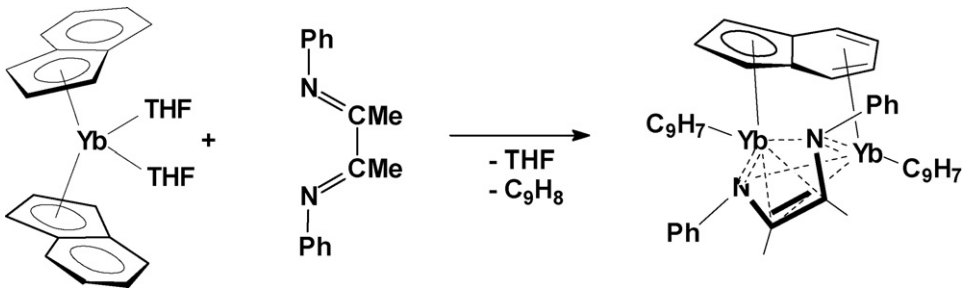

Scheme 76.

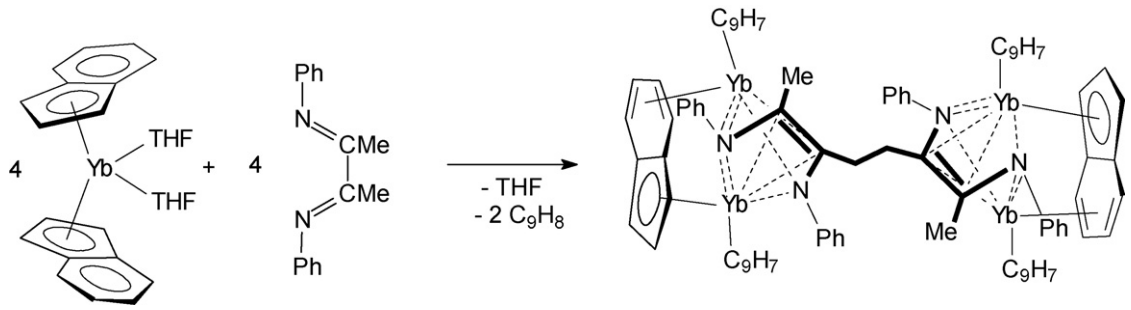

Scheme 77.

pentalenyl ligands (Scheme 75), including the scandium sandwich complex CpSc(C_8H_6) [68].

The outcome of the redox reaction of $(C_9H_7)_2Yb(THF)_2$ with the diazabutadiene ligand PhN=C(Me)–C(Me)=NPh (=DAD) was found to depend on the molar ratio of the reactants. Reaction in a 1:2 molar ratio according to Scheme 76 afforded the deep brown dinuclear mixed-valent complex $Yb_2(\mu\text{-}\eta^5\text{:}\eta^4\text{-}C_9H_7)(\eta^5\text{-}C_9H_7)_2[\mu\text{-}\eta^4\text{:}\eta^4\text{-PhNC(Me)=C(Me)NPh}]$ containing an indenyl ligand with an unusual $\mu\text{-}\eta^5\text{:}\eta^4$-bridging coordination. The molecular structure of this compound is depicted in Fig. 26 [69].

The analogous reaction of equimolar amounts of these compounds resulted in an organolanthanide-mediated reductive coupling of the DAD ligands and formation of the deep brown tetranuclear mixed-valent complex $[Yb_2(\mu\text{-}\eta^5\text{:}\eta^4\text{-}C_9H_7)(\eta^5\text{-}C_9H_7)_2[\mu\text{-}\eta^4\text{:}\eta^4\text{-PhNC(CH}_2\text{)=C(Me)NPh]}_2]$ (Scheme 77) with a novel tetradentate tetraimine ligand (Fig. 27) [69].

In a theoretical study, uni- and bimolecular C–H methane metathesis reactions of *ansa*-[bis(η^5-2-indenyl)methane]LnL (Ln = Sc, Y, Lu; L = Me, $CH_2{}^tBu$) with four *ansa*-indenyl ligands having various degrees of aromatic ring methylation were modeled with the MPW1K density functional and a relativistic effective core potential basis set. An analysis of theoretical trends as a function of metal and ligand indicated that, in contrast to the situation with analogous Cp^*_2Ln sandwich complexes, unimolecular metathesis reactions proceeding through tuck-in intermediates (Scheme 78) have significantly higher enthalpies of activation compared to alternative bimolecular pathways, so the latter dominate metathesis reactivity in every case under typical experimental conditions. The degree of methylation of the bis(indenyl) ligand was found to play no significant role in complex structure and reactivity [70].

The synthesis, characterization and catalytic activity of organolanthanide(II) complexes with 2-pyridylmethyl- and 3-pyridylmethyl-functionalized indenyl ligands were reported. The synthetic routes are outlined in Schemes 79 and 80. The lanthanide(III) amides $[(Me_3Si)_2N]_3Ln(\mu\text{-Cl})Li(THF)_3$ (Ln = Yb, Eu) were employed as starting materials, and in all cases reduction to the corresponding homoleptic lanthanide(II) products occurred [71].

In the case of a closely related indenyl ligand having a pendant piperidylethyl moiety, evidence was found for the first example of an organolanthanide(II) compound having an indenyl ligand bonded to the metal through the benzo ring in η^4-hapticity. Again the ytterbium(II) amide complex $[(Me_3Si)_2N]_3Yb(\mu\text{-Cl})Li(THF)_3$ was used as starting material in the protonolysis reaction with 2 equiv. of the free ligand as shown in Scheme 81. An X-ray structure analysis clearly revealed the peculiar η^4-bonding of ytterbium to one of the benzo rings (Fig. 28) [72].

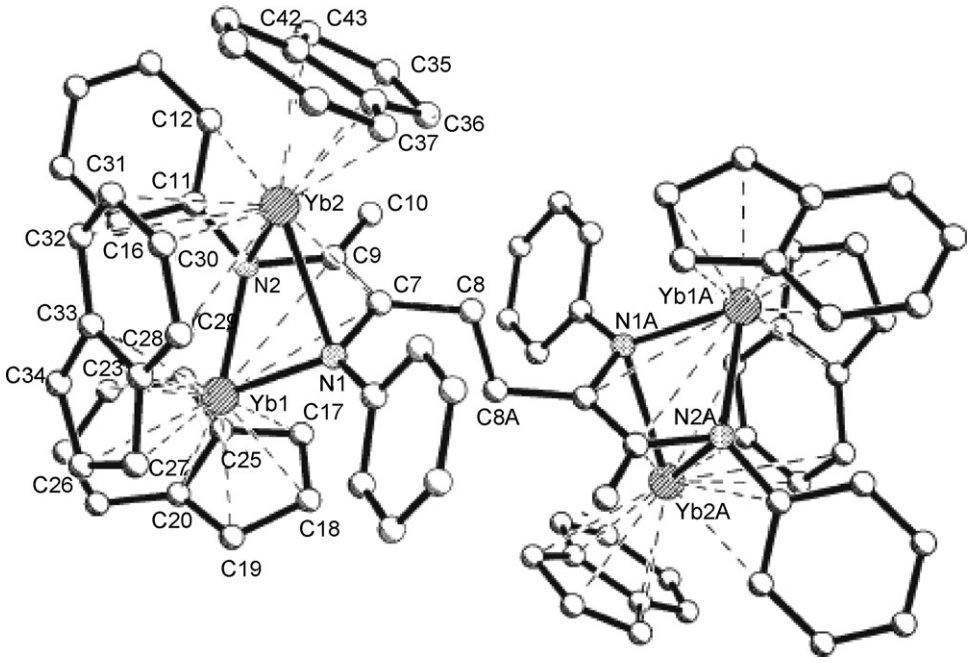

Fig. 27. Molecular structure of $[Yb_2(\mu\text{-}\eta^5\text{:}\eta^4\text{-}C_9H_7)(\eta^5\text{-}C_9H_7)_2[\mu\text{-}\eta^4\text{:}\eta^4\text{-PhNC(CH}_2\text{)=C(Me)NPh]}_2]$ [69].

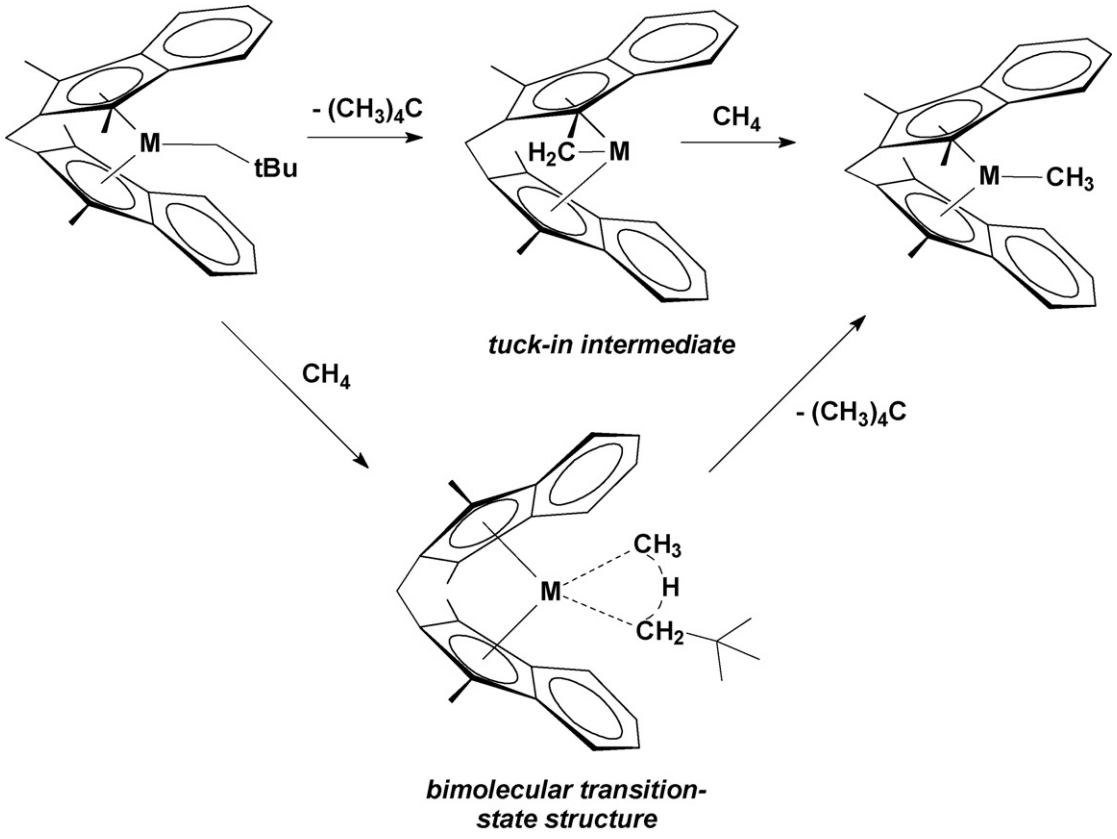

Scheme 78.

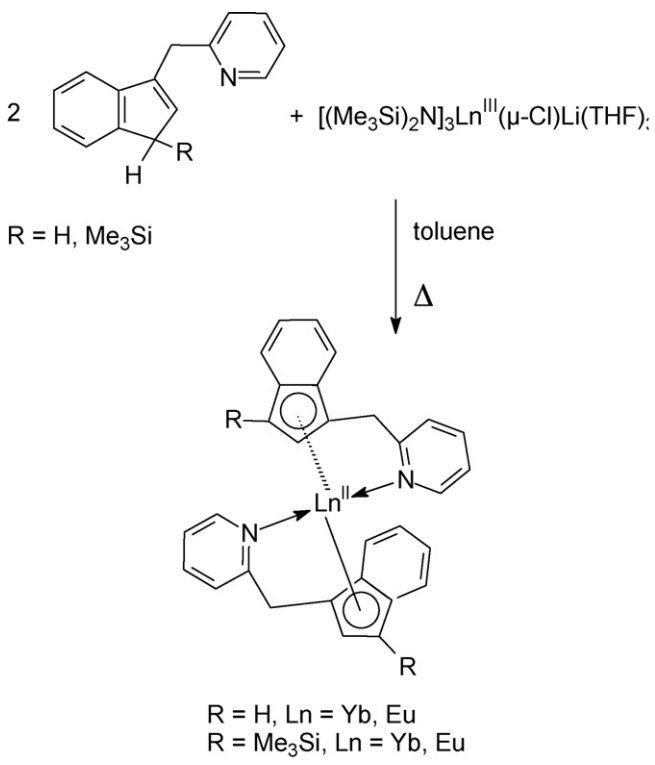

Scheme 79.

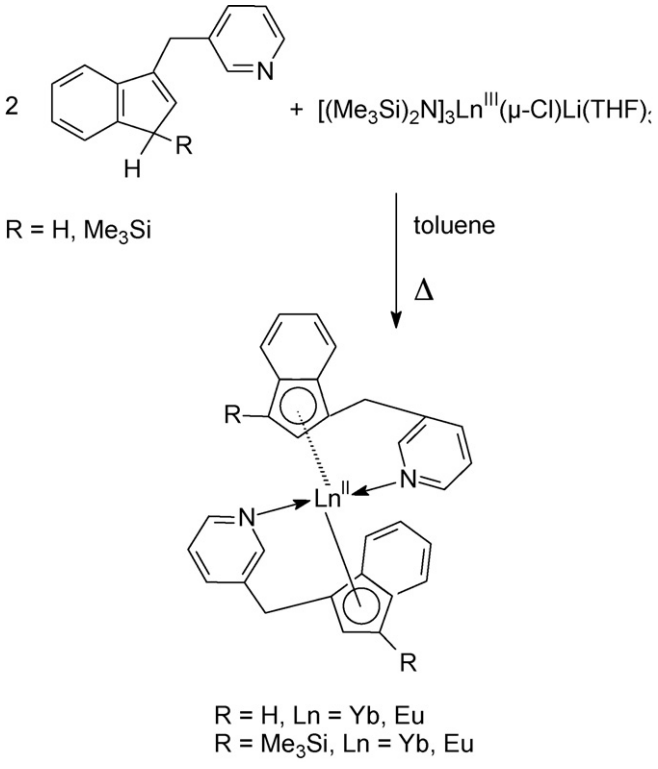

Scheme 80.

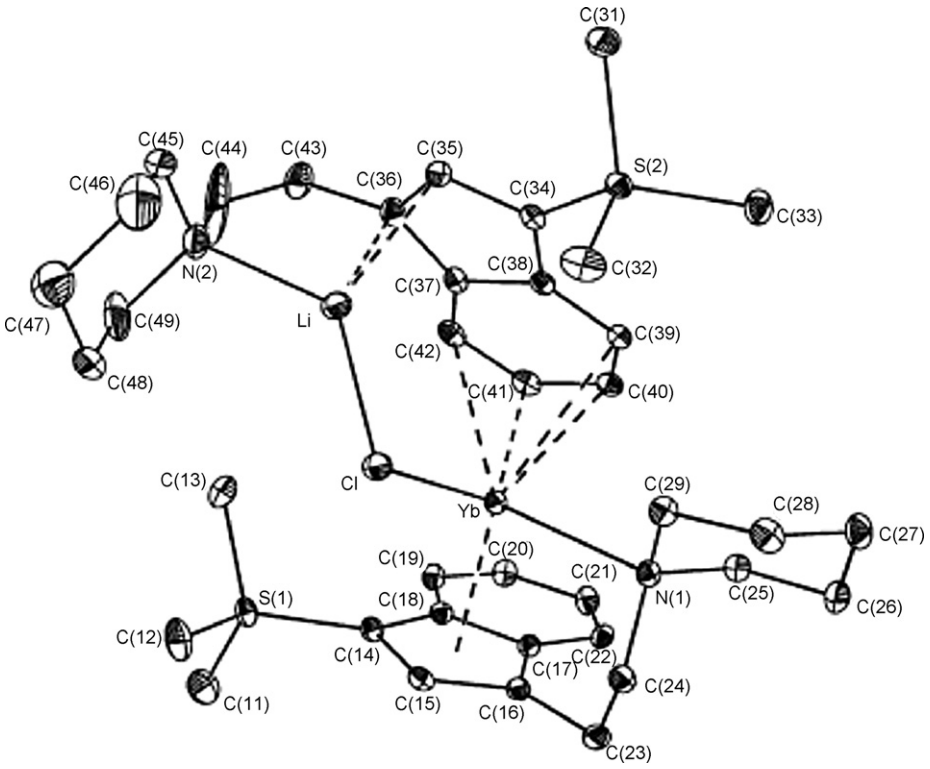

Fig. 28. Molecular structure of $[\eta^4{:}\eta^2{:}\eta^1\text{-}(C_5H_{10}NCH_2CH_2C_9H_5SiMe_3)Li(\mu\text{-}Cl)]Yb(\eta^5{:}\eta^1\text{-}C_5H_{10}NCH_2CH_2C_9H_5SiMe_3)$ [72].

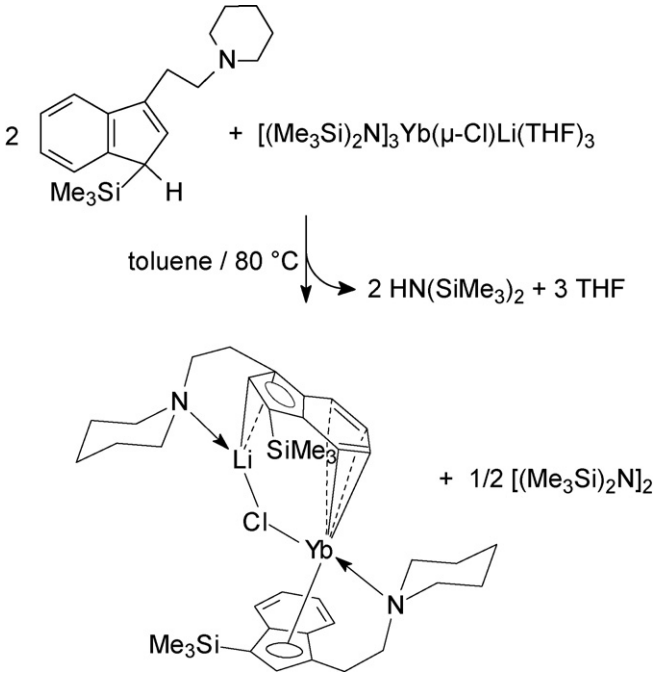

Scheme 81.

2.6. Organolanthanide complexes with cyclopentadienyl-like ligands

2.6.1. Compounds with heteroatom five-membered ring ligands

A new methylene-bridged ligand incorporation both indenyl and pyrrolyl moieties was prepared in low yield (27%) according to Scheme 82 [73].

Reactions of LnI_2 (Ln = Sm, Yb) with the dilithiated ligand followed by recrystallization from DME afforded the corresponding dinuclear organolanthanide(II) complexes as DME solvates in moderate yields (Scheme 83). The samarium(II) compound was isolated in the form of black crystals, while the ytterbium(II) complex crystallizes as dark red blocks [73].

Dimeric "ate" complexes incorporating lithium chloride were obtained when the dilithiated ligand was treated with either $SmCl_3$ or $ErCl_3$. The products are depicted in Scheme 84 [73].

The synthesis, characterization, and reactivity of new tetramethylphospholyl complexes of scandium was reported. Reaction of $(C_4Me_4P)Li(TMEDA)$ (TMEDA = tetramethylethylenediamine) with $ScCl_3(THF)_3$ in a molar ratio of 2:1 gave the new compound $(\eta^5\text{-}C_4Me_4P)_2Sc(\mu\text{-}Cl)_2Li(TMEDA)$ (Scheme 85), which was characterized by X-ray crystallography. The product is a typical "*ate*-complex" formed through incorporation of lithium chloride in order to increase the coordination number around the scandium center [74].

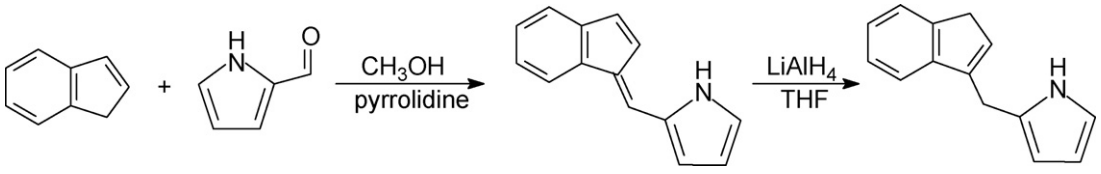

Scheme 82.

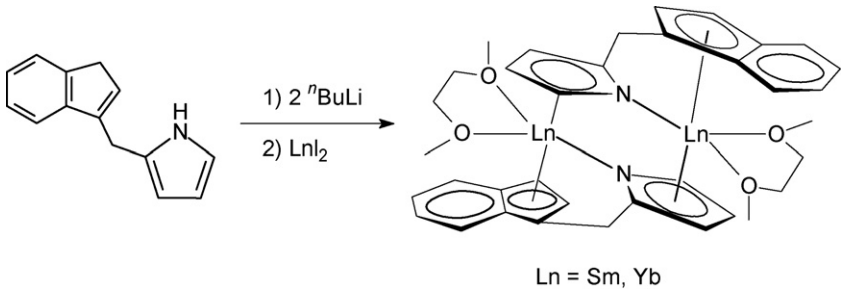

Scheme 83.

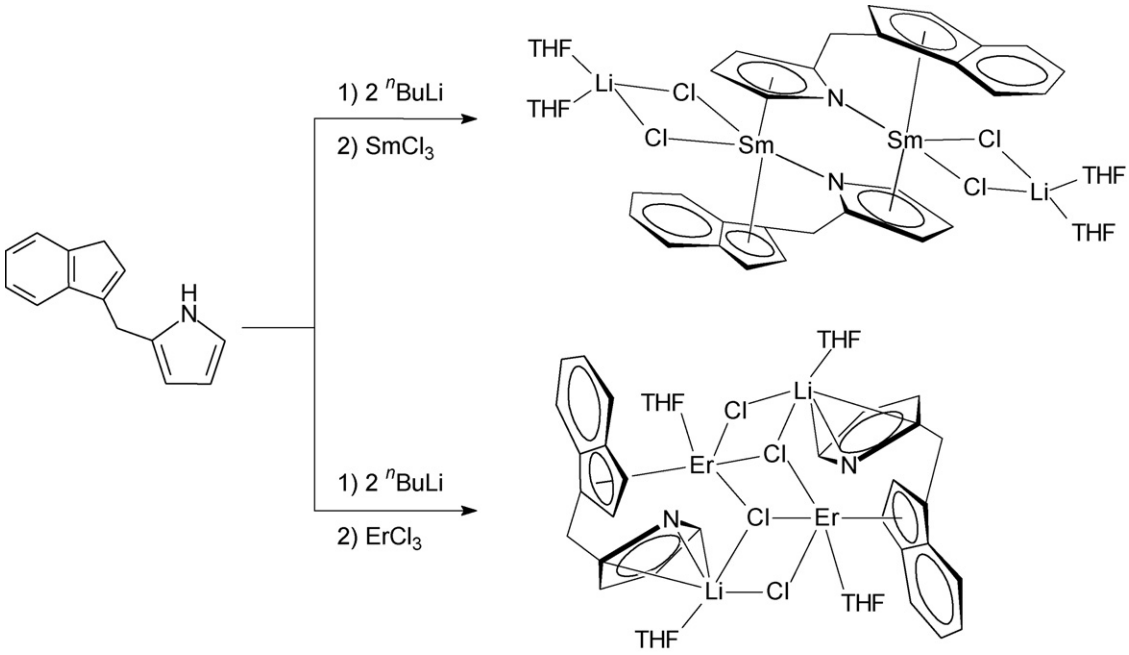

Scheme 84.

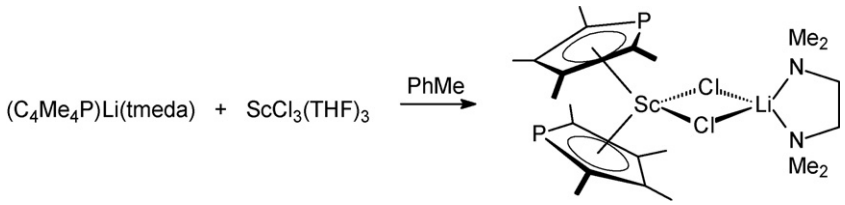

Scheme 85.

Reactions of $(\eta^5\text{-}C_4Me_4P)_2Sc(\mu\text{-}Cl)_2Li(TMEDA)$ with organolithium reagents showed that one phospholyl moiety in this complex is labile, as demonstrated *e.g.* by the reaction with $LiCH(SiMe_3)_2$ according to Scheme 86. Attempts to generate σ-alkyl derivatives of the general type $(\eta^5\text{-}C_4Me_4P)_2ScR$ (R = alkyl) using this approach were unsuccessful [74].

Treatment of $(\eta^5\text{-}C_4Me_4P)_2Sc(\mu\text{-}Cl)_2Li(TMEDA)$ with LiCp* also resulted in replacement of one phospholyl group by a Cp* ligand and

Scheme 86.

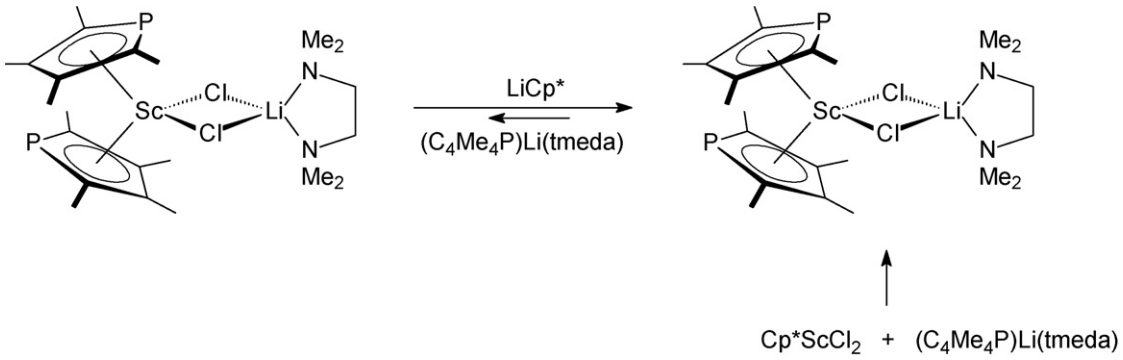

Scheme 87.

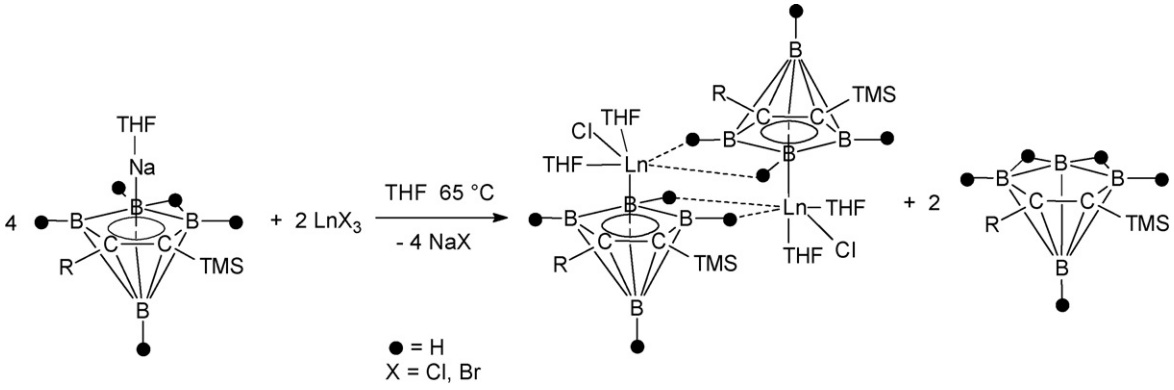

Scheme 88. TMS = $SiMe_3$.

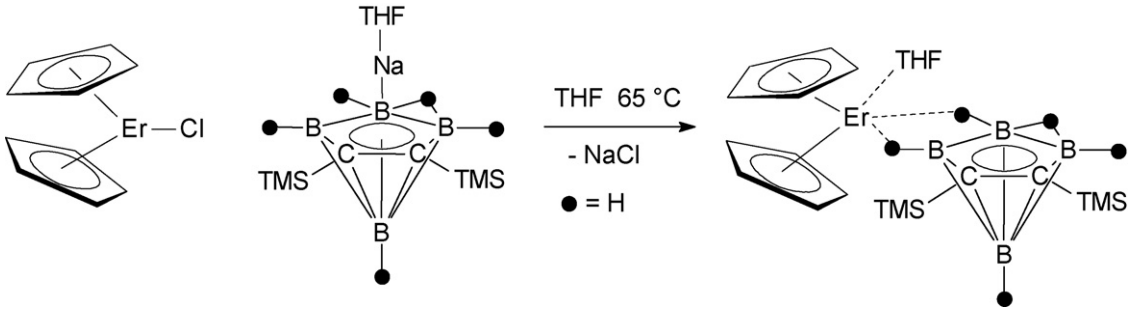

Scheme 89.

formation of (η^5-C_4Me_4P)Cp*Sc(μ-Cl)$_2$Li(TMEDA) as illustrated in Scheme 87. The same compound was obtained when Cp^*ScCl_2 was allowed to react with (C_4Me_4P)Li(TMEDA) [74].

2.6.2. Compounds with carboranyl ligands

The reactivity of the monosodium-complexed carborane precursors *nido*-1-Na(THF)-2-(R)-3-($SiMe_3$)-2,3-$C_2B_4H_5$ (R = Me, $SiMe_3$) with a number of lanthanide trihalides was investigated. Numerous half-sandwich lanthanacarborane complexes were isolated in high yields according to Scheme 88. Virtually all elements of the lanthanide series were employed in this study, and most of the products were structurally characterized by X-ray diffraction. The characteristic molecular structure of the half-sandwich lanthanacarboranes is displayed in Fig. 29, in which the solvate THF

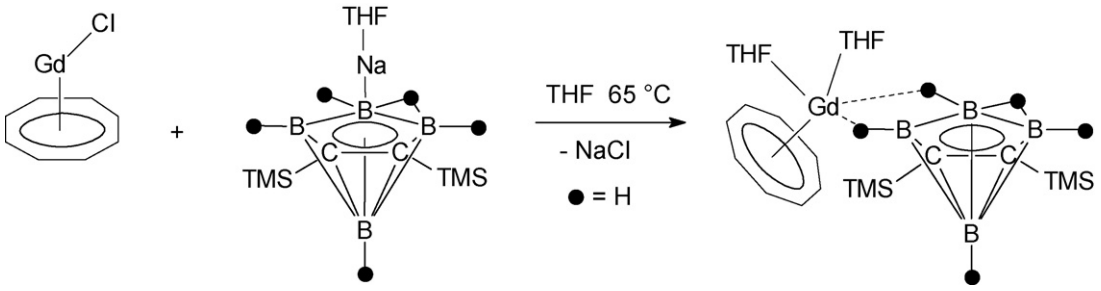

Scheme 90.

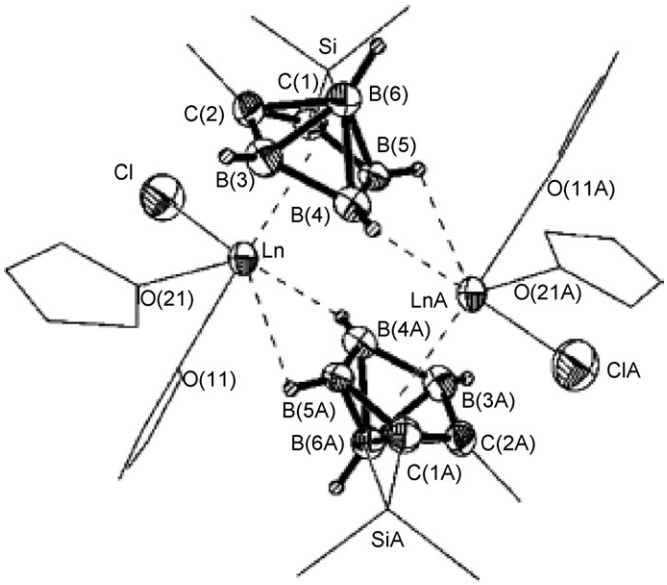

Fig. 29. Molecular structure of the half-sandwich lanthanacarboranes [75].

molecules and the *exo*-polyhedral $SiMe_3$ groups are drawn with thin lines [75].

In contrast, reactions of *nido*-1-Na(THF)-2,3-$(SiMe_3)_2$-2,3-$C_2B_4H_5$ with Cp_2ErCl (Scheme 89) and $(C_8H_8)GdCl$ (Scheme 90) in 1:1 molar ratios did not produce the half-sandwich lanthanacarboranes, but rather afforded the corresponding *exo*-polyhedral products as crystalline solids in 76 and 73% isolated yield, respectively. The molecular structure of the (cyclooctatetraenyl) gadolinium derivative is shown in Fig. 30 [75].

Two new directly attached carboranyl–indenyl compounds 2-(*o*-carboranyl)indene and 1-(*o*-carboranyl)indene were synthesized and their applications in lanthanide chemistry were explored. The two ligands were prepared by reactions of 2-indanone or indene epoxide with $Li_2C_2B_{10}H_{10}$ followed by dehydration reactions. Treatment of 2-(*o*-carboranyl)indene with excess sodium metal afforded an intermediate trisodium salt which upon subsequent treatment with anhydrous $LnCl_3$ (Ln = Y, Er) produced dinuclear indenyl–lanthanacarboranes as illustrated in Scheme 91 [76].

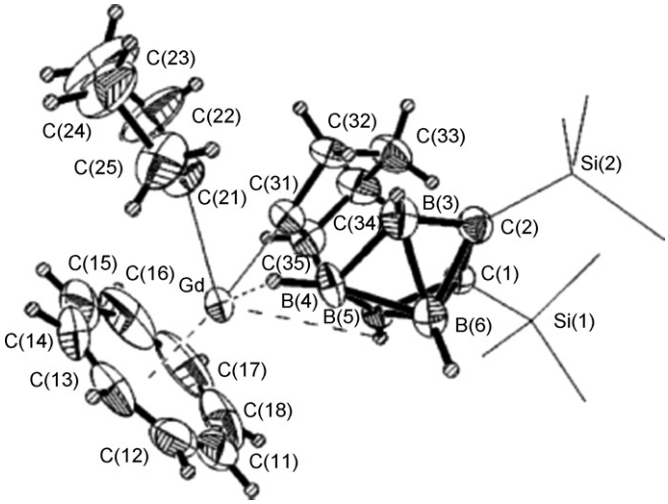

Fig. 30. Molecular structure of *exo*-(C8H8)Gd[4,5-(μ-H)-2,3-$(SiMe_3)_2$-2,3-$C_2B_4H_4$](THF)$_2$ [75].

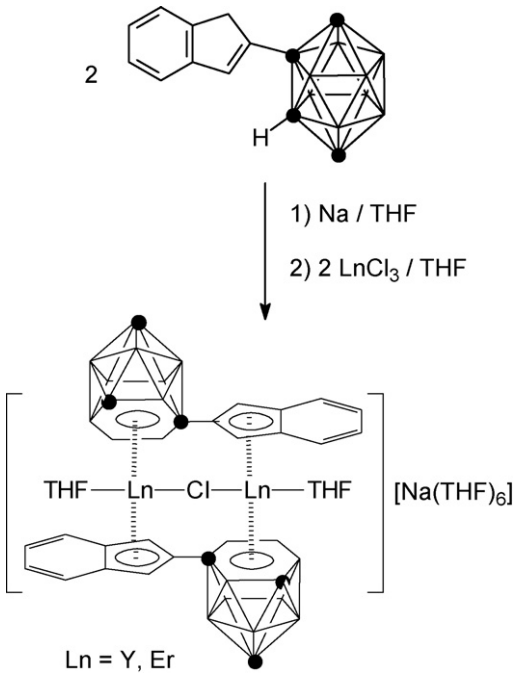

Scheme 91.

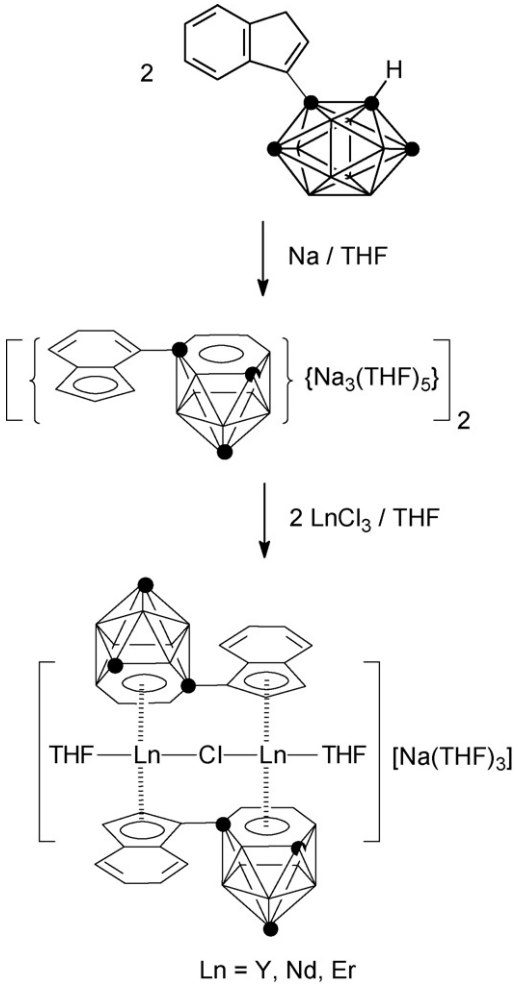

Scheme 92.

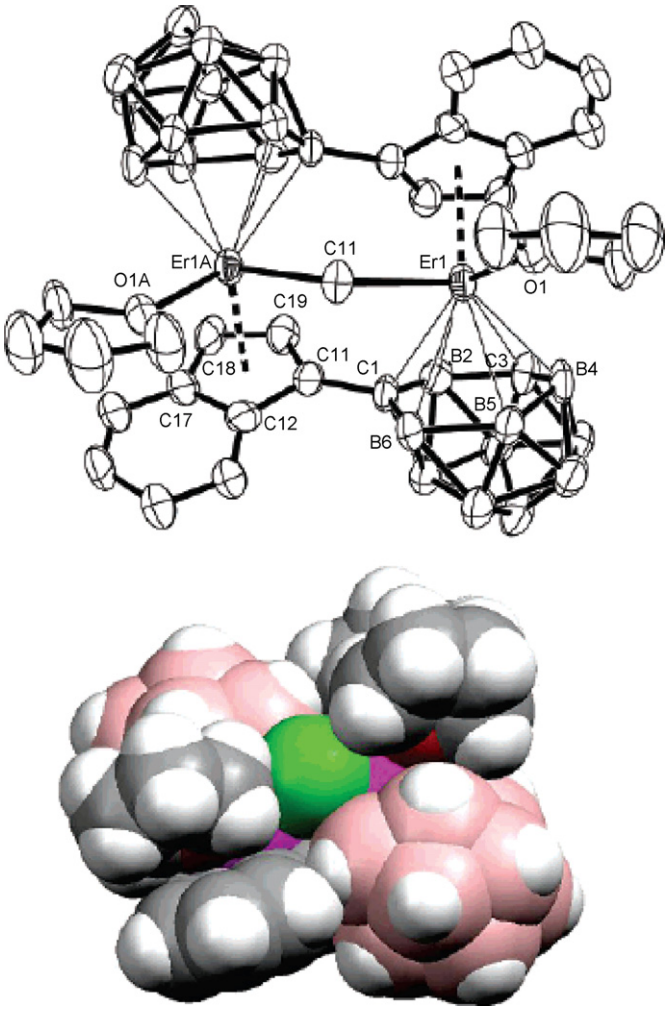

Fig. 31. Top: molecular structure of the anion in $[Na(THF)_3][\{\eta^5{:}\eta^6\text{-}(1\text{-}C_9H_6)(C_2B_{10}H_{11})Er(THF)\}_2(\mu\text{-}Cl)]$. Bottom: space-filling drawing of the anion [76].

In a similar manner, 1-(*o*-carboranyl)indene reacted with excess sodium metal yielding a trisodium intermediate bearing a six-membered C_2B_4 open face and a five-membered C_5 bonding face (Scheme 92). Reaction of this intermediate with $LnCl_3$ (Ln = Y, Nd, Er) afforded again dinuclear, chloro-bridged indenyl–lanthanacarborane complexes as shown in Scheme 92 [76].

An examination of the chemical properties of the indenyl–lanthanacarborane complexes shown in Schemes 91 and 92 revealed that they were surprisingly inert toward nucleophiles such as $NaBH_4$, CH_3COONa, sodium acetylacetonate, and $KOBu^t$ and toward chlorine-abstracting reagents such as AgOTf (OTf = triflate anion) and $AgNO_3$. To help understand these results, the space-filling drawing of the anion in the Er complex shown in Scheme 92 was generated using X-ray data (Fig. 31). The figure clearly shows that the coordination sphere of the lanthanide ion is fully occupied by the surrounding ligands, which prevents the lanthanide ion from any attack of nucleophiles. On the other hand, although the bridging Cl atom is accessible by Ag^+, such interactions may not be strong enough to break the Ln–Cl–Ln bonds [76].

A borohydride-bridged erbium complex of this type was synthesized by treatment of the trisodium salt of the ligand with $Er(BH_4)_3(THF)_3$ according to Scheme 93. The yellow crystalline material was isolated in 74% yield. Treatment of this borohydride with excess sodium metal generated the unbridged dinuclear erbium complex $[Na_4(THF)_8][\eta^5{:}\eta^7\text{-}(1\text{-}C_9H_6)(C_2B_{10}H_{11})Er(THF)_2]_2$ which was also isolated in the form of yellow crystals (68% yield, Scheme 93). The molecular structures of the two dinuclear erbium complexes are shown in Figs. 32 and 33 [76].

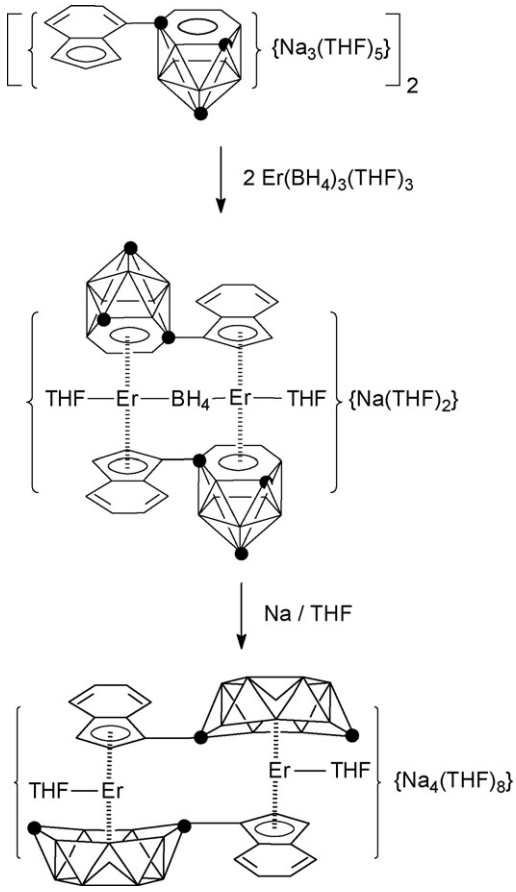

Scheme 93.

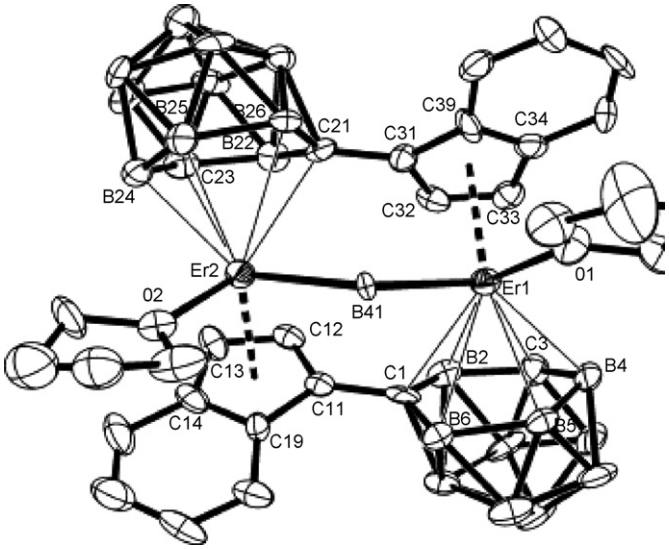

Fig. 32. Molecular structure of the anion in $[Na(THF)_2][\{\eta^5{:}\eta^6\text{-}(1\text{-}C_9H_6)(C_2B_{10}H_{11})Er(THF)\}_2(\mu\text{-}BH_4)]$ [76].

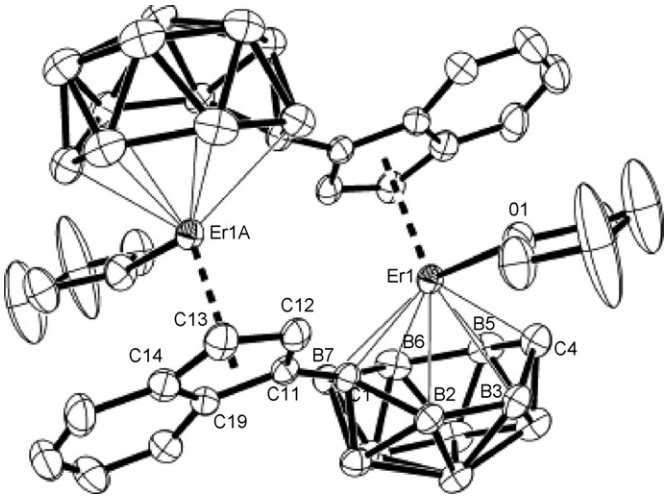

Fig. 33. Molecular structure of the anion in $[Na_4(THF)_8][\eta^5{:}\eta^7\text{-}(1\text{-}C_9H_6)(C_2B_{10}H_{11})Er(THF)_2]_2$ [76].

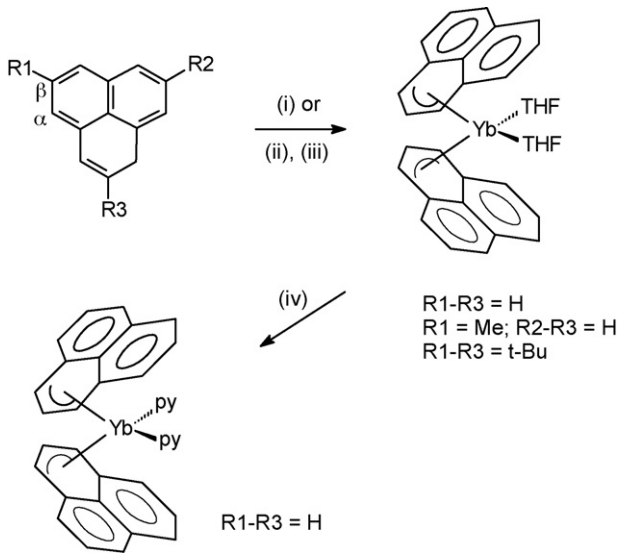

Scheme 94. Reagents and conditions: (i) $Yb[N(SiMe_3)_2](THF)_2$ (0.5 equiv.), toluene, 18 h; (ii) ^{n}BuLi (1 equiv.), THF, 0 °C; (iii) YbI_2 (0.5 equiv.), THF, 18 h; (iv) excess pyridine, 1 h, RT.

2.7. Lanthanide arene complexes

The scandium arene complex Sc(biphenyl), $Sc(C_{12}H_{10})$, was prepared by the reaction of scandium atoms and biphenyl vapor in a supersonic molecular beam source. From high-resolution photoelectron spectroscopy a clamshell structure was deduced for this compound, while a half-sandwich structure with Sc bonded to one phenyl ring only could be ruled out [77]. The electronic and magnetic properties of one-dimensional transition metal benzene sandwich polymers, including the paramagnetic scandium derivative $[Sc(C_6H_6)]_\infty$, have been investigated by means of density functional calculations [78].

The synthesis, X-ray structure and fluxional behavior of the first lanthanide complexes containing delocalized phenalenide anions were reported. Scheme 94 illustrates the preparative routes leading to ytterbium(II) complexes of this type [79].

Fig. 34 depicts the molecular structure of the bis(THF) adduct containing tri-*tert*-butylphenalenide ligands (red crystals). The latter are bonded to Yb(II) in an η^3-allylic fashion. ^{1}H NMR experiments showed a rapid migration of the η^3-bonded metal center between the ring systems of the π-system, thus establishing the first example for a degener-

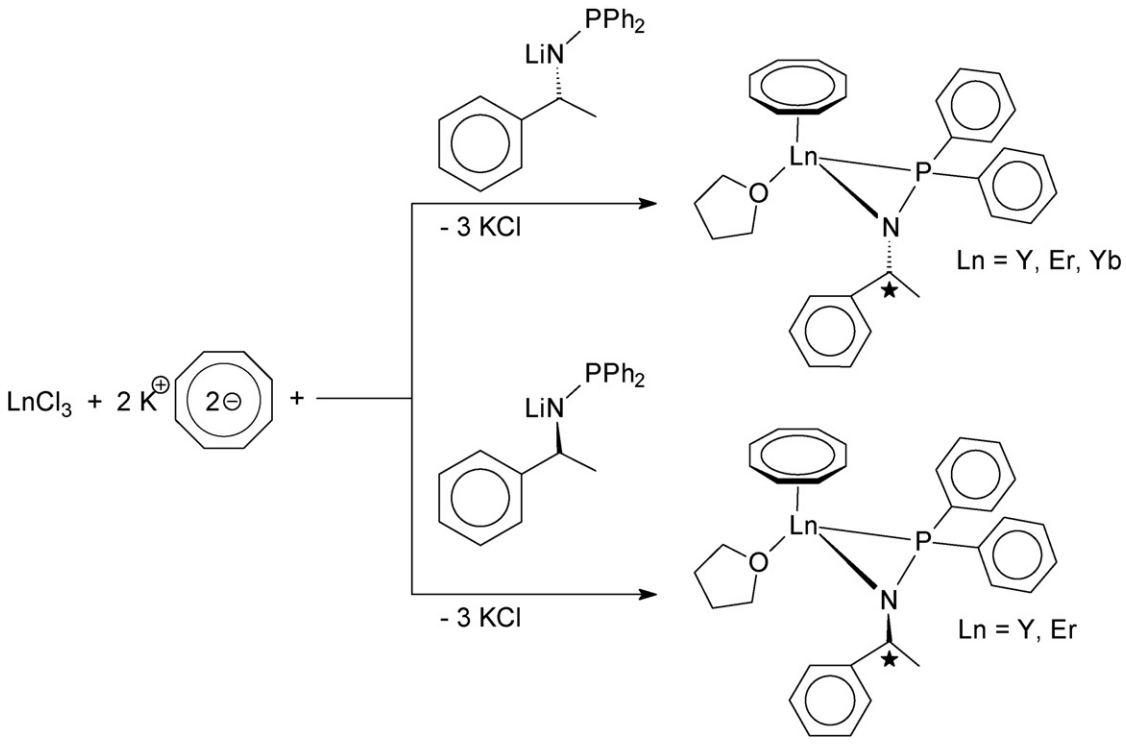

Scheme 95.

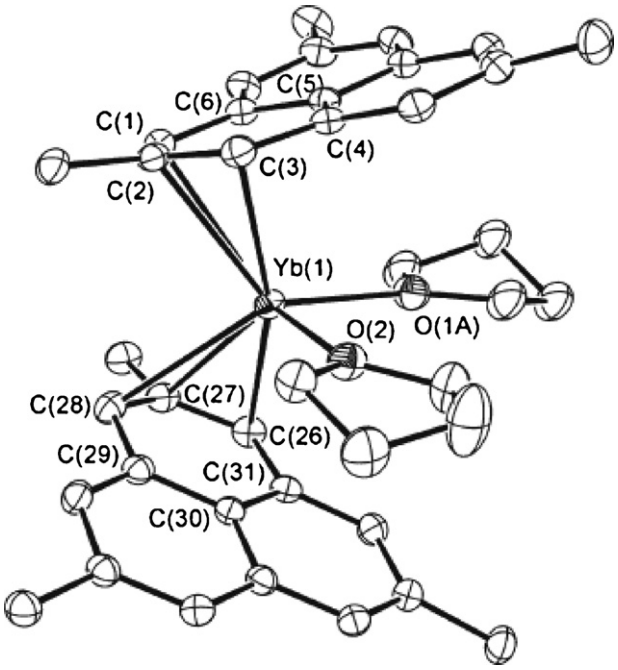

Fig. 34. Molecular structure of bis(tri-*tert*-butylphenalenide)Yb(THF)$_2$ (^{t}Bu methyl groups omitted for clarity) [79].

ate haptotropic rearrangement in organolanthanide chemistry [79].

2.8. Lanthanide cyclooctatetraenyl complexes

Chiral phosphanylamide ligands were introduced into rare-earth chemistry for the first time in 2006. In the course of this work, enantiomerically pure cyclooctatetraenyl lanthanide complexes containing these ligands were prepared according to Scheme 95 and their structures confirmed by single-crystal X-ray diffraction [80].

A rare example of a solvated trivalent mixed-ligand cyclopentadienyl/cyclooctatetraenyl compound was reported. Green needle-like crystals of (μ-dioxane)[Cp*Nd(COT)]$_2$ were isolated from a reaction mixture of [Cp*$_2$Nd][(μ-Ph)$_2$BPh$_2$] and K$_2$(COT) in benzene and crystallized from dioxane. The inverse-sandwich complex (μ-η^8:η^8-COT)[Cp*Yb(MeO^{t}Bu)]$_2$ was prepared in high yield (93%) to determine if, and how, methyl *tert*-butyl ether (=MTBE) would coordinate to a lanthanide. Orange needles of this compound crystallized readily from a solution of (μ-η^8:η^8-COT)[Cp*Yb]$_2$ in MTBE [62].

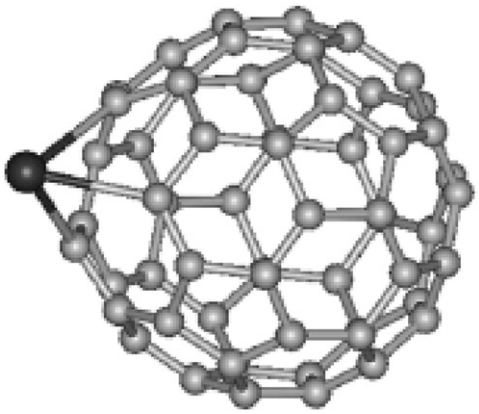

Fig. 35. The optimized structure of SmC$_{59}$ [83].

2.9. Lanthanide metallofullerenes

In a more general study, ultraviolet photoelectron spectra of mono- and multiple metal atoms entrapped metallofullerenes were compared and discussed for the effect of the metal atoms to the cage. Encapsulation of mono-metal atom was found to cause hardly any drastic change to the electronic structure of the cage, but it seems to be affected by multiple atom encapsulation [81]. A DFT investigation of substitutionally doped fullerenes MC$_{59}$ of second- and third-row transition metals (including Sc and Y) showed that their stability increases toward the right-hand side of the d-block. Whereas the structural deviation from that of C$_{60}$ depends on the size of the metal atom, stability is governed by electronic properties of the transition metal atom [82]. The geometric and electronic structures of metal-substituted fullerene SmC$_{59}$ and exohedral fullerene SmC$_{60}$ were studied using density functional theory. The geometric optimization showed that the replacement of a C atom with a Sm in C$_{60}$ yields a stable substitutionally doped fullerene SmC$_{59}$ (Fig. 35), and among the five possible optimized geometries for SmC$_{60}$, the most favorable exohedral sites are above the center of a hexagon and a pentagon ring. Because of the small energy gaps and the half occupation of the highest occupied molecular orbitals,

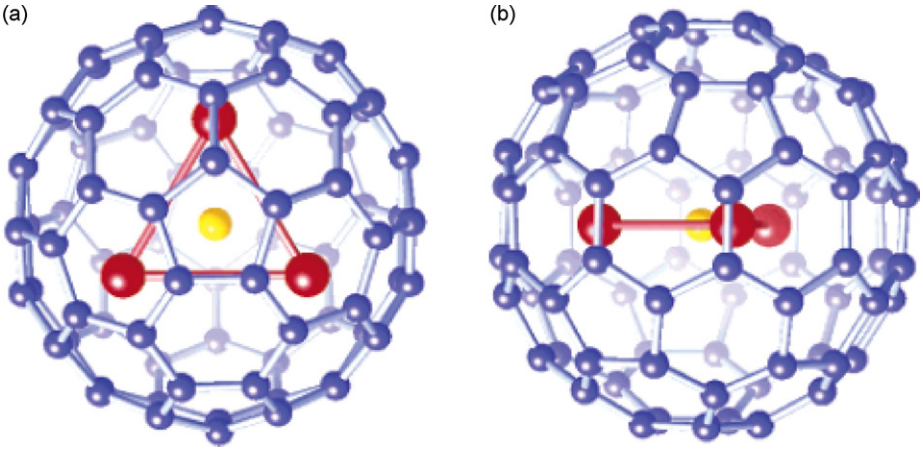

Fig. 36. The molecular structure models of (Sc$_3$C$_2$)@C$_{80}$ viewed along the (a) S_{10} and (b) C_2 axes determined by the MEM/Rietveld method from synchrotron X-ray powder diffraction data [85].

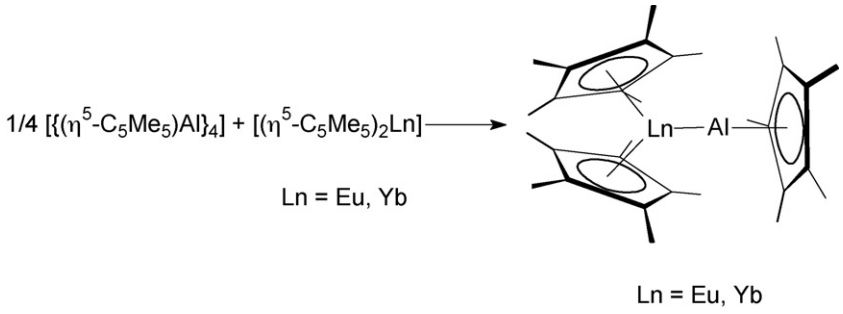

Scheme 96.

all the stable SmC_{60} isomers are inferred to be conductors. For SmC_{59} the calculations showed that it is possibly a semiconductor [83].

Several interesting papers dealing with endohedral metallofullerenes of scandium were published in 2006. A remarkable achievement in this field was the isolation and characterization of $Sc_2C_2@C_{68}$, the first metal-carbide endofullerene having a non-IPR (=isolated pentagon rule) cage. The IPR states that in the most stable fullerenes the pentagons are isolated from each other by hexagons. $Sc_2C_2@C_{68}$ was isolated as a black powder in low yield (0.1% of that of C_{70}) by adapting the procedures well established for the preparation of other scandium metallofullerenes. It was possible to clearly rule out by ^{13}C NMR spectroscopy the simple endohedral $Sc_2@C_{70}$ structure and to verify the metal-carbide structure $Sc_2C_2@C_{68}$. The successful isolation and characterization of $Sc_2C_2@C_{68}$ in combination with previous work on $Sc_3N@C_{68}$ showed that endohedral clusters such as Sc_2C_2 and Sc_3N can function as templates for the synthesis of different non-IPR C_{68} cages [84].

The X-ray structure of the open-shell metal-carbide endofullerene $(Sc_3C_2)@C_{80}$ (=Sc_3C_{82}) was redetermined by the MEM/Rietveld method by using synchrotron radiation powder data. The encapsulated three scandium atoms form a triangle inside a C_{80} fullerene cage. A spherical charge distribution originating from the C_2 molecule is located at the center of the triangle (Fig. 36). Interatomic distances between Sc and C are 3.61(3) Å in the triangle. The distance between Sc and the center of the C_2 molecule is 2.07(1) Å [85]. Density functional theory calculations showed that $(Sc_3C_2)@C_{80}$ has the valence state $(Sc^{3+})_3(C_2)^{3-}@C_{80}{}^{6-}$ [86]. In the previous literature, the scandium dimetallofullerene Sc_2C_{84} was widely believed to have the form $Sc_2@C_{84}$. However, a ^{13}C NMR spectroscopic study published in 2006 revealed that it is a scandium carbide metallofullerene, $Sc_2C_2@C_{82}$, which has a

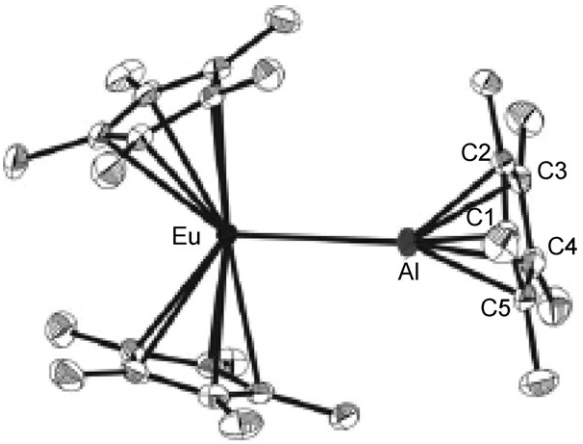

Fig. 37. Molecular structure of $Cp^*{}_2Eu–AlCp^*$ [89].

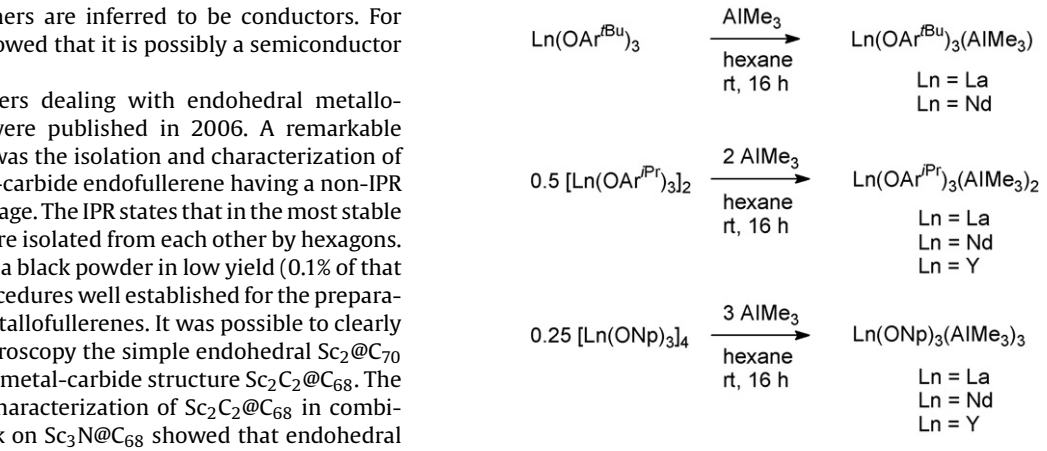

Scheme 97.

$C_{82}(C_{3v})$ cage structure [87]. In a theoretical study the geometric and electronic properties of the closely related scandium carbide-encaged fullerene derivative $Sc_2C_2@C_{84}$ were investigated. The Sc_2C_2 cluster was found to be stable inside the C_{84} cage, while the cage expands slightly. The Sc_2C_2 cluster can rotate freely in the

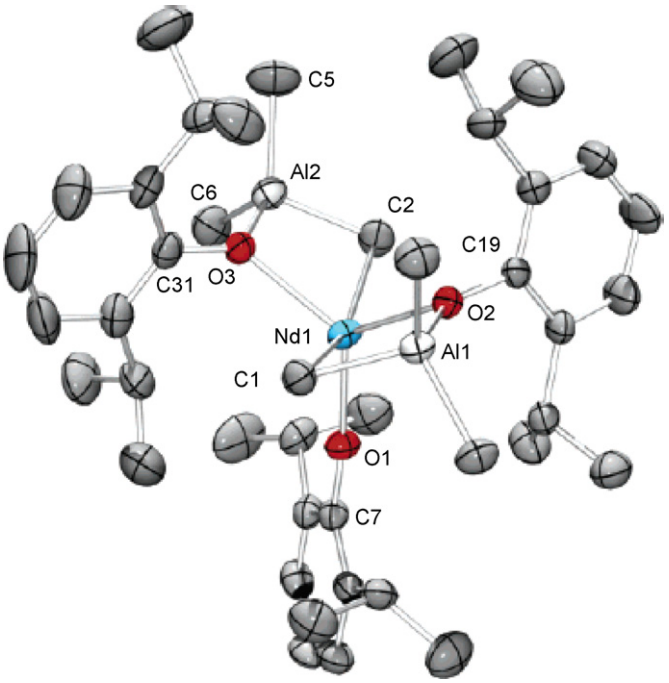

Fig. 38. Molecular structure of $Nd(OAr^{iPr})[(\mu\text{-}OAr^{iPr})(\mu\text{-}Me)AlMe_2]_2$ [91].

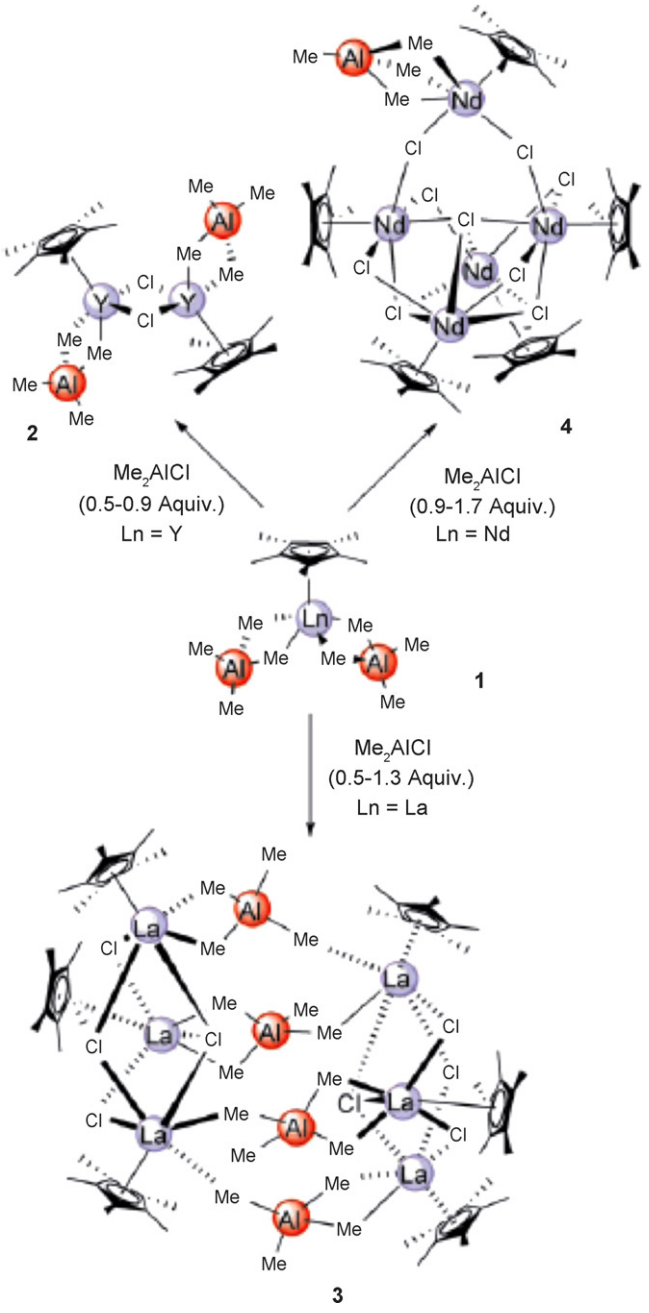

Scheme 98.

cage around the Sc–Sc axis which is coincident with the vertical principal axis of the cage [88].

2.10. Heterobimetallic organolanthanide complexes

One of the major achievements in organolanthanide chemistry reported in 2006 was the first realization of Al–Eu and Al–Yb donor–acceptor bonds. Prolonged heating of solid mixtures of $[Cp^*Al]_4$ and unsolvated Cp^*_2Ln (Ln = Eu, Yb) (molar ratio 1:4) in evacuated ampoules at 120 °C afforded red (Ln = Eu) or green (Ln = Yb) crystals of the composition $Cp^*_2Ln–AlCp^*$ in moderate yields. Scheme 96 illustrates the reaction [89].

The oxidation state of the central lanthanide ion in both compounds was unequivocally established to be +2. The presence of any bridging hydride ligands could be clearly ruled out. Fig. 37 displays the molecular structure of the Eu–Al complex. The Eu–Al bond length was determined as 3.3652(10) Å, while the Yb–Al distance in the ytterbium complex is 3.1981(11) Å [89].

A series of bimetallic complexes composed of lanthanide metallocene and trimethylaluminum, $Cp^*_2Ln[(\mu\text{-}Me)AlMe_2(\mu\text{-}Me)]_2LnCp^*_2$ (Ln = Ce, Pr, Nd, Sm, Gd, Tb, Dy, Ho, Tm, Yb, Lu) were prepared and used to catalyze polymerization of butadiene (*cf.* Section 2.11.2) [90]. Three series of lanthanide alkoxide/aryloxide trimethylaluminum adducts were synthesized with the aim of developing new isoprene polymerization catalysts (*cf.* Section 2.11.2). Scheme 97 summarizes the synthetic procedures ($Ar^{tBu} = C_6H_2{}^tBu_2$-2,6-Me-4; $Ar^{iPr} = C_6H_3{}^iPr_2$-2,6; Np = $CH_2{}^tBu$) [91].

The crystal structure of the purple neodymium complex $Nd(OAr^{iPr})[(\mu\text{-}OAr^{iPr})(\mu\text{-}Me)AlMe_2]_2$ was determined by X-ray diffraction (Fig. 38). The Nd center is five-coordinate in a distorted trigonal-bipyramidal fashion with bridging methyl groups in the apical positions [91].

Interesting novel organolanthanide tetramethylaluminates were synthesized and structurally characterized. Scheme 98 illustrates that reactions of $Cp^*Ln(AlMe_4)_2$ (Ln = Y, La, Nd) with various amounts of Me_2AlCl lead to products of different nuclearity depending on the stoichiometry of the reactants. Three products (**2**, Ln = Y; **3**, Ln = La; **4**, Ln = Nd) were structurally characterized by X-ray diffraction (Fig. 39). All three compounds are rare examples of alkali metal-free organolanthanide complexes containing both alkyl and chloro ligands [92].

Treatment of either the dinuclear yttrium complex **2** or the hexanuclear lanthanum species **3** with THF afforded two isostructural trinuclear complexes in which all the aluminum metal centers were displaced (Scheme 99). An X-ray crystal structure determination of the yttrium derivative revealed the presence of the first rare-earth metal methylidene complexes with a highly nucleophilic $CH_2{}^{2-}$ moiety stabilized by ionic interactions with three adjacent Ln^{3+} centers (Fig. 40) [93].

An unusual heterooctametallic Y–Al–methylidine cluster was obtained upon treatment of the half-sandwich tetramethylaluminate complex $Cp^*Y(AlMe_4)_2$ with diethyl ether. Scheme 100 illustrates the reaction pathways leading to this complex [94].

Interesting heterobimetallic complexes were isolated from reactions of non-classical lanthanide diiodides such as NdI_2 and DyI_2 with vanadocene or chromocene. A reaction of DyI_2 with Cp_2V in molten naphthalene at 100 °C produced the heterobimetallic cluster $[CpDy(\mu\text{-}I)_2]_7Cp_2V(\mu\text{-}I)$ which was isolated as violet crystals in low yield (5%). Fig. 41 shows the molecular structure of this unusual cluster species [39].

A reaction of DyI_2 with Cp_2Cr in benzene at 80 °C afforded mainly Cp_2DyI in addition to a few greenish-yellow crystals which were identified by an X-ray structural analysis to be the heterobimetallic "ate" complex $[Cp_2Cr][Cp_2DyI_2]$. The molecular structure of this salt-like species is shown in Fig. 42 [39].

2.11. Organolanthanide catalysis

2.11.1. Organolanthanide-catalyzed oligomerization reactions

In a study related to π-conjugated aromatic enynes as a single-emitting component for white luminescence, organolanthanide complexes were employed as catalysts to achieve the catalytic dimerization of terminal alkynes. Enynes derived from carbazole-substituted terminal phenylalkynes were easily prepared with excellent regio- and stereoselectivity using either $Cp^*_2LaCH(SiMe_3)_2$ or $[Me_2Si(C_5Me_4)\{N(C_6H_3Me_2$-2,6)$\}]Lu(CH_2SiMe_3)(THF)$ as catalysts [95].

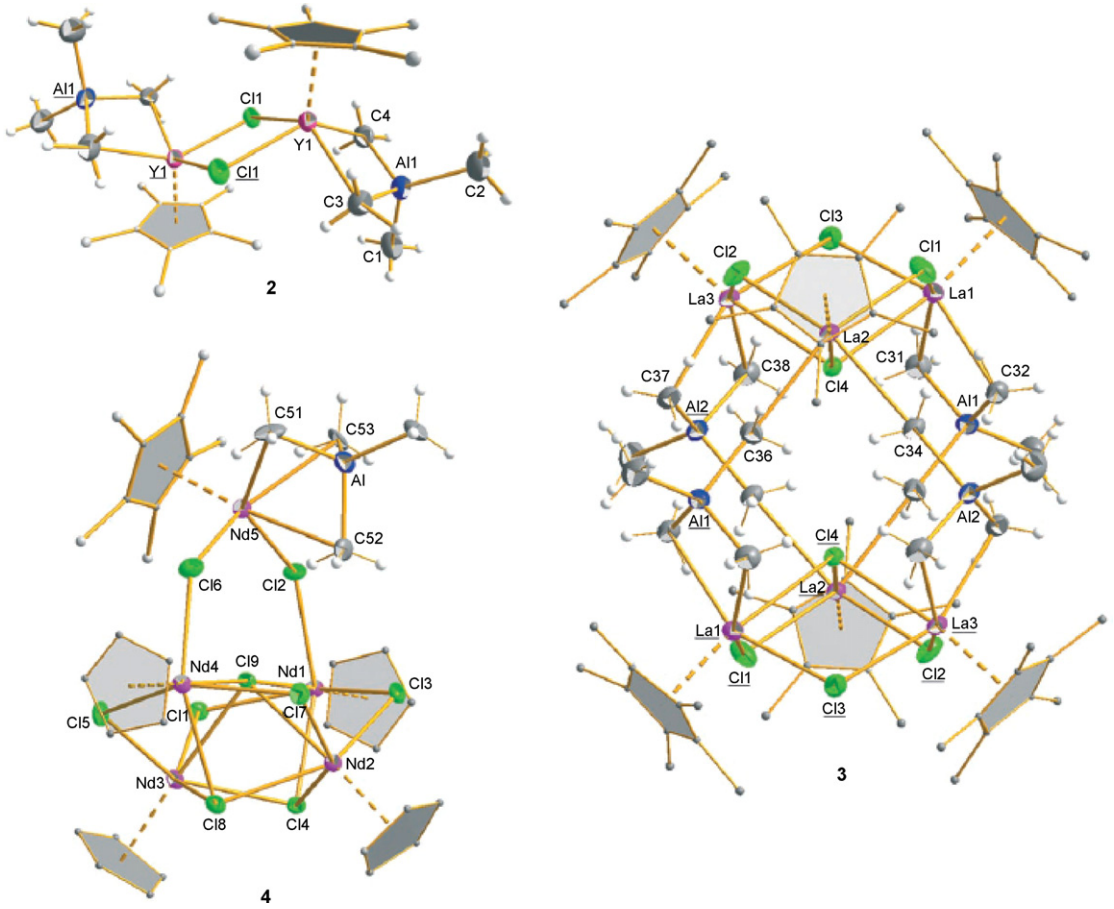

Fig. 39. Molecular structures of the heterobimetallic Al/Ln complexes **2**–**4** (*cf.* Scheme 98) [92].

2.11.2. Organolanthanide-catalyzed polymerization reactions

2.11.2.1. Monoolefins (ethylene, propene, styrene, etc.). A series of neutral and cationic lanthanum benzyl compounds were tested in ethylene polymerization experiments and was found to exhibit only moderate catalytic activity [13]. The catalytic activity of dimeric bis(guanidinato)lanthanide hydrido complexes of the type $[\{(Me_3Si)_2NC(N^iPr)_2\}_2Ln(\mu\text{-}H)]_2$ in the polymerization of ethylene, propene, and styrene was investigated. It was found that especially the Y and Sm derivatives displayed high catalytic activity in ethylene polymerization (1268 and 442 g mmol^{-1} h^{-1}, respectively) [20]. The neodymium complex $Cp^*_2Nd(BH_4)(THF)$ in combination with ^{n}BuEtMg affords a highly active catalyst for ethylene polymerization, the first one prepared from a borohydride organolanthanide pre-catalyst. Under the same experimental conditions, the catalytic behavior of $Cp^*_2Nd(BH_4)(THF)$ is similar to that of previously described $Cp^*_2Nd(\mu\text{-}Cl)_2Li(THF)_2$. The $Cp^*_2Nd(BH_4)(THF)/^n$BuEtMg system is not deactivated even in the presence of large excesses of THF [66].

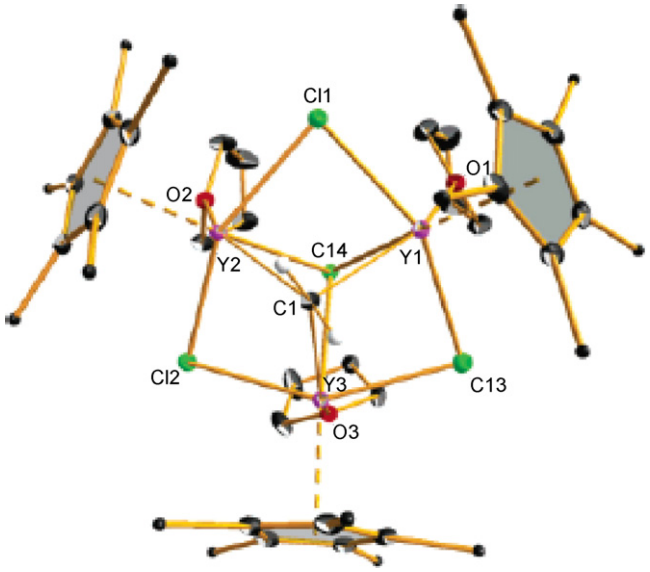

Fig. 40. Molecular structure of $Cp^*_3Y_3(\mu\text{-}Cl)_3(\mu_3\text{-}Cl)(\mu_3\text{-}CH_2)(THF)_3$ [93].

Organoeuropium compounds of the type $CpEuCl_2(PzA)_2$ and $CpEu(O_3SMe)_2(PzA)_2$ (O_3SMe^- = methanesulfonate, PzA = pyrazinamide) were found to be active in styrene polymerization, when methylaluminoxane (MAO) was used as cocatalyst. The catalytic systems produced polystyrene with activities up to 5.65 kg(PS) mol(Eu)$^{-1}$ h^{-1} ($CpEuCl_2(PzA)_2$, Al/Eu = 700, T = 60 °C, t = 4 h) in the absence of toluene. The presence of solvent led to a decrease of the catalytic activity. The compound containing the O_3SMe^- anion exhibited lower catalytic activity. The resulting polystyrene was atactic and had average molecular weights of 3.0 kg/mol [96].

2.11.2.2. Dienes (butadiene, isoprene, etc.). A series of bimetallic complexes composed of lanthanide metallocene and trimethylaluminum, $Cp^*_2Ln[(\mu\text{-}Me)AlMe_2(\mu\text{-}Me)]_2LnCp^*_2$ (Ln = Ce, Pr, Nd, Sm, Gd, Tb, Dy, Ho, Tm, Yb, Lu) were prepared, and the ability to catalyze the polymerization of butadiene in the presence of cocatalysts, AlR_3

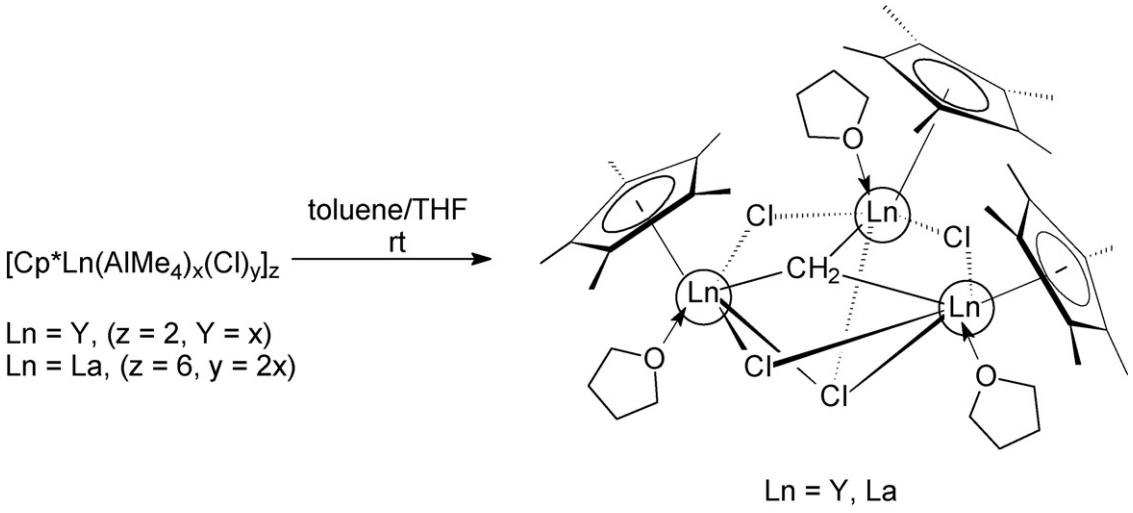

Scheme 99.

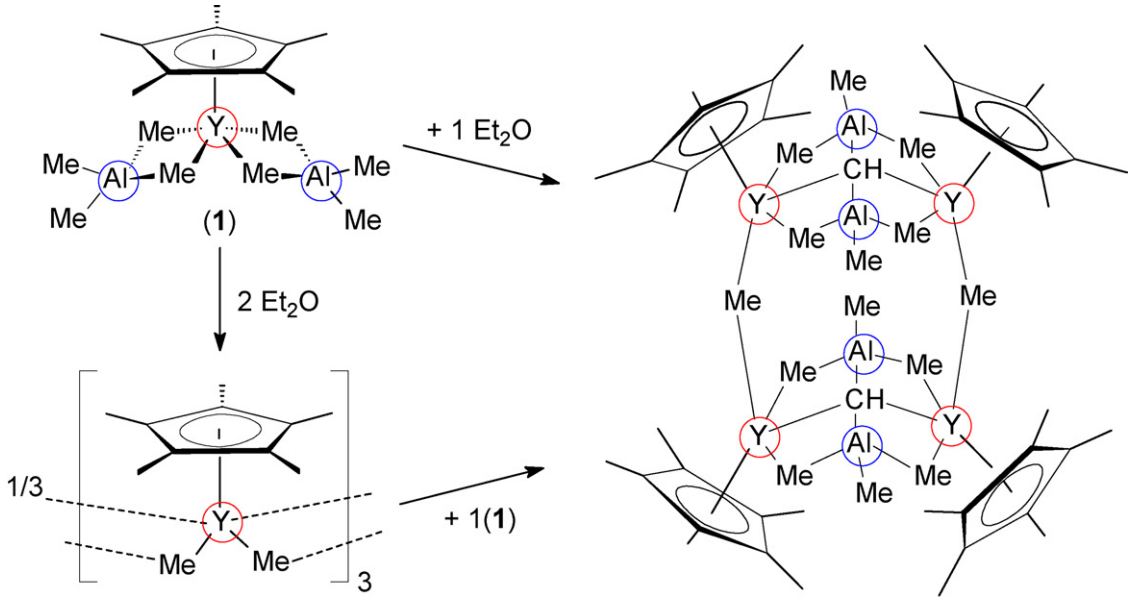

Scheme 100.

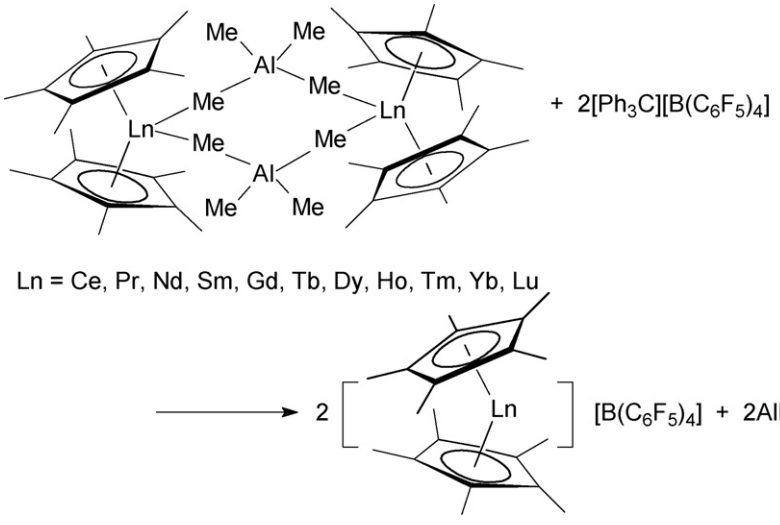

Scheme 101.

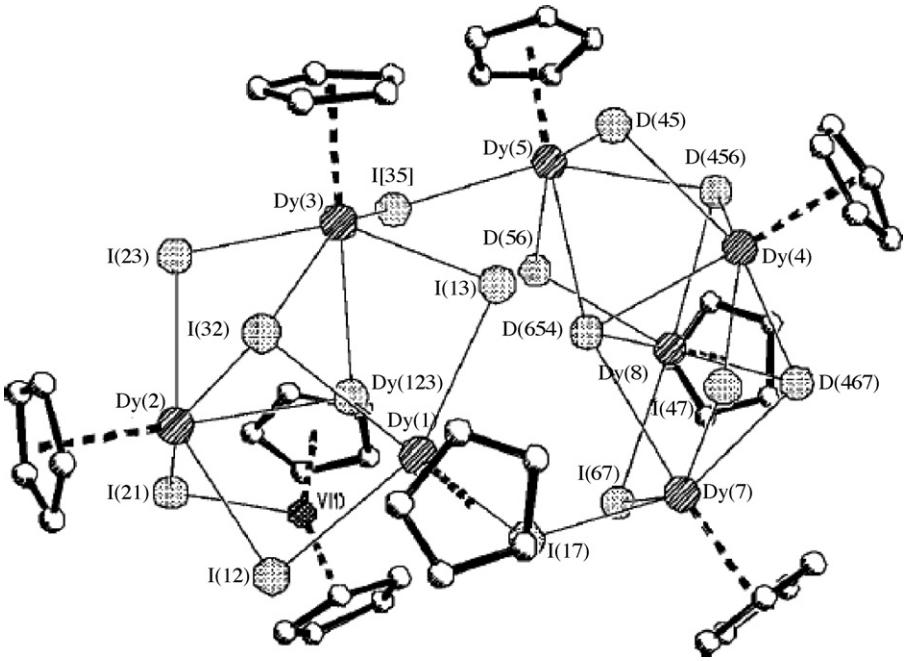

Fig. 41. Molecular structure of $[CpDy(\mu\text{-}I)_2]_7Cp_2V(\mu\text{-}I)$ [39].

(R = Me, ^{i}Bu) and $[Ph_3C][B(C_6F_5)_4]$, was studied as a function of the 11 different lanthanide metal species and the kind of alkylaluminum in the cocatalyst. Both catalytic activity and microstructure of polybutadiene were found to depend strongly on the kind of lanthanide metal and the trialkylaluminum. Apparently the role of the $[Ph_3C][B(C_6F_5)_4]$ is the *in situ* formation of cationic species $[Cp^*_2Ln][B(C_6F_5)_4]$ as illustrated in Scheme 101 [90].

Three series of lanthanide alkoxide/aryloxide trimethylaluminum adducts (*cf.* Section 2.10, Scheme 97) were tested as new isoprene polymerization catalysts. Using the binary initiating systems $Ln(OR)_3(AlMe_3)_x/Et_2AlCl$ (Ln = La, Nd, Y) the structure–reactivity relationship of the rare-earth metal aryl(alk)oxide-promoted polymerization of isoprene was investigated. Depending on the degree of the rare-earth metal aryl(alk)oxide prealkylation (x = 1–3), such discrete trimethylaluminum (TMA) adduct complexes of lanthanide alkoxide and aryloxide components displayed a distinct initiating capability. The heterobimetallic bis-TMA adducts $Ln(OAr^{iPr})_3(AlMe_3)_2$ ($Ar^{iPr} = C_6H_3{}^iPr_2$-2,6) and tris-TMA adducts $Ln(OCH_2{}^tBu)_3(AlMe_3)_3$ (Ln = La, Nd) produced highly reactive initiators, whereas the mono-TMA adducts $Ln(OAr^{tBu})_3(AlMe_3)$ ($Ar^{tBu} = C_6H_2{}^tBu_2$-2,6-Me-4) were catalytically inactive [91]. In a

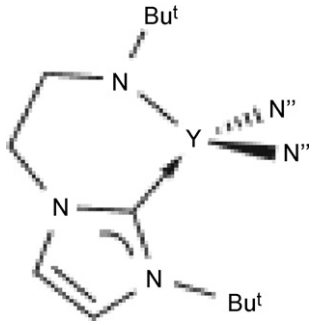

Scheme 102. $N'' = N(SiMe_3)_2$.

continuation of this work the organoaluminum-mediated alkylation of tailor-made rare-earth metal carboxylate complexes was studied, and implications of the degree of Ln alkylation and organoaluminum-chloride-mediated cation formation for 1,3-diene polymerization were investigated. Homoleptic $Ln(AlMe_4)_3$ species were found to play a crucial role as intermediates and were

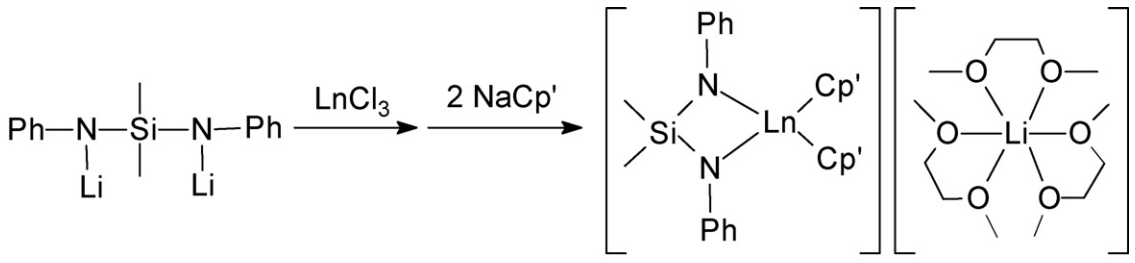

Ln = Yb, Cp' = C_5H_5
Ln = Sm, Cp' = C_5H_5
Ln = Yb, Cp' = MeC_5H_4

Scheme 103.

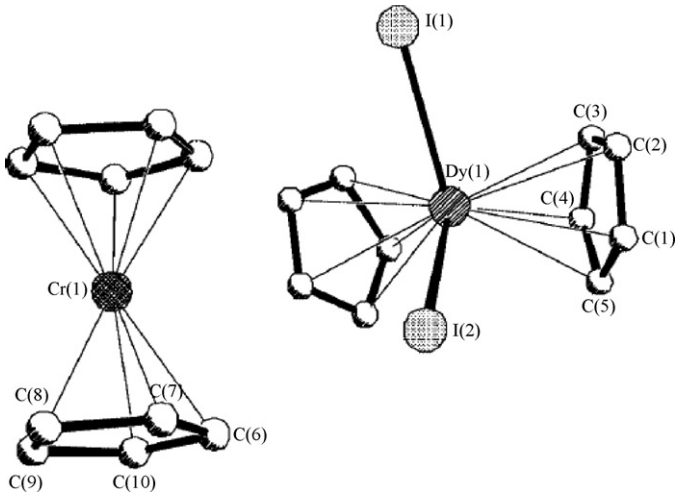

Fig. 42. Molecular structure of $[Cp_2Cr][Cp_2DyI_2]$ [39].

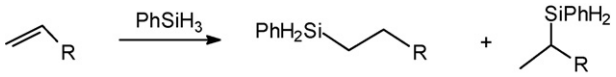

Scheme 104.

subsequently used for the high-yield synthesis of various alkylated lanthanide carboxylate complexes [97]. Addition of ^{n}BuEtMg to $Cp^*_2Nd(BH_4)(THF)$ afforded a catalyst for a *trans*-selective polymerization of isoprene. This is in contrast to the chloro homologue $Cp^*_2Nd(\mu\text{-}Cl)_2Li(THF)_2$ which did not afford a catalytically active species when associated with ^{n}BuEtMg [66].

2.11.2.3. Cyclic esters and amides (ε-caprolactone, δ-valerolactone, lactide, etc.). A Lewis acidic yttrium(III) complex of an anionic, metal-tethered carbene ligand (Scheme 102) was reported to act as bifunctional catalyst for the polymerization of D,L-lactide, using a combination of Lewis acid and base functionalities to initiate

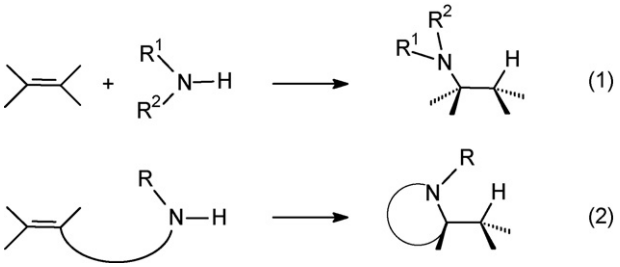

Scheme 106.

ring opening of the cyclic monomer. The alcohol- and amino-functionalized carbenes from which the complexes derive provide models for the first insertion step, and also display metal-free polymerization catalysts to generate polylactic acid [98].

2.11.2.4. Acrylic monomers (methyl methacrylate (MMA), acrylonitrile, etc.). A DFT study of the monometallic group transfer polymerization (GTP) of methyl acrylate (MA) catalyzed by Sm-based and Zr-based metallocenes was presented. The processes examined were the generation of the catalytically active species, the subsequent C–C coupling reaction, and the ring opening of a metallacyclic stable intermediate as resting state of the polymerization process, obtained from the C–C coupling. The mechanisms for a neutral zirconocene, a cationic zirconocene, and the neutral samarocene $Cp_2SmMe(THF)$ were compared [99]. A half-sandwich samarium(III) diketiminate bromide (*cf.* Scheme 45) was found to be active in methyl methacrylate polymerization. The effects of temperature, polymerization time and catalyst concentration were studied. Activities of *ca.* 18 kg of polymethyl methacrylate (PMMA) per mole of Sm per hour were obtained under optimum conditions (0 °C and a MMA/catalyst molar ratio of 100/1), giving a polymer with a molecular weight $M_n > 24\,000\ g\ mol^{-1}$. After 1 h of polymerization, conversions of MMA as high as 96% were observed [43]. A series of new lanthanide complexes supported by silylene-bridged diamide ligands were prepared (Scheme 103) and their catalytic activities in the polymerization of methyl methacrylate

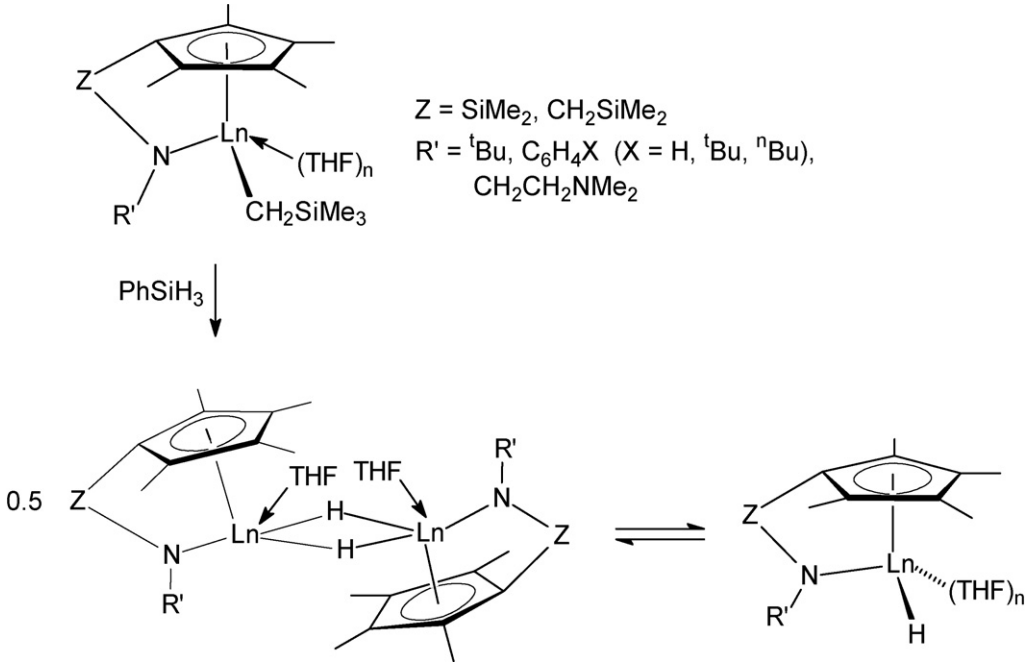

Scheme 105.

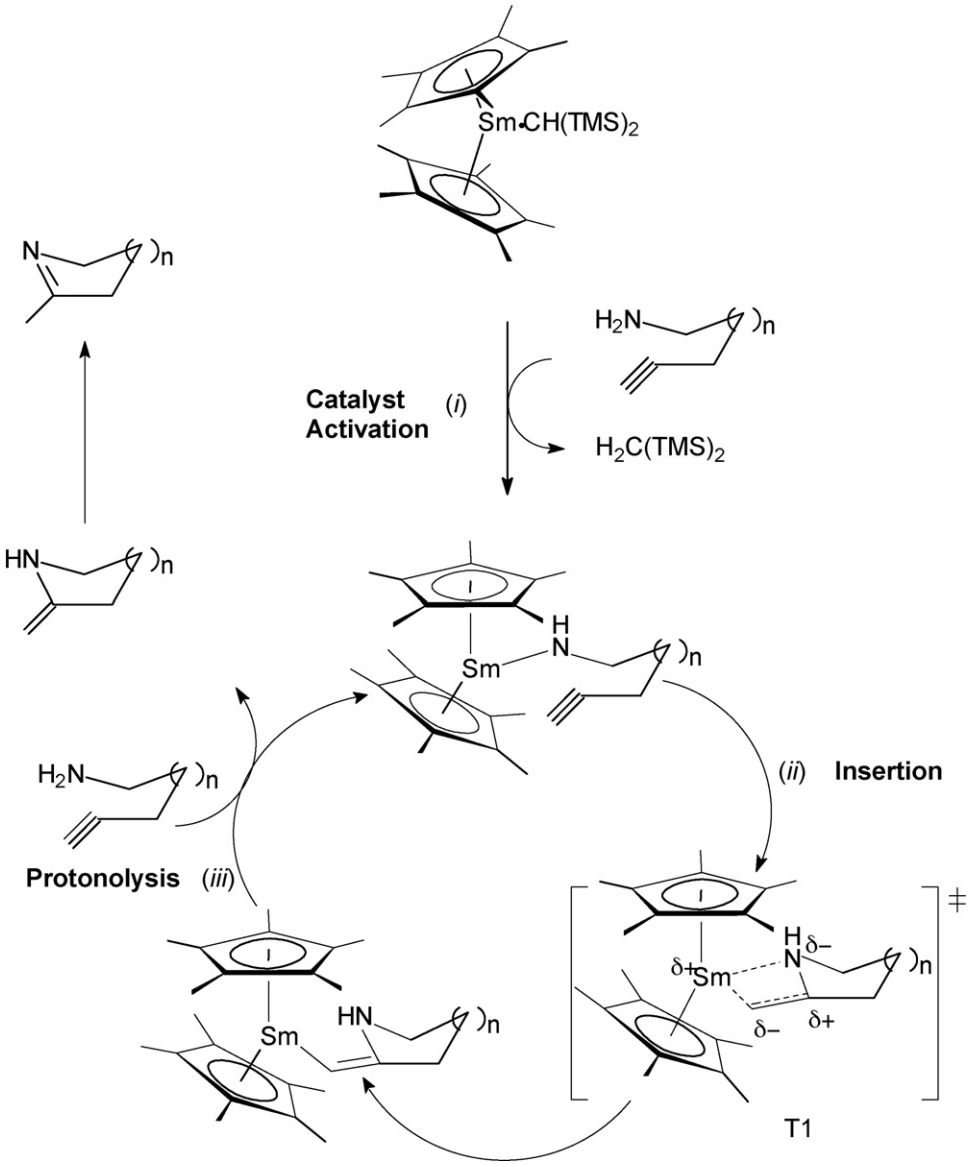

Scheme 107.

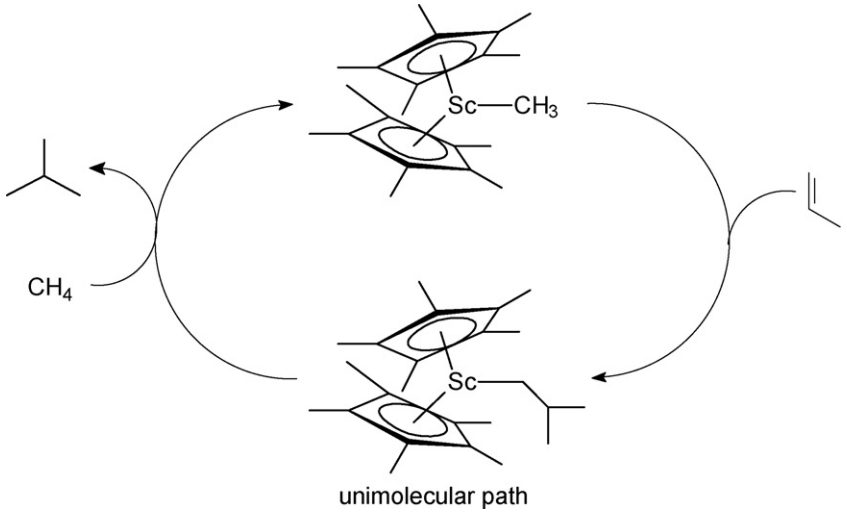

Scheme 108.

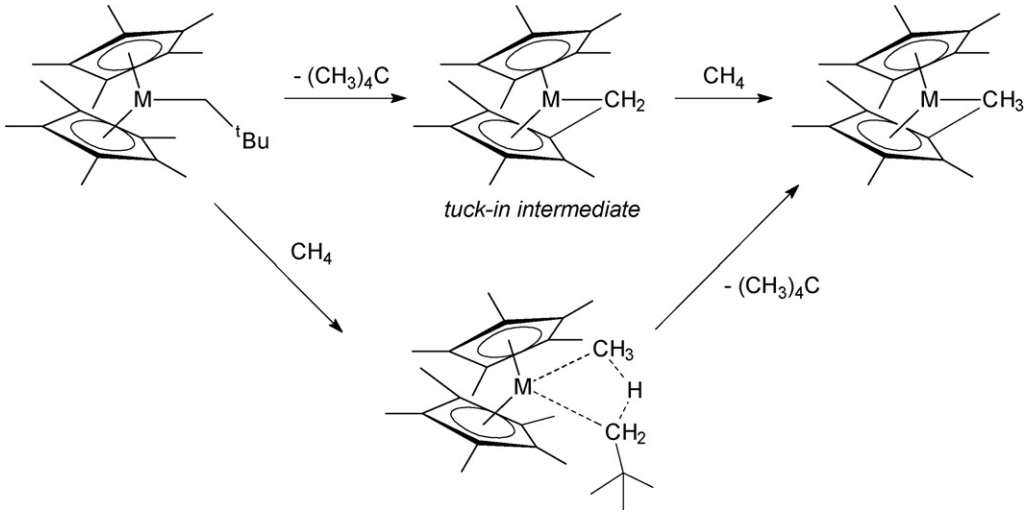

Scheme 109.

studied. These anionic complexes showed high activity for the polymerization of MMA at room temperature, giving syndiotactic-rich polymers with high molecular weights ($M_n > 10^4$) and relatively narrow molecular weight distributions ($M_w/M_n = 1.54–1.85$) [100].

It was reported that organolanthanide(II) complexes with 3-pyridylmethyl-functionalized indenyl ligands (*cf.* Scheme 80) can function as single-component MMA polymerization catalysts, while the complexes with a 2-pyridylmethyl substituent on the indenyl ligands (*cf.* Scheme 79) cannot catalyze MMA polymerization. Temperature and solvent effects on the MMA polymerization were also examined in this study [73].

2.11.3. Organolanthanide-catalyzed hydrosilylation reactions

A standard hydrosilylation reaction used for testing potential organolanthanide catalysts is the reaction of 1-decene (or styrene) with $PhSiH_3$ (Scheme 104) [42].

Using this standard reaction, a series of "constrained geometry" yttrium and lutetium alkyl complexes $(C_5Me_4ZNR)Ln(CH_2SiMe_3)(THF)_n$ (Ln = Y, Lu), prepared by treatment of the tris(trimethylsilylmethyl) precursors $Ln(CH_2SiMe_3)_3(THF)_2$ with different linked aminocyclopentadienes of the type $(C_5Me_4H)ZNHR$ (Z = $SiMe_2$, CH_2SiMe_2; R = ^{t}Bu, Ph, $C_6H_4{}^t$Bu-*p*, $C_6H_4{}^n$Bu-*p*) (*cf.* Section 2.5.2) was tested for their catalytic activity in hydrosilylation. A significant influence of the ligand structure on the catalytic properties (turnover frequency, regioselectivity) was observed, with the yttrium complex $(C_5Me_4SiMe_2N{}^t$Bu)Y(CH_2SiMe_3)(THF) being the most active for 1-decene hydrosilylation. ^{1}H NMR experiments in all cases evidenced the immediate and complete formation of the catalytically active dimeric μ-hydrido species (Scheme 105) [42].

Several neutral and cationic rare-earth metal silanolate complexes containing a σ-bonded CH_2SiMe_3 group were tested as olefin hydrosilylation pre-catalysts with a variety of substrates. The com-

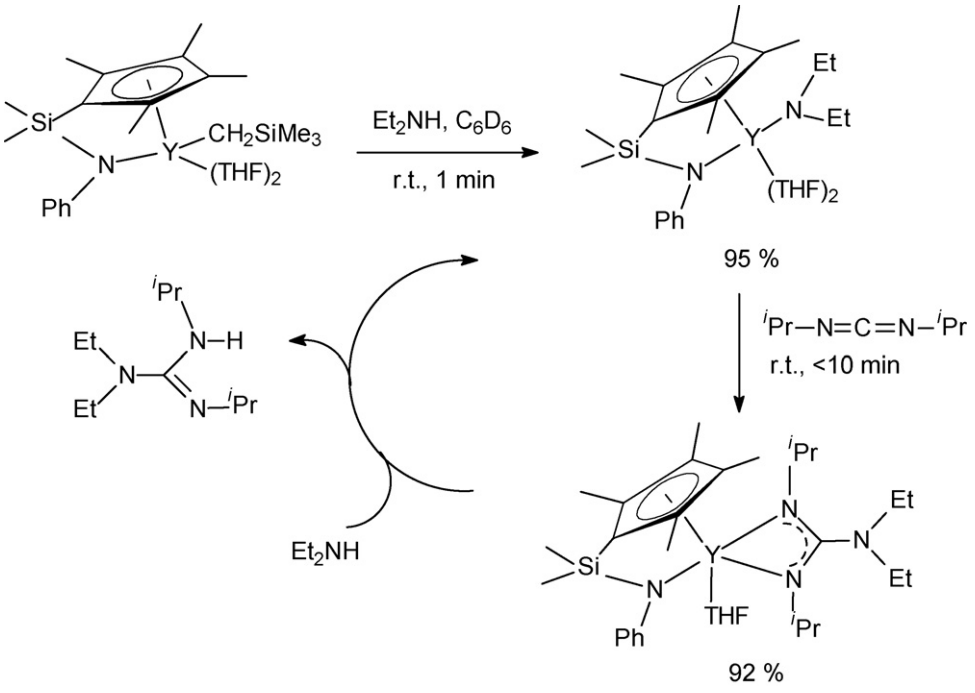

Scheme 110.

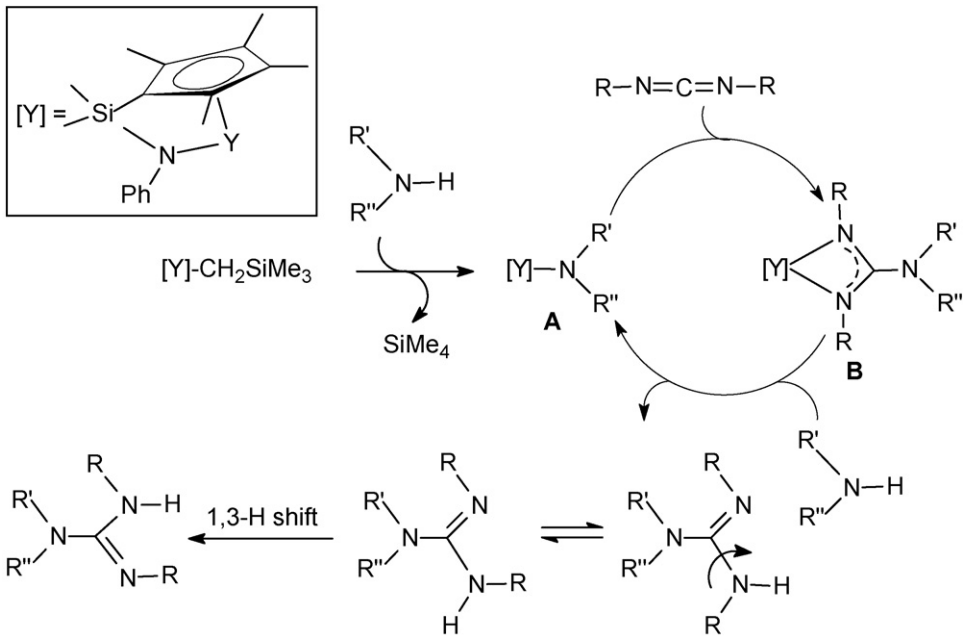

Scheme 111.

pound [Y{μ,η²-OSi(O^{t}Bu)$_3$}(CH$_2$SiMe$_3$)$_2$]$_2$ (*cf.* Section 2.2.2) was found to be highly active in 1-decene hydrosilylation [15].

2.11.4. Organolanthanide-catalyzed hydroamination and hydrophosphination reactions

Organolanthanide-catalyzed hydroamination reactions continued to find significant attention in 2006. Hydroamination, *i.e.* the addition of amine N–H functionalities to unsaturated carbon–carbon bond can be carried out either in an *inter*molecular (Scheme 106 (1)) or *intra*molecular (Scheme 106 (2)) fashion and generates amines in a waste-free, highly atom-economical manner starting from simple and inexpensive precursors.

Both neutral and cationic benzyl complexes of lanthanum were found to initiate the catalytic intramolecular hydroamination/cyclization of 2,2-dimethyl-4-pentenylamine [13]. In a closely related study, the relative catalytic activity of neutral dialkyl *versus* cationic monoalkyl Group 3 metal catalysts in the intramolecular hydroamination/cyclization of the 2,2-dimethyl-4-pentenylamine reference substrate. This was found to depend strongly on the nature of the monoanionic ancillary ligand. With a chelating amidinate ligand, the neutral catalysts were quite effective, but their cationic derivatives showed a much lower activity. In contrast, the neutral catalysts with tetradentate triamine-amide ligands showed a much lower activity than their cationic derivatives [101]. Several chiral 3,3′-bis(triarylsilyl)-substituted binaphtholate rare-earth metal complexes were also investigated and found to be efficient catalysts for the asymmetric hydroamination/cyclization of aminoalkenes such as 2,2-diphenyl-4-pentenylamine [25]. Ytterbium and lutetium ionic complexes derived from enantiopure substituted (*R*)-binaphthylamine ligands of the general formula [Li(THF)$_n$][Ln{(*R*)-C$_{20}$H$_{12}$(NR)$_2$}$_2$] have been investigated for the hydroamination/cyclization of several aminopentenes and an aminohexene. Complexes with isopropyl or cyclohexyl substituents on nitrogen were found to be efficient catalysts under mild conditions for the formation of N-containing heterocycles with enantiomeric excesses up to 78% [102].

Organolanthanide-mediated catalytic hydroamination processes were also studied using density functional theory. In this work

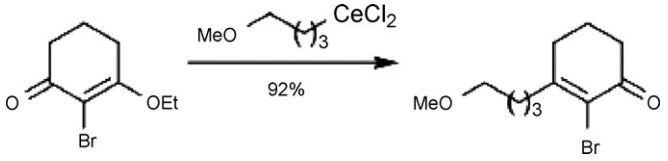

Scheme 112.

the exothermic hydroamination/cyclization of a prototypical aminoalkyne, H$_2$N(CH$_2$)$_3$C≡CR, mediated by Cp$_2$Sm complexes was analyzed. The reaction was found to proceed in two discrete steps, namely, cyclization with concerted Ln–C and C–N bond formation and subsequent Ln–C protonolysis. Dissociation of the cyclized amine then follows to regenerate the active catalyst. The proposed catalytic cycle for the organolanthanide-catalyzed hydroamination/cyclization of aminoalkynes is shown in Scheme 107 [103].

A series of divinylbenzene cross-linked, amino-functionalized polystyrene resins were used as supports for intramolecular hydroamination/cyclization catalysts such as Cp*$_2$LnCH(SiMe$_3$)$_2$ (Ln = La, Sm) and [Me$_2$Si(C$_5$Me$_4$)(NBu^t)]SmN(SiMe$_3$)$_2$. It was shown that these catalyst precursors can be immobilized on the polymer supports *via* transaminative protonolysis to give the corresponding bound pre-catalysts, which, in the presence of aminoalkene substrates, are transaminatively released for efficient homogeneous intramolecular hydroamination/cyclization processes. Upon substrate consumption, the catalysts are readsorbed on the supports. In many cases, these catalysts exhibit activities comparable to the

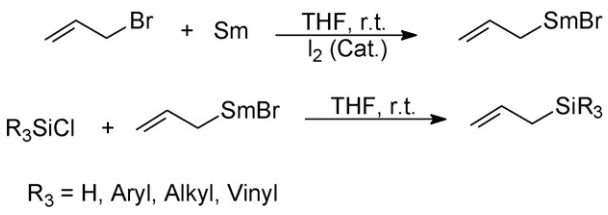

Scheme 113.

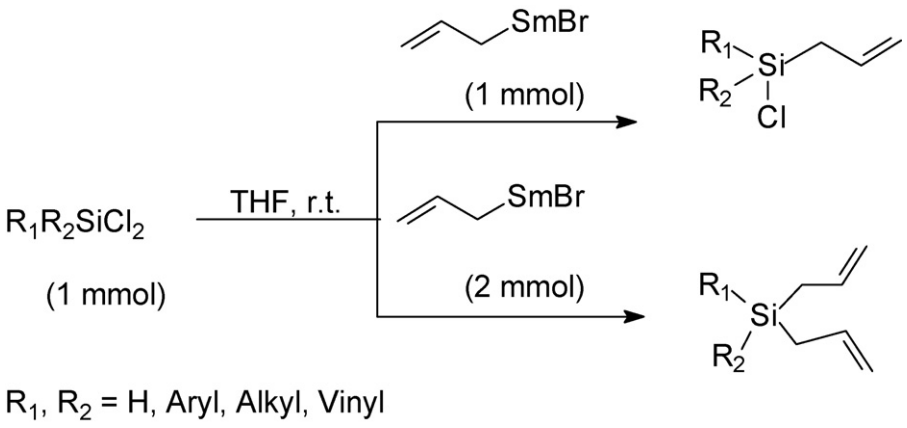

Scheme 114.

homogeneous precursors and are recoverable/recyclable with only minor to moderate loss of activity, depending on the particular resin amino substituents [104].

Formally related to hydroamination is hydrophosphination. Dual intermolecular hydrophosphination of conjugated diynes with 2 equiv. of diphenylphosphine was reported to be catalyzed by ytterbium complexes, Yb(η^2-Ph_2CNPh)$(HMPA)_3$ and Yb$[N(SiMe_3)_2]_3(HMPA)_2$ (HMPA = hexamethylphosphoric triamide), to give the corresponding 1,4-bis(diphenylphosphinyl) buta-1,3-dienes in high yields after oxidative work-up [105]. Intermolecular hydrophosphination of alkynes with Ph_2PH was also shown to be effectively catalyzed by the ytterbium imine complex Yb(η^2-Ph_2CNPh)$(HMPA)_3$. Ytterbium(II) mono- and diphosphido species, generated *in situ*, were identified as the active catalysts. When Ph_2PH was substituted by Ph_2PSiMe_3, silylphosphination of aromatic internal alkynes took place to afford 1-trimethylsilyl-2-diphenylphosphinoalkenes in moderate yields. Moreover, the one-pot synthesis of 1-diphenylphosphino-1,3-butadienes from terminal alkynes and Ph_2PH was achieved using $Y[N(SiMe_3)_2]_3$ as catalyst through alkyne dimerization and subsequent hydrophosphination [106].

2.11.5. Other organolanthanide-catalyzed reactions

A DFT study of the catalytic properties of Cp_2ScCH_3 and Cp_2LuCH_3 in the hydromethylation of propene has been performed. The catalytic behavior of Cp_2ScCH_3 in this reaction was confirmed, and the formation of secondary products rationalized. It was also shown that Cp_2LuCH_3 cannot exhibit catalytic behavior and that only stoichiometric conversions of propene to isobutane could be observed. The difference in reactivities between the two metallocenes was investigated, and an electronic explanation was given based on differences in the coordination of propene. However, it was proposed that the intrinsic reactivities of the two metallocenes are driven by both electronic and steric effects [107]. In a closely related theoretical study, density functional theory was employed to gain a better understanding of the carbometalation of propene catalyzed by Group 3 metal and lanthanide metallocenes. As illustrated in Scheme 108, a catalytic cycle was reported in 2003 [108] in which isobutane is produced when Cp^*_2ScMe is allowed to react with propene in the presence of excess methane, presumably by initial carbometalation and subsequent non-degenerate metathesis with excess methane.

The uni- and bimolecular C–H bond metathesis reactions of Cp^*_2LnL (Ln = Sc, Y, Lu; L = Me, $CH_2{}^tBu$) were modeled with MPW1K density functional theory and a relativistic effective core potential basis set. This level of theory, when combined with a one-dimensional tunneling model, provides enthalpies of activation that are in good agreement with experiment for known bimolecular reactions of methane with $Cp^*_2ScCH_2{}^tBu$ and Cp^*_2LuMe. Analysis of theoretical trends as a function of metal and ligand indicated that bimolecular reactions dominate in every case under typical experimental conditions (Scheme 109). However, unimolecular reactions proceeding through tuck-in complexes become increasingly competitive with increased steric bulk of the metal alkyl and also with metals having smaller ionic radii [108].

Stannane dehydrocoupling catalyzed by Cp_2LaH has also been elucidated by a DFT study. All the pathways leading to bis-stannane and regeneration of the catalyst Cp_2LaH for the stannane SnH_4 were computed using the DFT (B3PW91) method. In all cases, the reaction is at least a two-step process with a common first step, which is the Sn–H activation of the stannane, leading to the hydrostannyl complex Cp_2LaSnH_3 [109].

The catalytic addition of secondary amines to carbodiimides has been achieved by use of an yttrium half-sandwich alkyl complex, $[Me_2Si(C_5Me_4)(NPh)]Y(CH_2SiMe_3)(THF)_2$ (Scheme 110). This method offers a straightforward, atom-economical route to tetrasubstituted guanidines. As illustrated in Scheme 110, an yttrium guanidinate species has been confirmed to be a true catalytic species [110].

In detail, the 1:1 acid–base reaction between the alkyl precursor $[Me_2Si(C_5Me_4)(NPh)]Y(CH_2SiMe_3)(THF)_2$ with diethylamine in benzene yielded immediately the corresponding amido complex $[Me_2Si(C_5Me_4)(NPh)]Y(NEt_2)(THF)_2$. Nucleophilic addition of this amido species to *N,N′*-diisopropylcarbodiimide took place rapidly to give the guanidinate complex $[Me_2Si(C_5Me_4)(NPh)]Y[Et_2NC(NPr^i)_2](THF)$ in 92% yield. The

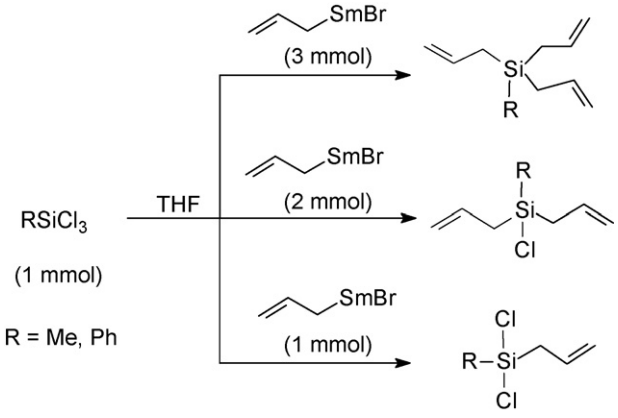

Scheme 115.

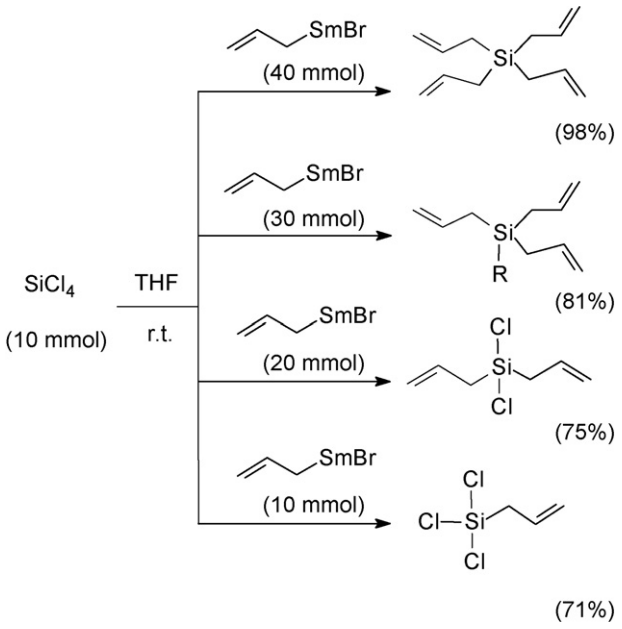

Scheme 116.

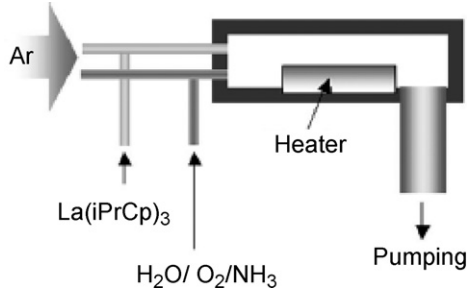

Fig. 43. Schematic view of the deposition chamber [118].

molecular structure of the guanidinate intermediate could be confirmed by an X-ray diffraction analysis. Upon heating of the guanidinate complex with diethylamine in a 1:1 mixture to 80 °C, the tetraalkylguanidine ^{i}PrN=C(NEt$_2$)NHPr^{i} and [Me$_2$Si(C$_5$Me$_4$)(NPh)]Y(NEt$_2$)(THF)$_2$ were formed almost quantitatively. More remarkably, catalytic formation of ^{i}PrN=C(NEt$_2$)NHPr^{i} was achieved when excess diethylamine and *N*,*N*′-diisopropylcarbodiimide were added to [Me$_2$Si(C$_5$Me$_4$)(NPh)]Y[Et$_2$NC(NPr^{i})$_2$](THF) in C$_6$D$_6$ at 80 °C. A possible catalytic cycle for this reaction is shown in Scheme 111 [110].

$$[Cp_2LnNH_2] + 2\,LiNH_2 \xrightarrow{\Delta T} LnN + 2\,LiCp + 2\,NH_3$$

$$[Cp_3LnNH_3] + 3\,LiNH_2 \xrightarrow{\Delta T} LnN + 3\,LiCp + 3\,NH_3$$

$$[Cp_2LnNH_2] + CaH_2 \xrightarrow{\Delta T} LnN + CaCp_2 + 2\,H_2$$

Scheme 117.

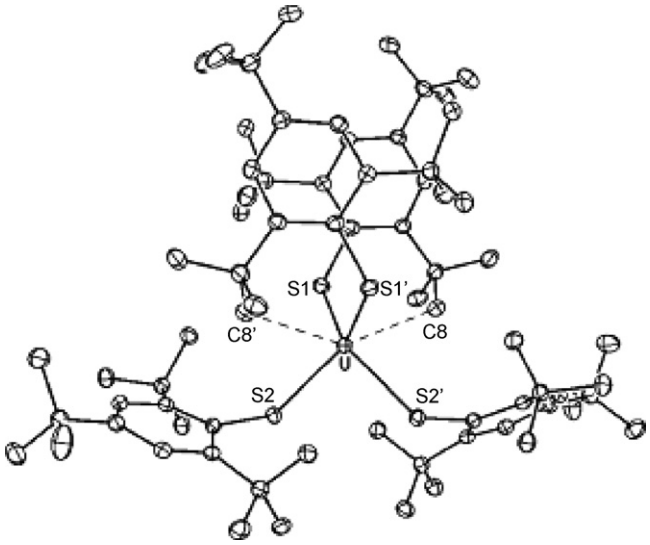

Fig. 45. Molecular structure of U(SMes*)$_4$ [126].

2.12. Organolanthanides in organic synthesis

Tri-*n*-butyllanthanum, *n*Bu$_3$La, was employed as an intermediate in the addition of silylglyoxylates to alcohols [111]. A methoxyalkylcerium(III) dichloride reagent was used in the reaction illustrated in Scheme 112. This was part of a study on the synthesis of spiro[4,5]decane CF-ring analogues of 1α,25-dihydroxyvitamin D$_3$ [112]. In a similar manner the functionalized alkenylcerium(III) dichloride reagent (EtO)$_2$CH–C(CeCl$_2$)=CHMe was generated from the corresponding bromide precursor [113].

Allylation of chlorosilanes has been achieved with allylsamarium bromide, especially in a controlled manner. The samarium reagent was made according to Scheme 113 from allyl bromide and samarium in the presence of a catalytic amount of iodine in dry THF. Allylation of trisubstituted chlorosilanes (R$_3$SiCl) afforded a variety of aryl-, aralkyl-, and alkenyl-substituted allylsilanes (Scheme 113) [114].

Using the same method, dichlorosilanes (R$_2$SiCl$_2$) can either afford monoallylated silanes or diallylated silanes depending

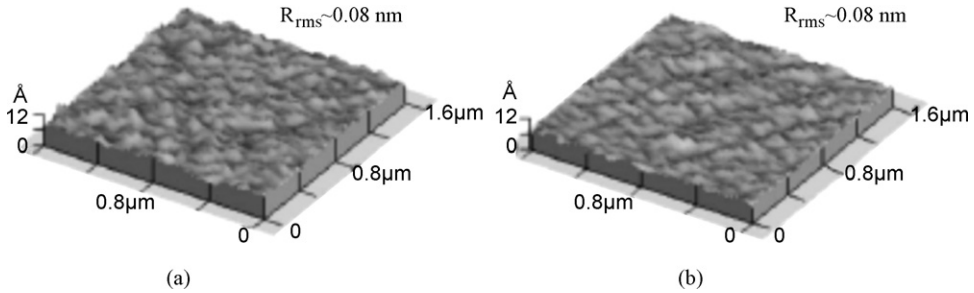

Fig. 44. AFM images of 5-nm thick La$_2$O$_3$ films (a) before RTA and (b) after RTA at 920 °C for 30 s [118].

on the amount of allylsamarium bromide used (Scheme 114) [114].

Similarly, trichlorosilanes ($RSiCl_3$) can selectively afford mono-, di-, and tri-allylation products as illustrated in Scheme 115 [114].

Finally, silicon tetrachloride ($SiCl_4$) was allylated stepwise, and the corresponding silanes containing one, two, three or four allylic groups, respectively, were obtained in satisfactory yields (Scheme 116) [114].

2.13. Organolanthanides in materials science

High-permittivity $YScO_3$ thin films have been deposited by atomic layer deposition using the organometallic cyclopentadienyl precursors $(C_5H_4Me)_3Y$ and Cp_3Sc at a deposition temperature of 300 °C. Ozone and water were used as oxygen sources in these processes. Metal ratio and film thickness were easily controlled by varying the metal precursor pulsing ratio and the number of deposition cycles. Stoichiometric $YScO_3$ films contained less than 1 atom% hydrogen and less than 0.2 atom% carbon. The as-deposited stoichiometric films were smooth, amorphous and they had high permittivity (14–16). Films deposited using the cyclopentadienyl precursor-based process started to crystallize at 800 °C, which significantly deteriorated the dielectric properties [115]. Lanthanum oxide is known to be suited as a gate oxide that can replace SiO_2 due to its high dielectric constant with a band gap of 4.3 eV and its thermal stability with silicon. Plasma-enhanced atomic layer deposition (PE-ALD) of La_2O_3 thin films by using an electron cyclotron resonance plasma source has been studied. The amorphous La_2O_3 films were deposited on Si substrates with $La(C_5H_4Et)_3$ as a precursor source and ozone as reactant gas. Secondary ion mass spectrometry and Rutherford backscattering measurements detected no carbon impurity content [116,117]. In a closely related study, $La(C_5H_4Pr^i)_3$ was used as organolanthanum precursor. Lanthanum oxide thin films were deposited at deposition temperatures ranging from 170 to 370 °C using alternate injection of tris(isopropylcyclopentadienyl)lanthanum and various reactants (H_2O, O_2, and NH_3). Fig. 43 provides a schematic view of the deposition chamber [118].

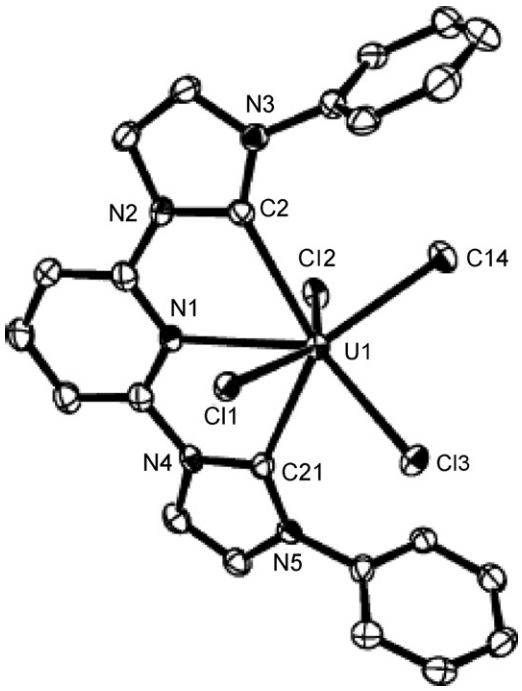

Fig. 46. Molecular structure of $(C–N–C)UCl_4$ [126].

It was possible to deposit films containing a carbon impurity concentration <1 atom%. The residual carbon could be further reduced

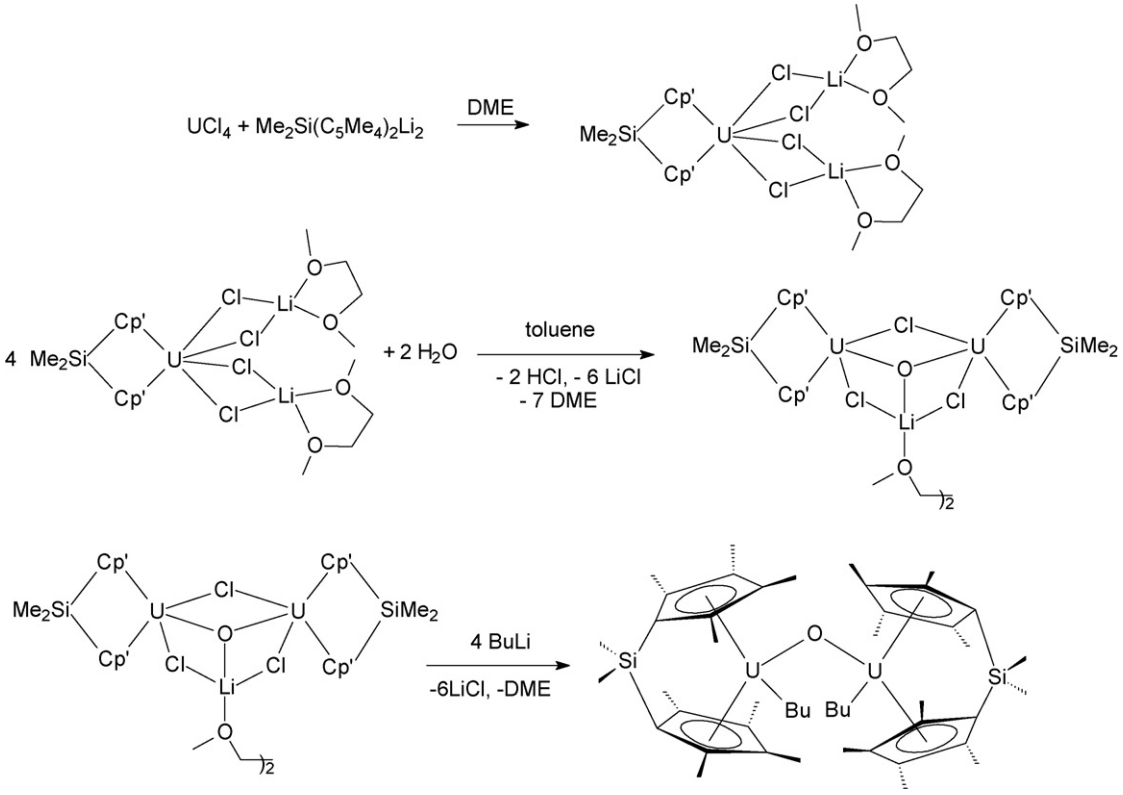

Scheme 118.

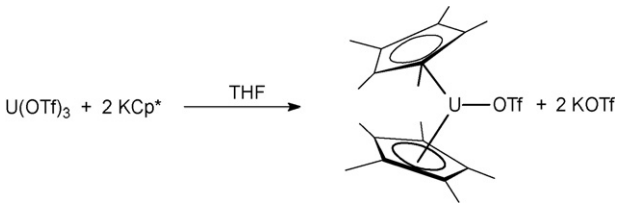

Scheme 119.

by postdeposition annealing. X-ray photoelectron spectroscopy (XPS) showed that after rapid thermal annealing (RTA, Fig. 44) the films transformed to La-silicate which increased the band gap of the films (7.0 ± 0.15 eV) [77].

Nanocrystalline lanthanide nitride materials were synthesized by thermal treatment of amido and ammine metallocenes. Thermolysis of either $Cp_3Ln(NH_3)$ or $[Cp_2Ln(\mu\text{-}NH_2)]_2$ (Ln = Sm, Gd, Dy, Ho, Er, Yb) in the presence of inorganic bases such as $LiNH_2$ or CaH_2 as illustrated in Scheme 117 yielded lanthanide nitride (LnN) powders with an estimated crystallite size of between 40 and 90 nm at unprecedented low temperatures of 240–300 °C. Temperature-dependent X-ray powder diffraction and transmission electron microscopy (TEM) investigations were performed and showed that the decomposition reaction yielded nanocrystalline material [57].

Tris(ethylcyclopentadienyl)erbium, $Er(C_5H_4Et)_3$, and *tert*-butylphosphine were employed as precursors for the deposition of ErP layers by low-pressure organometallic vapor phase epitaxy (LP-OMVPE). In this study the surface morphology of ErP/GaInP/GaAs and ErP/InP was investigated. In both samples, Er exists in the form of ErP with the rock-salt structure. The growth rate of ErP on GaInP was 1.8 ML/h. The surface roughness of ErP on GaInP was smaller than that of ErP on InP. Moreover, it was found that an ErP layer exists underneath the surface about 2 ML and the surface roughness does not depend on the ErP thickness in the range of 2.2–13.7 ML [119].

3. Actinides

An excellent review article entitled "The vitality of uranium molecular chemistry at the dawn of the XXIst century" was published in 2006 by Ephritikhine. In this article, recent advances in uranium molecular chemistry were highlighted, with the results reported during the 2000–2006 period. It was clearly pointed out the this discipline is currently witnessing an impressive development, together with the theoretical chemistry and solid-state chemistry of the f-elements, and that its face has profoundly changed, revealing unsuspected structural and reactivity features. This progress required and was facilitated by the use of new precursors. Studies of low-valent compounds gave a better insight into lanthanide(III)/actinide(III) differentiation and led to the discovery of unusual reactions, including activation of small molecules. A number of tetravalent uranium complexes, in particular polynuclear compounds have been synthesized within the period of time covered, which exhibit exciting structures and physicochemical properties. The potential of uranium(III) and uranium(IV) complexes in catalysis has been confirmed. The uranyl complexes, from mononuclear species to supramolecular assemblies, reveal a variety of novel structures, changing the generally accepted ideas

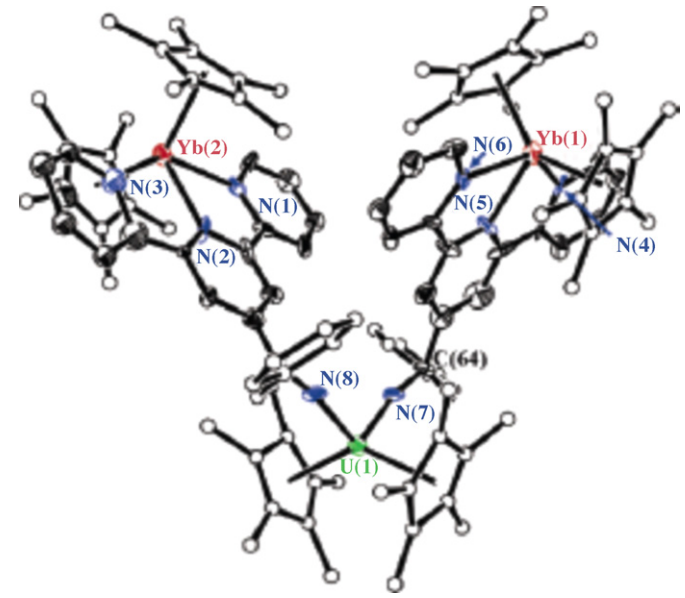

Fig. 47. Molecular structure of $Cp^*_2U[N{=}C(CH_2Ph)\{(tpy\text{-}CN)YbCp^*_2\}]_2$ [129].

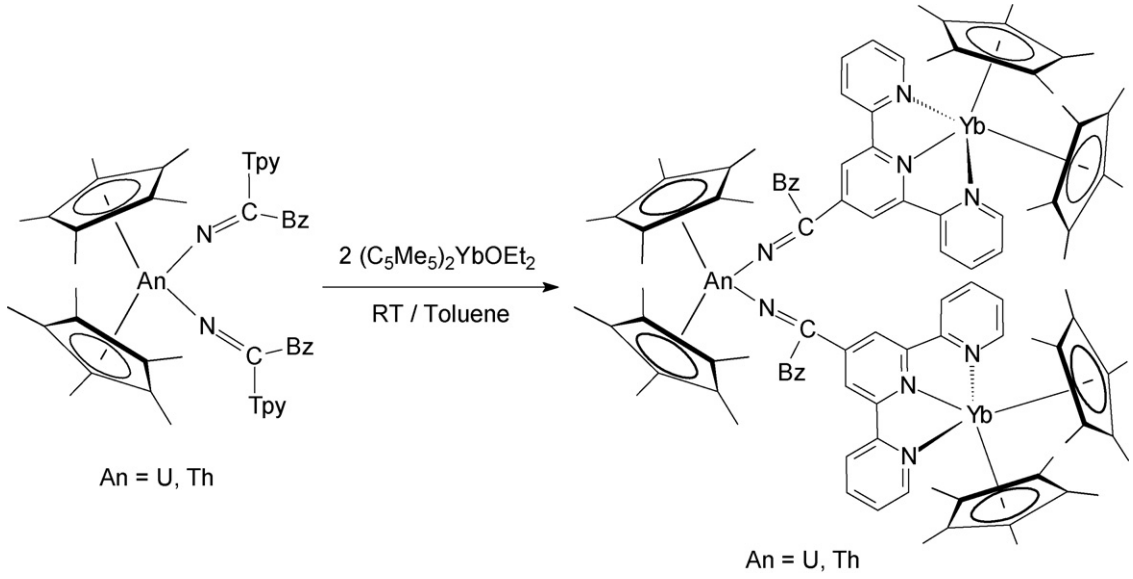

Scheme 120.

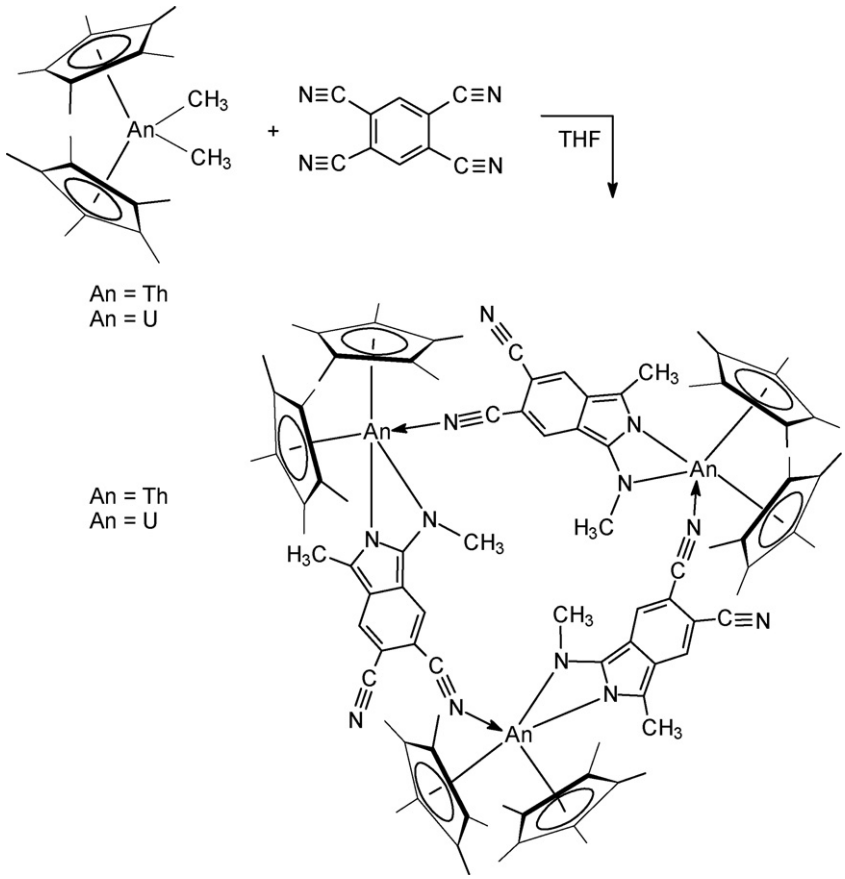

Scheme 121.

on the coordination geometry and the stability of the UO_2^{2+} ion [120].

3.1. Actinide carbonyls

The electronic structure and prediction of atomization energy of naked homoleptic uranium hexacarbonyl $U(CO)_6$ were studied by *ab initio* all-electron fully relativistic Dirac–Fock and nonrelativistic Hartree–Fock self-consistent field (SCF) calculation. From these calculations, $U(CO)_6$ (O_h) was predicted to be very stable in view of a predicted large atomization energy (~49 eV) and stability (~4 eV) with respect to dissociation into U plus six CO molecules. It was concluded that innovative techniques should be devised for the synthesis of uranium hexacarbonyl since the usual synthetic methods have failed so far for this naked actinide hexacarbonal [121].

3.2. Actinide hydrocarbyls

A "Comprehensive Theoretical View of the Bonding in Actinide Molecular Complexes" was published in 2006. This study was based on model complexes of the general formula F_3MCO (M = Nd, Am, U), I_3AmCO, and I_3UCO [122]. Density functional theory and Hartree–Fock effective core potential calculations were performed to investigate the reactivity of neutral f-block atoms (lanthanides and thorium) toward methane C–H bond activation. The first step of the methane dehydrogenation process, which corresponds to an oxidative insertion and formation of $HThCH_3$, was studied. The

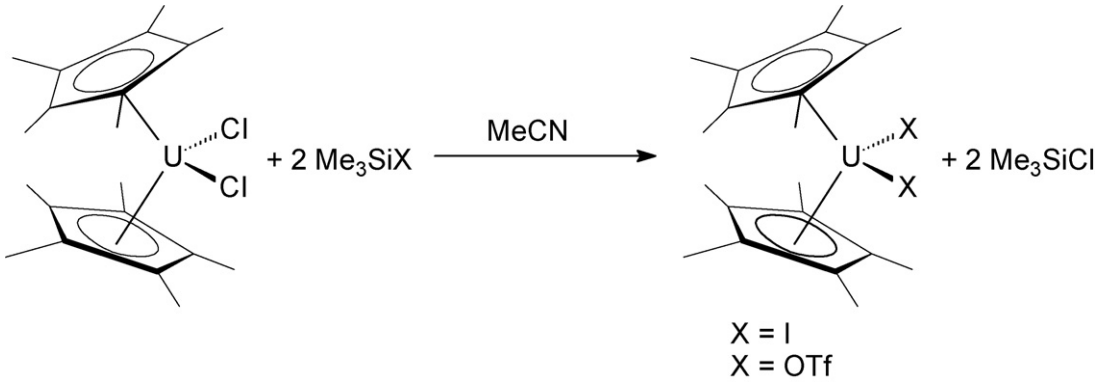

Scheme 122.

performance of a Th neutral atom was found to overshadow the catalytic power of the best of the lanthanides, Ce, in the $[4f^0]6s^25d^2$ electronic configuration. One of the most important factors for this effectiveness comes from the 5f-orbital radial overlap onto the 7s6d valence shell, which enhances the ability of thorium as a catalyst for methane C–H bond activation [9]. The reactions between uranium atoms and CH_3X (X = F, Cl, Br) molecules were investigated in a solid argon matrix. The major products formed on ultraviolet irradiation were the CH_2=UHX methylidene complexes. DFT calculations predict these triplet ground-state structures to be stable and to have significant agostic interactions. Parallels between the uranium and analogous thorium methylidene complexes were also discussed in this contribution [123].

The natural tendency of a uranium atom to be preferentially complexed by a ligand, rather than to explicitly form a direct U–U bond, has to date precluded the isolation of stable uranium species exhibiting direct metal–metal bonding. Quantum chemical calculations published in 2006 have now predicted the diphenyl diuranium compound PhUUPh to have a stable ^1A_g ground state. The paper also addressed the question of how to make PhUUPh and similar species experimentally. Similar to previously detected diuranium polyhydride species, PhUUPh could in principle be formed in a matrix by laser ablation of uranium and co-deposition with biphenyl in an inert matrix. The phenyl ligand might however be too large to be made in a matrix, and a species such as CH_3UUCH_3 may be more feasible [124]. The paucity of molecular actinide complexes with unsupported metal–metal bonds was the subject of yet another theoretical study published in 2006. This paper presented a comparative investigation of the electronic structure and metal–metal bonding in U_2X_6 (X = Cl, F, OH, NH_2, CH_3) complexes and d-block analogues (Mo, W). A generally weak electrostatic stabilization was found to account for a large pre-relaxation destabilization in the U complexes and, ultimately, for the relative weakness of the U–U bonds. Thus the synthesis of a stable actinide compound with an unsupported metal–metal bond remains somewhat similar to a "Holy Grail" in actinide chemistry [125].

Agostic Ln···H–C interactions were detected in a series of homoleptic and heteroleptic uranium arylthiolates containing the bulky "supermesityl" thiolate ligand SMes* (Mes* = $C_6H_2Bu^t_3$-2,4,6). For example, the black uranium(III) compound $U(SMes^*)_3$ was prepared in high yields by protonolysis of $U[N(SiMe_3)_2]_3$ with HSMes* in cyclohexane. Other uranium compounds containing the SMes* ligand include $U(SMes^*)_3(NEt_2)(py)$, $U(SMes^*)[N(SiMe_3)_2]_3$, $U(SMes^*)_3[N(SiMe_3)_2]$, and homoleptic $U(SMes^*)_4$. The latter was isolated as a black solid in 64% yield from the reaction of $U(BH_4)_4$ and KSMes*. An X-ray crystal structure analysis of $U(SMes^*)_4$

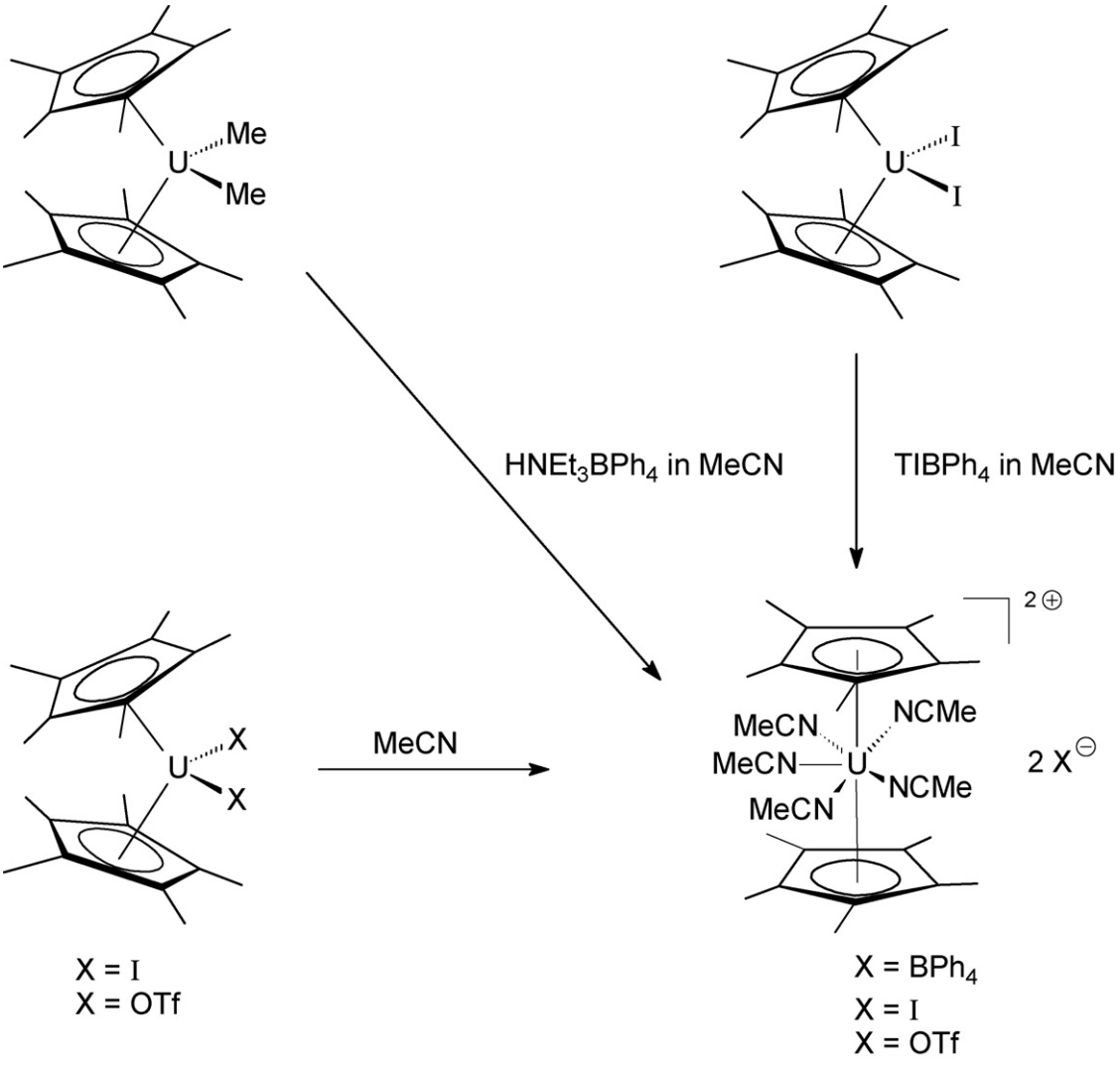

Scheme 123.

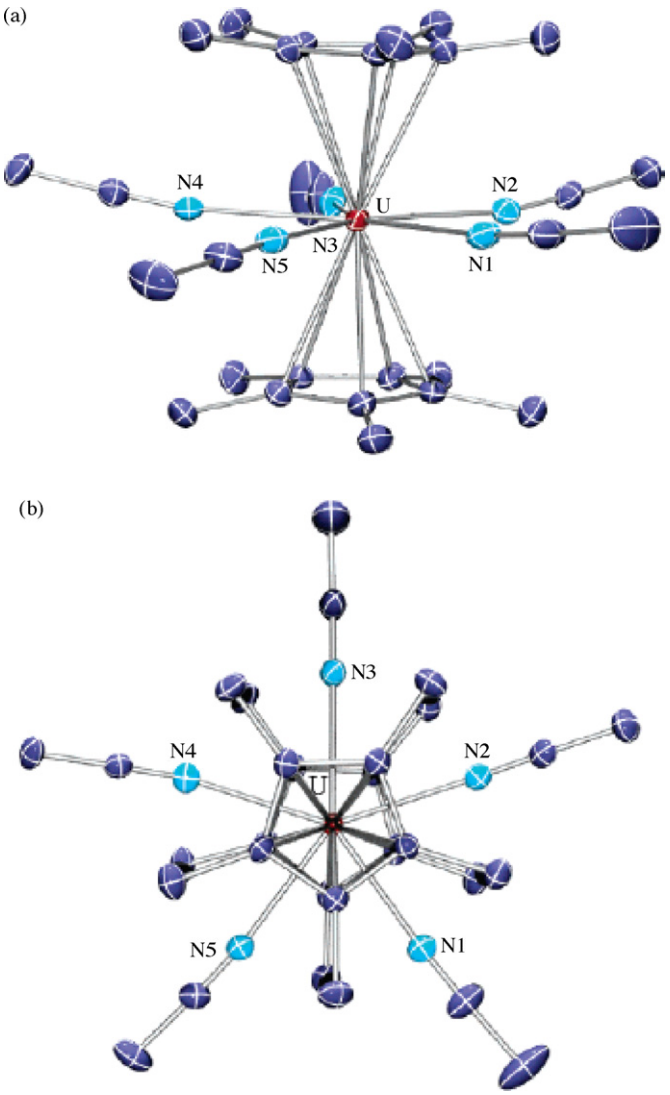

Fig. 48. Views of the dication $[Cp^*_2U(NCMe)_5]^{2+}$ parallel (a) and perpendicular (b) to the cyclopentadienyl rings [131].

revealed a novel η^3-ligation mode for the arylthiolate ligand involving two U···H–C γ-agostic interactions as depicted in Fig. 45 [8].

Uranium complexes containing *N*-heterocyclic carbene (NHC) ligands are still fairly rare. A complex of uranium tetrachloride with the "pincer" dicarbene ligand 2,6-bis(arylimidazol-2-ylidene)pyridine (=C–N–C; aryl = 2,6-$Pr^i_2C_6H_3$) was prepared and structurally characterized by X-ray diffraction methods. The compound was isolated in 50% yield as a yellow-green solid. Despite crystallization from THF the product was obtained solvent-free. As shown in Fig. 46, the central uranium atom is seven-coordinated with the "pincer" dicarbene ligand acting as tridentate ligand [126].

3.3. Actinide cyclopentadienyl compounds

3.3.1. Cp_2AnX, Cp_3An and Cp_3AnL compounds

The binding of *N*-heterocyclic carbenes to Cp_2MI compounds [M = Ce(III), U(III)] was characterized by quantum chemical methods. Density functional methods were found to be in qualitative agreement with experiment that binding to U(III) is more favorable than to Ce(III) [46].

3.3.2. $CpAnX_3$, Cp_2AnX_2 and Cp_3AnX compounds

An oxo-bridged dinuclear uranium(IV) complex containing *ansa*-dimethylsilyl-bis(tetramethylcyclopentadienyl) ligands was prepared following the reaction sequence outlined in Scheme 118. Although the final product was not obtained as single-crystals, the two *n*-butyl groups were confirmed by its reaction with an excess amount of $PhSiH_3$ to produce only 2 equiv. of the corresponding $PhSiH_2{}^nBu$. The oxide-bridged dibutyl uranium complex was found to catalyze the cross-metathesis reaction of $Me_3SiC{\equiv}CR$ with $R'C{\equiv}CH$ (*cf.* Section 3.5) [127].

3.3.3. Pentamethylcyclopentadienyl compounds

3.3.3.1. Cp^*AnX_2 and Cp^*_2AnX compounds. When treated with Me_3SiOTf, the uranium(III) species $Cp^*_2UCl_2Na(THF)_2$ did not afford the trivalent complex $Cp^*_2U(OTf)$ but gave crystals of the dimeric uranium(IV) "ate" compound $[Cp^*_2U(OTf)_3Na(THF)_2]_2{\cdot}2THF$. The first organouranium(III) triflate, $Cp^*_2U(OTf)$, was isolated in 90% yield from the reaction of $U(OTf)_3$ with 2 equiv. of KCp^* in THF as shown in Scheme 119. Dissolution of $Cp^*_2UI(py)$ in acetonitrile gave the adduct $Cp^*_2UI(NCMe)_2$, which, like its cerium analogue, adopts a bent sandwich structure in its crystalline form [128].

3.3.3.2. Bis(pentamethylcyclopentadienyl) actinide(IV), actinide(V), and actinide(VI) compounds. Unprecedented 4f–5f heterotrimetallic complexes exhibiting electrochemical and magnetic communication were reported in 2006. Reaction of $Cp^*_2An(CH_2Ph)_2$ (An = U, Th) with 2 equiv. of 4′-cyano-2,2′:6′,2″-terpyridine in toluene afforded the corresponding terpyridyl-functionalized ketimide complexes. These possess terpyridyl (tpy) groups suitable for the introduction of two additional metal ions and subsequently react with 2 equiv. of $Cp^*_2Yb(OEt_2)$ (Scheme 120) to give the novel 4f–5f heterotrimetallic product in greater than 65% yield. The molecular structure of the uranium derivative, shown in Fig. 47, is one of only three known structures of a complex containing both lanthanide and actinide ions [129].

Actinide-mediated cyclization of 1,2,4,5-tetracyanobenzene led to the discovery of an unusual class of self-assembled trinuclear thorium and uranium macrocycles. Addition of 1 equiv. of 1,2,4,5-tetracyanobenzene to a THF solution of $Cp^*_2AnMe_2$ (An = Th, U) as shown in Scheme 121 at ambient temperature afforded the corresponding trinuclear actinide macrocycles as dark purple solids in 61% (Th) and 47% (U) yield, respectively. The macrocyclic structure was verified by an X-ray diffraction study of the uranium derivative showing a triangular array of uranium atoms bridged by three unusual 5,6-dicyano-1-methyl-3-(*N*-methylamino)isoindolyl ligands. The macrocycle has C_{3h} symmetry and each 9-coordinate uranium atom adopts a typical bent-metallocene geometry [130].

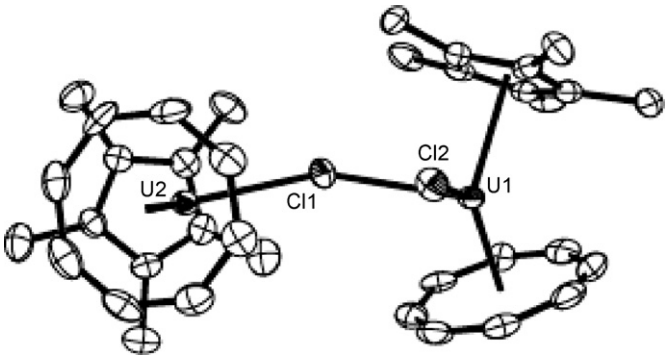

Fig. 49. Molecular structure of $Cp^*(COT)ClU(\mu\text{-}Cl)U(COT)Cp^*$ [135].

The formation of the first linear uranium metallocenes was the subject of two important contributions in 2006 [128,131]. Reactions of $Cp^*_2UCl_2$ with a slight excess of Me_3SiI or Me_3SiOTf in acetonitrile provided convenient routes to $Cp^*_2UI_2$ or $Cp^*_2U(OTf)_2$, which were isolated in excellent yields (Scheme 122) [128].

Crystals of the bent metallocenes $Cp^*_2UI_2(NCR)$ (R = Me, ^{t}Bu) were obtained by addition of excess RCN to a toluene solution of $Cp^*_2UI_2$. The triflate analogue $Cp^*_2U(OTf)_2(NCMe)$ contains monodentate OTf ligands. Treatment of $Cp^*_2UMe_2$ with 2 equiv. of $[HNEt_3][BPh_4]$ in acetonitrile led to the immediate formation of $[Cp^*_2U(NCMe)_5][BPh_4]_2$ as shown in Scheme 123. Previously it had been observed that the ^{1}H NMR spectra of $Cp^*_2UCl_2$ and $Cp^*_2UI_2$ were quite different in acetonitrile, exhibiting signals at δ 12.7 and 35.1, respectively, while the Cp* resonances are in the range of δ 9–18 in benzene or pyridine [131]. In fact, the ^{1}H NMR spectra of $Cp^*_2UI_2$ and $Cp^*_2U(OTf)_2$ in acetonitrile were found to be similar to that of $[Cp^*_2U(NCMe)_5][BPh_4]_2$, indicating the presence of the dicationic species $[Cp^*_2U(NCMe)_5][X]_2$ (X = I, OTf; Scheme 123) in this solvent. The three cationic compounds represent the first linear metallocenes of an f-element and exhibit an unprecedented structure with auxiliary donor ligands in the equatorial plane parallel to the cyclopentadienyl rings (Fig. 48) [128,131].

3.4. Organoactinide complexes with heteroatom five-membered ring ligands

Various unusual thorium complexes involving pyrrolyl π-coordination were reported. Reduction of the tetravalent complex [{2,5-[$(C_4H_3N)CPh_2$]$_2$[$C_4H_2N(Me)$]}$ThCl_2(THF)$]·THF of the tripyrrolide dianion 2,5-[$(C_4H_3N)CPh_2$]$_2C_4H_2N(Me)$ afforded different prod-

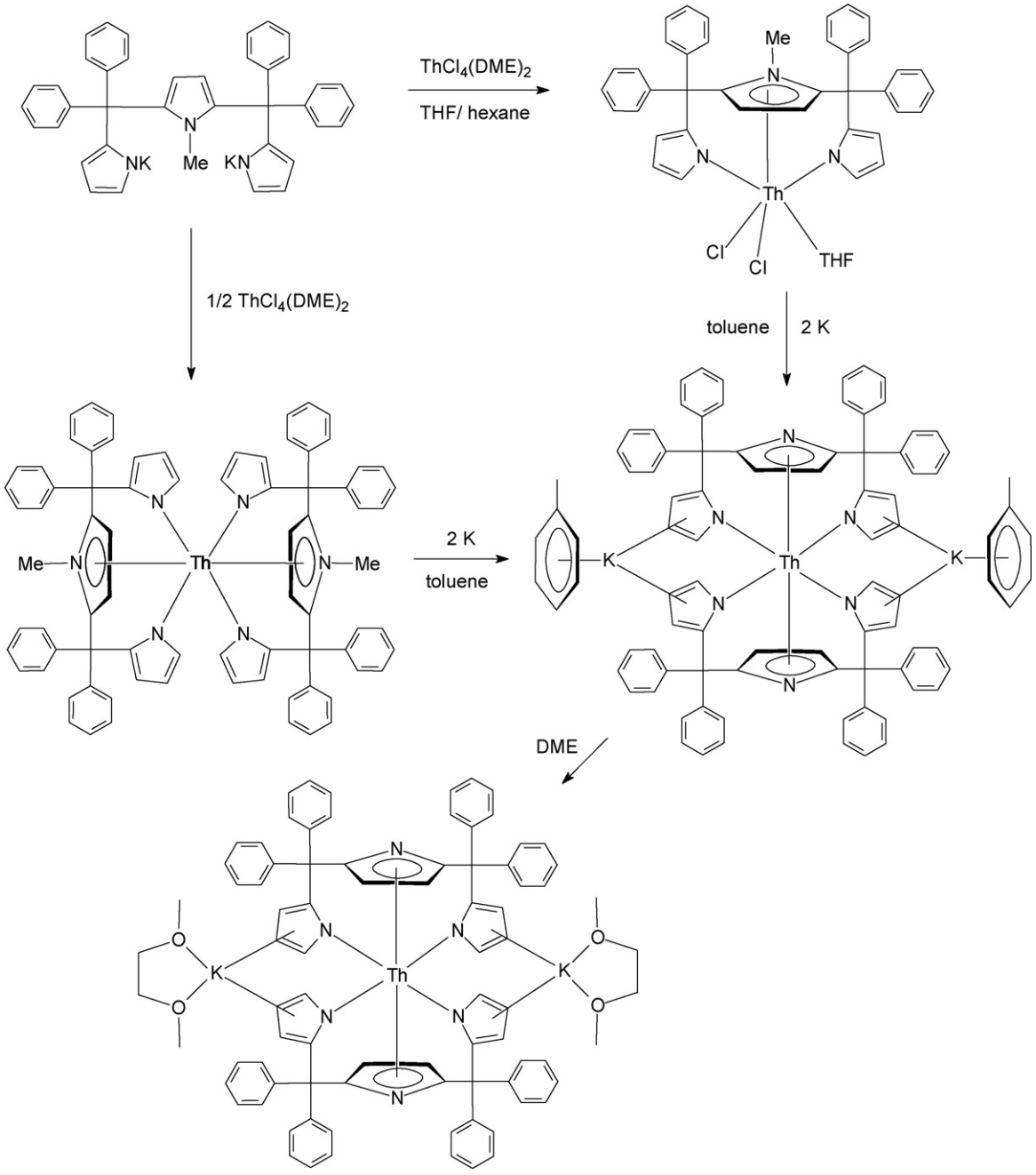

Scheme 124.

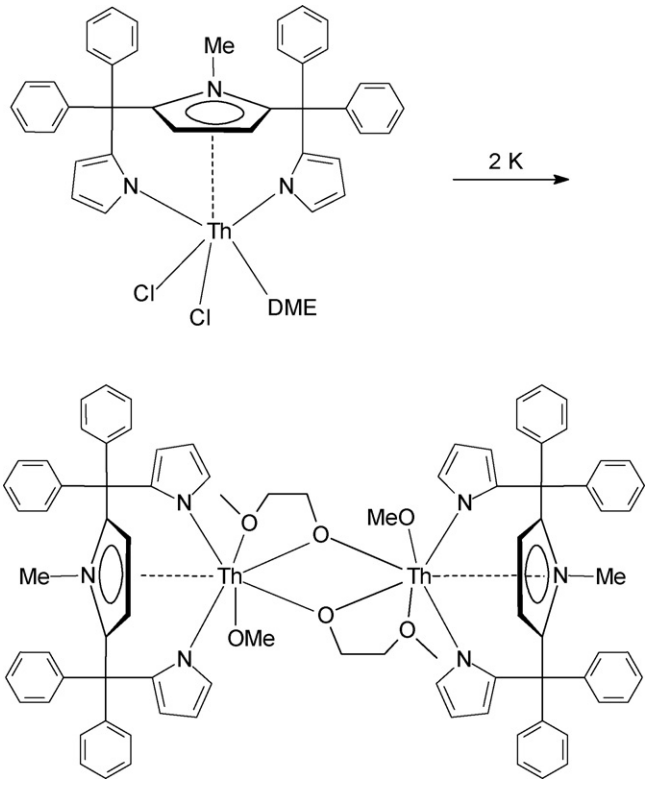

Scheme 125.

ucts depending on the reaction conditions (Scheme 124). In every case, the reaction proceeded *via* the initial formation of a reduced species, as indicated by the very rapid formation of a dark red color followed by slow and complete discoloration. In the case of the reduction in toluene, the complexes $(\{2,5\text{-}[(C_4H_3N)CPh_2]_2[C_4H_2N]\}_2Th[K(toluene)]_2)\cdot 1.5(toluene)$

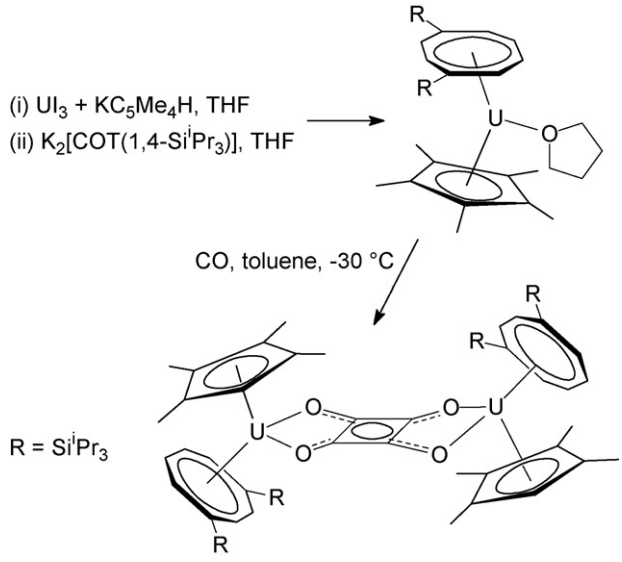

Scheme 127.

and $\{2,5\text{-}[(C_4H_3N)CPh_2]_2[C_4H_2N]\}_2Th[K(DME)]_2$ were obtained, depending on the crystallization solvent (toluene *versus* DME). In both cases, the products arose from a loss of the methyl group attached to the central pyrrole ring N atom [132].

When the reduction was carried out directly in DME as a solvent, the complex $\{[\{2,5\text{-}[(C_4H_3N)CPh_2]_2[C_4H_2N(Me)]\}Th(OMe)]_2(m\text{-}OC_2H_4OMe)_2\}\cdot 0.75(hexane)$ was isolated (Scheme 125). This species is derived from two different pathways of C–O cleavage of the DME solvent [132].

3.5. Actinide cyclooctatetraenyl complexes

One of the most spectacular results in organoactinide chemistry published in 2006 was the reductive cyclotrimerization of

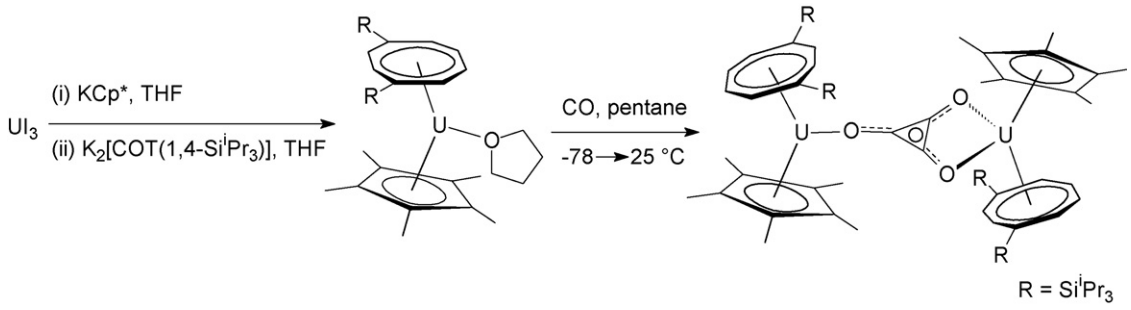

Scheme 126.

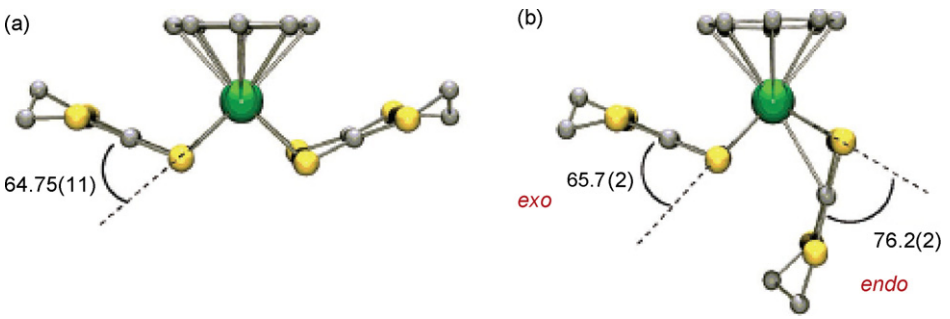

Fig. 50. Side view of the (a) U(IV) and (b) U(V) anions [136].

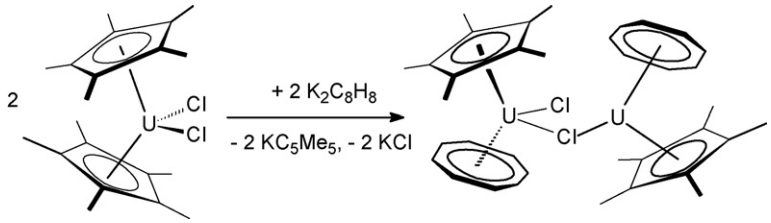

Scheme 128.

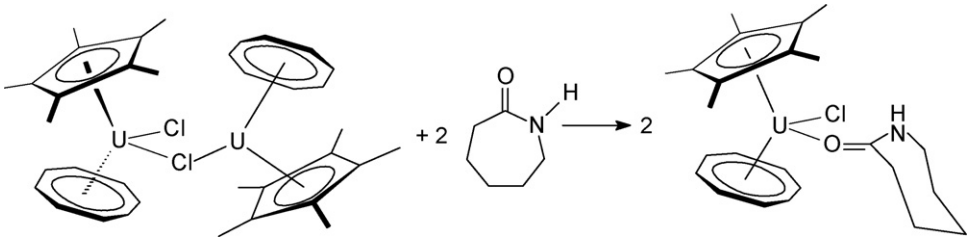

Scheme 129.

carbon monoxide to the deltate dianion by an organometallic uranium complex. The precursor, $(COT^{\dagger})UCp^{*}(THF)$ [$COT^{\dagger}$ = 1,4-bis(triisopropylsilyl)cyclooctytetraenide dianion] was prepared by reaction of UI_3 with KCp^{*} in THF to give the intermediate $Cp^{*}UI_2(THF)_3$, directly followed by treatment with $K_2[COT^{\dagger}]$ in THF, thereby affording $(COT^{\dagger})UCp^{*}(THF)$ as a dark purple, crystalline material in 39% overall yield after recrystallization from pentane at −50 °C (Scheme 126). $(COT^{\dagger})UCp^{*}(THF)$ was structurally characterized by X-ray diffraction. As shown in Scheme 126, this compound reacts with ambient pressures (1 bar) of CO in pentane to give the dimeric U(IV) complex $(\mu\text{-}C_3O_3)[(COT^{\dagger})UCp^{*}]_2$ which was isolated in the form of dark red needles in 40% isolated yield. X-ray crystallography revealed the presence of a deltate dianionic ligand as a reductively homologated CO trimer held between the two uranium(IV) centers. This finding suggested that tuning the ligand environment around U(III) may give access to higher homologues of the dianion as well [133].

The assumption that subtle variations in the steric and/or electronic properties of the starting $COT^{R}/Cp^{R'}$ uranium(III) complex was soon verified experimentally. Also in 2006, the synthesis of a new complex containing a slight modification of the ligand architecture of $(COT^{\dagger})UCp^{*}(THF)$, *via* replacement of the Cp* ligand by Cp^{Me_4H}, and its subsequent reaction with CO was published. The complex $(COT^{\dagger})UCp^{Me_4H}(THF)$ was prepared as a dark-black crystalline material in moderate yield (41%), following a method similar to that used for the synthesis of $(COT^{\dagger})UCp^{*}(THF)$ (Scheme 127) [134].

The structure of $(COT^{\dagger})UCp^{Me_4H}(THF)$ was found to be almost identical to that of $(COT^{\dagger})UCp^{*}(THF)$. Exposure of $(COT^{\dagger})UCp^{Me_4H}(THF)$ to ambient pressures (1 bar) of CO at −30 °C gave a dimeric uranium(IV) squarate complex (Scheme 127) as a red crystalline solid, in 66% yield following recrystallization from a mixture of THF and Et_2O. According to an X-ray structure analysis, the molecule has an inversion center at the midpoint of the C_4O_4 ring. The $C_4O_4^{2-}$ moiety is held between two U(IV) centers in a manner similar to that observed in the deltate complex (*cf.* Scheme 126) [133], with similar accompanying U–COT and U–Cp ring centroid distances. As expected, the oxocarbon unit was found to be planar [134].

$K_2C_8H_8$ (=K_2COT) reacts with $Cp^{*}_2UCl_2$ not by substitution of both chlorides, but by Cl and Cp* ligand displacement to form an asymmetric, sterically unsaturated, mixed-ligand metallocene chloride complex, $Cp^{*}(COT)ClU(\mu\text{-}Cl)U(COT)Cp^{*}$ (Scheme 128). This compound is a tetravalent uranium analogue of the asymmetric trivalent yttrium bimetallic complex $Cp^{*}_2ClY(\mu\text{-}Cl)YCp^{*}_2$, that has been used earlier to evaluate coordination of bases with electropositive trivalent metallocenes. Fig. 49 displays the molecular structure of $Cp^{*}(COT)ClU(\mu\text{-}Cl)U(COT)Cp^{*}$ [135].

Tetravalent $Cp^{*}(COT)ClU(\mu\text{-}Cl)U(COT)Cp^{*}$ similarly coordinates Lewis bases as demonstrated by its reaction with ε-caprolactam (Scheme 129) that generates a complex with four different ligands, $Cp^{*}(COT)UCl[OCNH(CH_2)_5]$ [135].

Dinuclear $Cp^{*}(COT)ClU(\mu\text{-}Cl)U(COT)Cp^{*}$ also participates in ionic salt metathesis reactions with $KN(SiMe_3)_2$ to form $Cp^{*}(COT)U[N(SiMe_3)_2]$ according to Scheme 130. From this reaction the silylamide derivative was isolated as a red solid in 92% yield [135].

The dithiolene ligand conformation in analogous U(IV)/U(V) complexes was investigated by X-ray diffraction and density functional theory analysis of the U···(C=C) interaction. Elucidation of the crystal structure of the dianionic complex $[Na(18\text{-crown-}6)(THF)_2]_2[(COT)U(dddt)_2]$ (dddt = 5,6-dihydro-1,4-

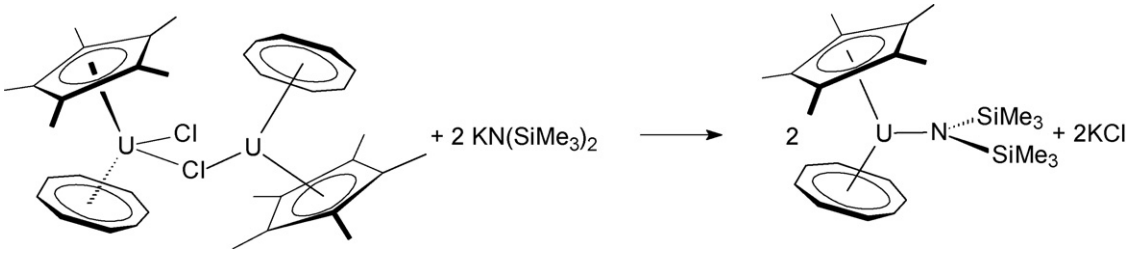

Scheme 130.

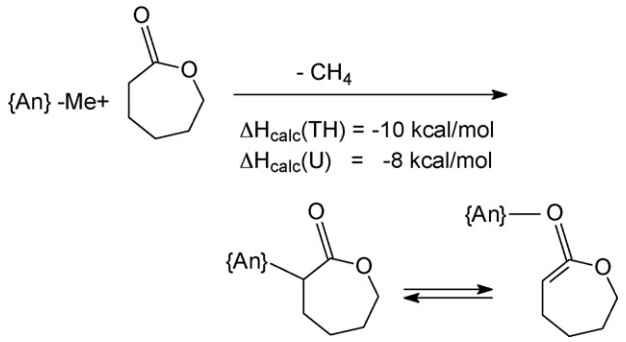

Scheme 131.

dithiin-2,3-dithiolate), complementing that of [Na(18-crown-6)(THF)][(COT)U(dddt)$_2$], allowed the first structural comparison of analogous uranium(IV) and uranium(V) compounds with anionic sulfur ligands. The distinct conformations of the dithiolene ligands, *exo–exo* and *exo–endo* in the uranium(IV) and uranium(V) complexes, respectively, were shown to be the observable manifestations of the differences in the metal-ligand bonding according to the oxidation state of the metal. DFT calculations revealed the occurrence in the uranium(V) anionic species of a significant intramolecular interaction involving the 5f metal orbitals and the C=C double bond of the *endo* dithiolene ligand, which stabilizes its peculiar *exo–endo* conformation (Fig. 50). Such an interaction does not exist in the uranium(IV) complex [136].

3.6. Organoactinides in catalysis

The oxide-bridged dibutyl uranium complex (μ-O)[{$Me_2Si(C_5Me_4)_2$}U^{n}Bu]$_2$ (*cf.* Scheme 118) was found to catalyze the cross-metathesis reaction of $Me_3SiC{\equiv}CR$ with $R'C{\equiv}CH$ (R = Me, $SiMe_3$; R′ = Me, ^{i}Pr, ^{n}Bu, ^{t}Bu, Ph) [127]. The use of the neutral organoactinide complexes $Cp^*_2AnMe_2$ (An = Th, U) and the cationic complex [$(Et_2N)_3U$][BPh_4] for the ring-opening polymerization (ROMP) of ε-caprolactone and L-lactide has been reported [137]. Despite their highly oxophilic nature, these complexes show high activity for polymerization, yielding high-molecular-weight polymers with a low-molecular-weight distribution. In several cases the polymerization proceeds in a living fashion. The first step in the polymerization reaction is the abstraction of the α-hydrogen of the monomer to form the actinide enolate and methane (Scheme 131). From ligand bond dissociation energies this step was calculated to be exothermic with positive entropy and hence spontaneous.

The following steps (chain growth, *cf.* Scheme 132) should also be exothermic (similar bonds are formed and broken, the monomer ring opens to release ring strain) with a negative entropy (due to the reduction in the number of molecules) [137].

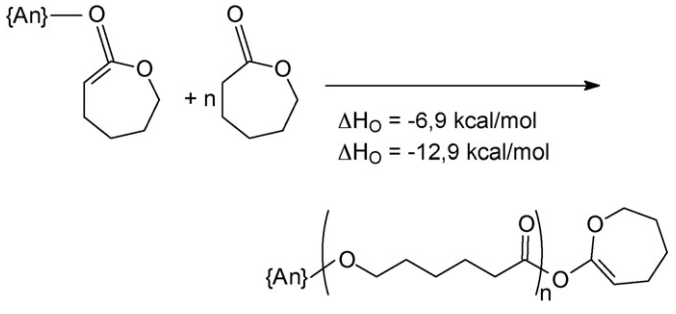

Scheme 132.

References

[1] L. Jiang, Q. Xu, J. Phys. Chem. A 110 (2006) 5636.
[2] Q. Xu, L. Jiang, R.-Q. Zou, Chem. Eur. J. 12 (2006) 3226.
[3] M. Zhou, X. Jin, J. Li, J. Phys. Chem. A 110 (2006) 10206.
[4] X. Jin, L. Jiang, Q. Xu, M. Zhou, J. Phys. Chem. A 110 (2006) 12585.
[5] A.B. Baker, L. Andrews, J. Phys. Chem. A 110 (2006) 10419.
[6] P. Redondo, C. Barrientos, A. Largo, J. Phys. Chem. A 110 (2006) 4057.
[7] H.M. Dietrich, C. Meermann, K.W. Törnroos, R. Anwander, Organometallics 25 (2006) 4316.
[8] M. Roger, N. Barros, T. Arliguie, P. Thuéry, L. Maron, M. Ephritikhine, J. Am. Chem. Soc. 128 (2006) 8790.
[9] K.J. de Almeida, A. Cesar, Organometallics 25 (2006) 3407.
[10] C. Raynaud, J.-P. Daudey, F. Jolibois, L. Maron, J. Phys. Chem. A 110 (2006) 101.
[11] S. Arndt, B.R. Elvidge, P.M. Zeimentz, T.P. Spaniol, J. Okuda, Organometallics 25 (2006) 793.
[12] L.J. Brown, K. Izod, W. Clegg, R.W. Harrington, Organometallics 25 (2006) 2999.
[13] S. Bambirra, A. Meetsma, B. Hessen, Organometallics 25 (2006) 3454.
[14] G.B. Deacon, G.D. Fallon, C.M. Forsyth, S.C. Harris, P.C. Junk, B.W. Skelton, A.H. White, Dalton Trans. (2006) 802.
[15] B.J. Elvidge, S. Arndt, T.P. Spaniol, J. Okuda, Dalton Trans. (2006) 890.
[16] E.W.Y. Wong, A.K. Das, M.J. Katz, Y. Nishimura, J. Batchelor, M. Onishi, D.B. Leznoff, Inorg. Chim. Acta 359 (2006) 2826.
[17] R.G. Howe, C.S. Tredget, S.C. Lawrence, S. Subongkoj, A.R. Cowley, P. Mountford, Chem. Commun. (2006) 223.
[18] S. Ge, S. Bambirra, A. Meetsma, B. Hessen, Chem. Commun. (2006) 3320.
[19] S. Bambirra, A. Meetsma, B. Hessen, A.P. Bruins, Organometallics 25 (2006) 3486.
[20] A.A. Trifonov, G.G. Skvortsov, D.M. Lyubov, N.A. Skorodumova, G.K. Fukin, E.V. Baranov, V.N. Glushakova, Chem. Eur. J. 12 (2006) 5320.
[21] A.A. Trifonov, D.M. Lyubov, G.K. Fukin, E.V. Baranov, Yu.A. Kurskii, Organometallics 25 (2006) 3935.
[22] A.A. Trifonov, D.M. Lyubov, E.A. Fedorova, G.K. Fukin, H. Schumann, S. Mühle, M. Hummert, M.N. Bochkarev, Eur. J. Inorg. Chem. (2006) 747.
[23] S.K. Ibrahim, A.V. Khvostov, M.F. Lappert, L. Maron, L. Perrin, C.J. Pickett, A.V. Protchenko, Dalton Trans. (2006) 2591.
[24] L.K. Knight, W.E. Piers, R. McDonald, Organometallics 25 (2006) 3289.
[25] D.V. Gribkov, K.C. Hultzsch, F. Hampel, J. Am. Chem. Soc. 128 (2006) 3748.
[26] M. Niemeyer, Inorg. Chem. 45 (2006) 9085.
[27] P.L. Arnold, S.T. Liddle, Organometallics 25 (2006) 1485.
[28] Z.-G. Wang, H.-M. Sun, H.-S. Yao, Q. Shen, Y. Zhang, Organometallics 25 (2006) 4436.
[29] Z.-G. Wang, H.-M. Sun, H.-S. Yao, Q. Shen, Y. Zhang, J. Organomet. Chem. 691 (2006) 3383.
[30] T. Cantat, F. Jaroschik, L. Ricard, P. Le Floch, F. Nief, N. Mézailles, Organometallics 25 (2006) 1329.
[31] K.A. Rufanov, B.H. Müller, A. Spannenberg, U. Rosenthal, New J. Chem. 30 (2006) 29.
[32] G. Wang, M. Chen, Y. Zhao, M. Zhou, Chem. Phys. 322 (2006) 354.
[33] C.M. Forsyth, G.B. Deacon, L.D. Field, C. Jones, P.C. Junk, D.L. Kay, A.F. Masters, A.F. Richards, Chem. Commun. (2006) 1003.
[34] L.F. Sánchez-Barba, D.L. Hughes, S.M. Humphrey, M. Bochmann, Organometallics 25 (2006) 1012.
[35] R.E. White, T.P. Hanusa, B.E. Kucera, J. Am. Chem. Soc. 128 (2006) 9622.
[36] R.E. White, C.N. Carlson, J.M. Veauthier, C.K. Simpson, J.D. Thompson, B.L. Scott, T.P. Hanusa, K.D. Scott, Inorg. Chem. 45 (2006) 7004.
[37] F. Jaroschik, F. Nief, L. Ricard, Chem. Commun. (2006) 426.
[38] S. Schinzel, M. Bindl, M. Visseaux, H. Chermette, J. Phys. Chem. A 110 (2006) 11324.
[39] M.E. Burin, M.V. Smirnova, G.K. Fukin, E.V. Baranov, M.N. Bochkarev, Eur. J. Inorg. Chem. (2006) 351.
[40] S.D. Daniel, J.-S.M. Lehn, P. van der Heide, Y. Wang, D.M. Hoffman, Inorg. Chim. Acta 359 (2006) 257.
[41] T. Schroeder, V. Ugrinova, B.C. Noll, S.N. Brown, Dalton Trans. (2006) 1030.
[42] D. Robert, A.A. Trifonov, P. Voth, J. Okuda, J. Organomet. Chem. 691 (2006) 4393.
[43] F. Fabri, R.B. Muterle, W. de Oliveira, U. Schuchardt, Polymer 47 (2006) 4544.
[44] F. Yuan, H. Qian, X. Min, Inorg. Chem. Commun. 9 (2006) 391.
[45] M.D. Walter, F. Weber, G. Wolmershäuser, H. Sitzmann, Angew. Chem. 118 (2006) 1937;
M.D. Walter, F. Weber, G. Wolmershäuser, H. Sitzmann, Angew. Chem. Int. Ed. 45 (2006) 1903.
[46] L. Gagliardi, C.J. Cramer, Inorg. Chem. 45 (2006) 9442.
[47] C. Zhang, R. Liu, J. Zhang, Z. Chen, X. Zhou, Inorg. Chem. 45 (2006) 5867.
[48] J. Zhang, R. Cai, L. Weng, X. Zhou, Dalton Trans. (2006) 1168.
[49] R.A. Layfield, A. Bashall, M. McPartlin, J.M. Rawson, D.S. Wright, Dalton Trans. (2006) 1660.
[50] (a) R. Liu, C. Zhang, Z. Zhu, J. Luo, X. Zhou, L. Weng, Chem. Eur. J. 12 (2006) 6940;
(b) C.-M. Zhang, R.-T. Liu, Z.-X. Chen, X.-G. Zhou, Chin. J. Chem. 24 (2006) 231;
(c) L. Ma, J. Zhang, Z. Zhang, R. Cai, Z. Chen, X. Zhou, Organometallics 25 (2006) 4571.
[51] P. Sekar, J.A. Ibers, Inorg. Chim. Acta 359 (2006) 2751.
[52] M.-Q. Xue, Y.-M. Yao, Q. Shen, K.-B. Yu, Chin. J. Struct. Chem. 25 (2006) 139.

[53] P.B. Hitchcock, A.G. Hulkes, M.F. Lappert, A.V. Protchenko, Inorg. Chim. Acta 359 (2006) 2998.
[54] H. Hamaed, A.Y.H. Lo, D.S. Lee, W.J. Evans, R.W. Schurko, J. Am. Chem. Soc. 128 (2006) 12638.
[55] A.J. Rossini, R.W. Schurko, J. Am. Chem. Soc. 128 (2006) 10391.
[56] U. Baisch, S. Pagano, M. Zeuner, J. Schmedt auf der Günne, O. Oeckler, W. Schnick, Organometallics 25 (2006) 3027.
[57] U. Baisch, S. Pagano, M. Zeuner, N. Barros, L. Maron, W. Schnick, Chem. Eur. J. 12 (2006) 4785.
[58] M.J. Davies, M.F. Lappert, Polyhedron 25 (2006) 397.
[59] M.D. Walter, D.J. Berg, R.A. Andersen, Organometallics 25 (2006) 3228.
[60] C.N. Carlson, C.J. Kuehl, R.E. da Re, J.M. Veauthier, E.J. Schelter, A.E. Milligan, B.L. Scott, E.D. Bauer, J.D. Thompson, D.E. Morris, K.D. John, J. Am. Chem. Soc. 128 (2006) 7230.
[61] J.A. Moore, A.H. Cowley, J.C. Gordon, Organometallics 25 (2006) 5207.
[62] W.J. Evans, T.M. Champagne, B.L. Davis, N.T. Allen, G.W. Nyce, M.A. Johnston, Y.-C. Lin, A. Khvostov, J.W. Ziller, J. Coord. Chem. 59 (2006) 1069.
[63] W.J. Evans, D.S. Lee, J.W. Ziller, N. Kaltsoyannis, J. Am. Chem. Soc. 128 (2006) 14176.
[64] W.J. Evans, K.A. Miller, J.W. Ziller, Inorg. Chem. 45 (2006) 424.
[65] W.J. Evans, D.B. Rego, J.W. Ziller, Inorg. Chem. 45 (2006) 3437.
[66] M. Visseaux, T. Chenal, P. Roussel, A. Mortreux, J. Organomet. Chem. 691 (2006) 86.
[67] W.J. Evans, B.L. Davis, T.M. Champagne, J.W. Ziller, Proc. Natl. Acad. Sci. U.S.A. 103 (2006) 12678.
[68] S. Bendjaballah, S. Kahlal, K. Costuas, E. Bévillon, J.-Y. Saillard, Chem. Eur. J. 12 (2006) 2048.
[69] A.A. Trifonov, E.A. Fedorova, G.K. Fukin, E.V. Baranov, N.O. Druzhkov, M.N. Bochkarev, Chem. Eur. J. 12 (2006) 2752.
[70] J.L. Lewin, N.L. Woodrum, C.J. Cramer, Organometallics 25 (2006) 5906.
[71] S. Wang, Y. Feng, L. Mao, E. Sheng, G. Yang, M. Xie, S. Wang, Y. Wei, Z. Huang, J. Organomet. Chem. 691 (2006) 1265.
[72] S. Wang, X. Tang, A. Vega, J.-Y. Saillard, E. Sheng, G. Yang, S. Zhou, Z. Huang, Organometallics 25 (2006) 2399.
[73] C. Pi, Z. Zhang, R. Liu, L. Weng, Z. Chen, X. Zhou, Organometallics 25 (2006) 5156.
[74] F.-G. Fontaine, K.A. Tupper, T.D. Tilley, J. Organomet. Chem. 691 (2006) 4595.
[75] J. Wang, J. Smith, C. Zheng, J.A. Maguire, N.S. Hosmane, Organometallics 25 (2006) 4118.
[76] H. Shen, H.-S. Chan, Z. Xie, Organometallics 25 (2006) 2617.
[77] B.R. Sohnlein, J.F. Fuller, D.-S. Yang, J. Am. Chem. Soc. 128 (2006) 10692.
[78] H. Xiang, J. Yang, J.G. Hou, Q. Zhu, J. Am. Chem. Soc. 128 (2006) 2310.
[79] D.J. Berg, J. Sun, B. Twamley, Chem. Commun. (2006) 4019.
[80] T.K. Panda, M.T. Gamer, P.W. Roesky, Inorg. Chem. 45 (2006) 910.
[81] S. Hino, J. Low Temp. Phys. 142 (2006) 127.
[82] M. Sparta, K.J. Børve, V.R. Jensen, J. Phys. Chem. A 110 (2006) 11711.
[83] G. Lu, K. Deng, H. Wu, J. Yang, X. Wang, J. Chem. Phys. 124 (2006) 054305.
[84] Z.-Q. Shi, X. Wu, C.-R. Wang, X. Lu, H. Shinohara, Angew. Chem. 118 (2006) 2161;
Z.-Q. Shi, X. Wu, C.-R. Wang, X. Lu, H. Shinohara, Angew. Chem. Int. Ed. 45 (2006) 2107.
[85] E. Nishibori, I. Terauchi, M. Sakata, M. Takata, Y. Ito, T. Sugai, H. Shinohara, J. Phys. Chem. B 110 (2006) 19215.
[86] K. Tan, X. Lu, J. Phys. Chem. A 110 (2006) 1171.
[87] Y. Iiduka, T. Wakahara, K. Nakajima, T. Tsuchiya, T. Nakahodo, Y. Maeda, T. Akasaka, N. Mizorogi, S. Nagase, Chem. Commun. (2006) 2057.
[88] H. Wu, K. Deng, G. Lu, Y. Yuan, J. Yang, X. Wang, J. Phys.: Condens. Matter 18 (2006) 7115.
[89] M.T. Gamer, P.W. Roesky, S.N. Konchenko, P. Nava, R. Ahlrichs, Angew. Chem. 118 (2006) 4558;
M.T. Gamer, P.W. Roesky, S.N. Konchenko, P. Nava, R. Ahlrichs, Angew. Chem. Int. Ed. 45 (2006) 4447.
[90] S. Kaita, M. Yamanaka, A.C. Horiuchi, Y. Wakatsuki, Macromolecules 39 (2006) 1359.
[91] A. Fischbach, C. Meermann, G. Eickerling, W. Scherer, R. Anwander, Macromolecules 39 (2006) 6811.
[92] H.M. Dietrich, O. Schuster, K.W. Törnroos, R. Anwander, Angew. Chem. 118 (2006) 4977;
H.M. Dietrich, O. Schuster, K.W. Törnroos, R. Anwander, Angew. Chem. Int. Ed. 45 (2006) 4858.
[93] H.M. Dietrich, K.W. Rörnroos, R. Anwander, J. Am. Chem. Soc. 128 (2006) 9298.
[94] H.M. Dietrich, H. Grove, K.W. Törnroos, R. Anwander, J. Am. Chem. Soc. 128 (2006) 1458.
[95] Y. Liu, M. Nishiura, Y. Wang, Z. Hou, J. Am. Chem. Soc. 128 (2006) 5592.
[96] R.D. Miotti, A. de Souza Maia, J.G. Rodrigues, W. de Oliveira, Inorg. Chem. Commun. 9 (2006) 228.
[97] A. Fischbach, F. Perdih, E. Herdtweck, R. Anwander, Organometallics 25 (2006) 1626.
[98] D. Patel, S.T. Liddle, S.A. Mungur, M. Rodden, A.J. Blake, P.L. Arnold, Chem. Commun. (2006) 1124.
[99] S. Tomasi, H. Weiss, T. Ziegler, Organometallics 25 (2006) 3619.
[100] L. Zhou, Y. Yao, C. Li, Y. Zhang, Q. Shen, Organometallics 25 (2006) 2880.
[101] S. Bambirra, H. Tsurugi, D. van Keusen, B. Hessen, Dalton Trans. (2006) 1157.
[102] D. Riegert, J. Collin, A. Meddour, E. Schulz, A. Trifonov, J. Org. Chem. 71 (2006) 2514.
[103] A. Motta, I.L. Fragalà, T.J. Marks, Organometallics 25 (2006) 5533.
[104] J. Zhao, T.J. Marks, Organometallics 25 (2006) 4763.
[105] K. Komeyama, D. Kobayashi, Y. Yamamoto, K. Takehira, K. Takaki, Tetrahedron 62 (2006) 2511.
[106] K. Takaki, K. Komeyama, D. Kobayashi, T. Kaeabata, K. Takehira, J. Alloys Compd. 408–412 (2006) 432.
[107] N. Barros, O. Eisenstein, L. Maron, T.D. Tilley, Organometallics 25 (2006) 5699.
[108] N.L. Woodrum, C.J. Cramer, Organometallics 25 (2006) 68.
[109] C. Raynaud, L. Perrin, L. Maron, Organometallics 25 (2006) 3143.
[110] W.-X. Zhang, M. Nishiura, Z. Hou, Synlett (2006) 1213.
[111] X. Linghu, A.D. Satterfield, J.S. Johnson, J. Am. Chem. Soc. 128 (2006) 9302.
[112] W. Schepens, D. van Haver, M. Vandewalle, R. Bouillon, A. Verstuyf, P.J. de Clercq, Org. Lett. 8 (2006) 4247.
[113] Y. Liu, S. Luo, X. Fu, F. Fang, Z. Zhuang, W. Xiong, X. Jia, H. Zhai, Org. Lett. 8 (2006) 115.
[114] Z. Li, X. Cao, G. Lai, J. Liu, Y. Ni, J. Wu, H. Qiu, J. Organomet. Chem. 691 (2006) 4740.
[115] P. Myllymäki, M. Nieminen, J. Niinistö, M. Putkonen, K. Kukli, L. Niinistö, J. Mater. Chem. 16 (2006) 563.
[116] B.-Y. Kim, M.-G. Ko, E.-J. Lee, M.-S. Hong, Y.-J. Jeon, J.-W. Park, J. Korean Chem. Soc. 49 (2006) 1303.
[117] E.-J. Lee, M.-G. Ko, B.-Y. Kim, S.-K. Park, H.-D. Kim, J.-W. Park, J. Korean Chem. Soc. 49 (2006) 1243.
[118] S.Y. No, D. Eom, C.S. Hwang, H.J. Kim, J. Appl. Phys. 100 (2006) 024111.
[119] A. Koizumi, H. Ohnishi, T. Inoue, T. Yamauchi, I. Yamakawa, H. Ofuchi, M. Tabuchi, A. Nakamura, Y. Takeda, Thin Solid Films 515 (2006) 543.
[120] M. Ephritikhine, Dalton Trans. (2006) 2501.
[121] G.L. Malli, J. Chem. Phys. 124 (2006) 021102.
[122] L. Petit, L. Joubert, P. Maldivi, C. Adamo, J. Am. Chem. Soc. 128 (2006) 2190.
[123] J.T. Lyon, L. Andrews, Inorg. Chem. 45 (2006) 1847.
[124] G. La Macchia, M. Brynda, L. Gagliardi, Angew. Chem. 118 (2006) 6356;
G. La Macchia, M. Brynda, L. Gagliardi, Angew. Chem. Int. Ed. 45 (2006) 6210.
[125] G. Cavigliasso, N. Kaltsoyannis, Inorg. Chem. 45 (2006) 6828.
[126] D. Pugh, J.A. Wright, S. Freeman, A.A. Danopoulos, Dalton Trans. (2006) 775.
[127] J. Wang, Y. Gurevich, M. Botoshansky, M.S. Eisen, J. Am. Chem. Soc. 128 (2006) 9350.
[128] J. Maynadié, J.-C. Berthet, P. Thuéry, M. Ephritikhine, Organometallics 25 (2006) 5603.
[129] E.J. Schelter, J.M. Veauthier, J.D. Thompson, B.L. Scott, K.D. John, D.E. Morris, J.L. Kiplinger, J. Am. Chem. Soc. 128 (2006) 2198.
[130] J.L. Kiplinger, J.A. Pool, E.J. Schelter, J.D. Thompson, B.L. Scott, D.E. Morris, Angew. Chem. 118 (2006) 2090;
J.L. Kiplinger, J.A. Pool, E.J. Schelter, J.D. Thompson, B.L. Scott, D.E. Morris, Angew. Chem. Int. Ed. 45 (2006) 2036.
[131] J. Maynadié, J.-C. Berthet, P. Thuéry, M. Ephritikhine, J. Am. Chem. Soc. 128 (2006) 1082.
[132] A. Arunachalampillai, P. Crewdson, I. Korobkov, S. Gambarotta, Organometallics 25 (2006) 3856.
[133] O.T. Summerscales, F.G.N. Cloke, P.B. Hitchcock, J.C. Green, N. Hazari, Science 311 (2006) 829.
[134] O.T. Summerscales, F.G.N. Cloke, P.B. Hitchcock, J.C. Green, N. Hazari, J. Am. Chem. Soc. 128 (2006) 9602.
[135] W.J. Evans, S.A. Kozimor, J.W. Ziller, Polyhedron 25 (2006) 484.
[136] L. Belkhiri, T. Arliguie, P. Thuéry, M. Formigué, A. Boucekkine, M. Ephritikhine, Organometallics 25 (2006) 2782.
[137] E. Barnea, D. Moradove, J.-C. Berthet, M. Ephritikhine, M.S. Eisen, Organometallics 25 (2006) 320.